Design, synthesis and catalytic applications of NiO-Al_2O_3 materials for hydrogenation and oxidative dehydrogenation reactions

by

Majid Darestani Farahani

(MSc)

Submitted in the fulfillment of the academic requirements for the degree of Doctor of Philosophy in the School of Chemistry and physics, University of KwaZulu-Natal, Durban, South Africa.

March 2017

NOTE: This thesis has been prepared according to Format 3 as outlined in the guidelines from the Collage of Agriculture, Engineering and Science which state:

This is a thesis in which the chapters are written as a set of discrete research papers, with an Overall Introduction and Final Discussion. These research papers would not be published yet, but at least one paper would have been submitted for publication. The references are reformatted to a uniform standard.

As the candidate's supervisor, I have approved this thesis for submission

Prof. Holger B. Friedrich_____ Date:_____

Abstract

This thesis shows the synthesis of $NiO\text{-}Al_2O_3$ based catalysts using solution combustion as well as glycol-thermal techniques and explains the roles of catalyst porosity and the presence of $NiAl_2O_4$ spinel in the hydrogenation of octanal. The oxidative dehydrogenation of *n*-octane was also investigated. Furthermore, the effects of Nb doping in $NiO\text{-}Al_2O_3$ based catalysts and $NiAl_2O_4$ spinel were probed using different characterization techniques such as PXRD, UV-DRS, SEM, HR-TEM, N_2 physisorption, H_2-TPR and NH_3-TPD, and oxidative dehydrogenation of *n*-octane as a model reaction, since doping is known to play major role in oxidative reactions.

Four catalysts with the molar ratio of Ni : Al (1 : 2) were prepared by solution combustion synthesis (SCS) and sol-gel auto combustion synthesis (SGCS) techniques and used for the hydrogenation of octanal to octanol. The effect of two different fuels (urea and oxalyldihydrazide [ODH]) and water concentration on the final physicochemical properties of catalysts were investigated. Pure phase and porous NiO/Al_2O_3 (free of spinel) was achieved by application of SGCS and urea as a fuel, which resulted in high activity for hydrogenation of octanal at relatively low temperature (110 °C). Furthermore, SCS using ODH as a fuel gave the best comparative aldehyde conversion and alcohol selectivity (98 % and 97 %, respectively), albeit at a higher temperature of 150 °C. The formation of $NiAl_2O_4$ seems to block the acidic sites of alumina and improve the selectivity towards the desired product. The presented $NiAl_2O_4$ seems to also offer the advantage of a slow release of fresh metallic Ni sites in the hydrogenation reactions.

In the second project, four catalysts with different doping concentrations of niobium were prepared using sol-gel auto combustion (SGCS). All fresh and used catalysts were characterized using different techniques and showed the partial substitution of Nb in the

$NiAl_2O_4$ spinel lattice and $NiNb_2O_6$. Nb was found to prefer the occupancy of the octahedral sites of the spinel, which resulted in modification of nickel migration, electronic profile, redox properties and surface textures. These catalysts were used for the oxidative dehydrogenation of *n*-octane. The catalytic results supported the characterization data and also revealed the role of Nb in the modification of acidic sites. Coke formation was found to facilitate nickel migration from octahedral to tetrahedral sites and result in a smaller crystallite size of $NiAl_2O_4$ spinel, which seems to be positively involved during the catalytic reactions.

The third project was the synthesis of four 25 wt% [NiO-Nb_2O_5]-Al_2O_3 nano-composites with different loadings of NiO and Nb_2O_5 using the glycol-thermal synthesis technique. These catalysts were used for the oxidative dehydrogenation of *n*-octane. Different characterization techniques confirmed the successful synthesis of these nano-composites with small crystallite sizes. This technique resulted in the formation of mesoporous materials with nanorod like morphology. Furthermore, the synthesis of ordered mesoporous alumina (OMA) was achieved using this synthetic technique without using any expensive templates. The addition of Nb was found to influence the physical texture, acidity and redox nature of these materials. It was also found to diminish the contribution of the "confinement-effect" between the mesoporous alumina and the nickel, resulting in enhanced redox properties over these catalysts. However, the fast reduction and oxidation of the involved nickel in these catalysts seem to have negative effects on the catalytic reaction and result in higher selectivity towards CO_x. All characterization data show good correlation with the obtained data from the ODH reaction of *n*-octane.

Thus two different techniques for the synthesis of NiO-Al_2O_3 based materials with tuneable physicochemical properties are shown. The properties of these materials could be tuned using different fuels, water concentration and loading of Nb as a dopant in the case of

combustion synthesis and the variation of Nb content in the case of catalysts prepared using glycol-thermal synthesis. The role of different parameters, such as phase composition, crystallite size, surface morphology, porosity, acidity, metal migration, metal dispersion, the confinement effect, doping and coke formation in the hydrogenation of octanal (metallic Ni as active sites) and ODH of *n*-octane (NiO as active sites) were investigated where applicable.

Preface

The experimental work described in this thesis was carried out in the School of Chemistry and Physics in the University of KwaZulu Natal, Westville campus, Durban. Starting from March 2014 under the guidance and supervision of Professor Holger B. Friedrich.

These studies represent original work by the author and have not otherwise been submitted in any form for any degree or diploma to any tertiary institution. Where use has been made of work of other it is duly acknowledged in the text.

Majid Darestani Farahani

B.Sc (Payam-e Noor University, Tehran), MSc (University of KwaZulu-Natal, Westville campus)

Declaration 1

Plagiarism

I, Majid Darestani Farahani

1. The research reported in this thesis, except where otherwise indicated, is my original research.
2. This thesis has not been submitted for any degree or examination at any other university.
3. This thesis does not contain other person's data, pictures, graphs or other information, unless specifically acknowledged as being sourced from other persons.
4. This thesis does not contain other person's writing, unless specifically acknowledged as being sourced from other researchers. Where other written sources have been quoted, then:
    a. Their words have been re-written but the original information attributed to them has been referenced.
    b. Where their exact words have been used, then their writing has been placed in italics and inside quotation marks, and referenced.
5. This thesis does not contain text, graphics or tables copied and pasted from internet, unless specifically acknowledge, and the source being detailed in the thesis and in the reference sections.

_____

Majid Darestani Farahani

Declaration 2

Publications and conference contributions

DETAILS OF CONTRIBUTION TO PUBLICATIONS that form part and/or include research presented in this thesis (include publications in preparation, submitted, in press and published and give details of the contributions of each author to the experimental and writing of each publication).

Publications

1.

Authors: Majid D. Farahani, Jignesh Valand, Abdul S. Mahomed and Holger B. Friedrich

Title: A comparative study of NiO/Al_2O_3 catalysts prepared by different combustion techniques for octanal hydrogenation

Status: Published, *Catal. Lett.*, 2016, 146, 2441–2449

Contribution: I carried out all catalysts preparation, characterisations and manuscript preparation under the supervision of Prof. Holger B. Friedrich. Dr. Jignesh Valand carried out the catalytic testing and Dr. Abdul S. Mahomed contributed with the discussion during the manuscript preparation.

2.

Authors: Majid D. Farahani and Holger B. Friedrich

Title: Oxidative dehydrogenation of *n*-octane over niobium doped $NiAl_2O_4$: A novel example of beneficial coking in catalysis over spinel base catalyst

Status: Manuscript in preparation

Contribution: I carried out all experimental work under the supervision of Prof. Holger B. Friedrich.

3.

Authors: Majid D. Farahani, Nadir S. E. Osman, Itegbeyogene P. Ezekiel, Thomas Moyo and Holger B. Friedrich

Title: Niobium, as a modifier of the "confinement effect", in ordered mesoporous NiO-Al_2O_3 catalysts with nanorod morphology, used for activation of *n*-octane

Status: Manuscript in preparation

Contribution: I carried out all characterisations, catalytic testing and manuscript preparation under the supervision of Prof. Holger B. Friedrich. Dr. Nadir S. E. Osman and Mr. Itegbeyogene P. Ezekiel prepared the catalysts under the supervision of Dr. Thomas Moyo.

Conference contributions

1.

Oral presentation, Hydrogenation of octanal over NiO/Al_2O_3 synthesised via Solution Combustion Synthesis (SCS) and Sol-Gel auto Combustion Synthesis (SGCS), CATSA conference, Stellenbosch, South Africa, 2015.

2.

Oral presentation, Oxidative dehydrogenation of *n*-octane over mesoporous nanorod composite 25 wt% [NiO-Nb_2O_5]-Al_2O_3 catalysts, CATSA conference, Drakensberg, South Africa, 2016.

3.

Poster presentation, Hydrogenation of octanal over NiO/Al_2O_3 catalysts prepared via Solution Combustion Synthesis (SCS) and Sol-Gel auto Combustion Synthesis (SGCS), Research day (UKZN), Durban, South Africa, 2016.

Content overview

This thesis is formatted as a combination of three technical papers. Each paper has the general structure of a manuscript including abstract, experimental, results and discussion and conclusion, as well as figures, tables and schemes.

- Chapter one is the introduction chapter, which is focused on the application of nickel based materials in catalysis. Solution Combustion Synthesis (SCS) for preparation of materials is briefly introduced, and the focus is on the synthesis of doped metal oxides using this technique. Different techniques for the preparation of the supported metal oxides are discussed and introduced in this chapter. In addition, a short introduction to the $NiAl_2O_4$ spinel is provided. The chemistry behind the hydrogenation of aldehydes, as well as the oxidative dehydrogenation of paraffins, using heterogeneous catalysts, is discussed in this chapter, with specific attention on nickel based catalysts, since these catalytic reactions are the chosen models throughout this study.
- Chapter two contains the first paper, which describes NiO/Al_2O_3 catalysts that were synthesised using SCS and Sol-gel auto Combustion (SGCS) with two different fuels, and used for hydrogenation of octanal as a catalytic model reaction. The effects of the varied parameters during the synthesis of these catalysts on their physiochemical properties as well as catalytic performance are discussed. Furthermore, the role of the formed $NiAl_2O_4$ spinel in the hydrogenation of octanal was investigated.
- Chapter three contains the second paper, which describes the use of Nb as a dopant for the $NiAl_2O_4$ spinel and the use of these materials for the oxidative dehydrogenation of *n*-octane. These catalysts were synthesised using SGCS and characterised by different means to better understand the role of Nb doping on the alteration of the physicochemical properties of these materials. The used catalysts were also characterised to probe the influence of the slight coke formation over these catalysts, formed during the ODH of *n*-octane, on catalytic performance, as well as the general properties of these catalysts.
- Chapter four contains the third paper, where mesoporous NiO/Al_2O_3 catalysts with different Nb loadings, prepared using the glycol-thermal synthesis, described. These materials were characterised using different techniques and used as catalysts for the oxidative activation of *n*-octane. The approximately similar surface textures for these catalysts allowed the better understanding of Nb addition on the modification of the

chemical properties of these nickel based catalysts, which resulted in different catalytic performances.

- Chapter five provides an overall summary and conclusion of all chapters.
- This is followed by the Appendix.

Table of contents

List of figures

(Figures are reprinted with the permission of the publisher where applicable)

List of tables

List of schemes

(Scheme 1.1 is reprinted with the permission of the publisher)

Acknowledgements

Firstly, I would like to thank to my parents, Mohammadreza and Sadigheh Darestani Farahani, who are my roots. I appreciate their supports, encouragements and the manner that they chose to raise me as their son. To my parents, thank you very much for teaching me the lessons of life, which are with me every time and everywhere. My thanks also go to my sister Maryam Darestani Farahani for her encouragement throughout these years.

I also want to thank my supervisor Prof. Holger Friedrich for taking me into his research group, providing me all requirements to focus on my projects and to carry them out. In particular, I appreciate the freedom that he offered me to design the focus of this study. His excellent management, valuable supervisions and guidance will be always remembered and used in my professional, as well as personal lives.

My thanks also go to the National Research Foundation (NRF), South Africa, the University of KwaZulu-Natal and Sasol for their financial supports throughout this study.

I would like to thank Dr. Abdul S. Mahomed, Dr. Sooboo Singh, Dr Mayashree Bux (Sasol) and Dr. Michael Datt (Sasol) for their valuable and treasured guidance during my research. I am also thankful to Dr. Nadir S. E. Osman, Mr. Itegbeyogene P. Ezekiel and their supervisor Dr. Thomas Moyo from the condensed materials group in the discipline of Physics (University of KwaZulu-Natal, Westville campus) for their help in this project. I would like to extend my thanks to Dr. Jignesh Valand for all of the scientific discussion and support.

This work required the applications of different instruments for different parts of the study. Therefore, I would like to thank all staff members in the School of Chemistry and Physics (University of KwaZulu-Natal, Westville campus), in particular Mrs A. Naidoo, and the electron microscopy unit in the University of KwaZulu-Natal, Westville campus.

I would like to take this opportunity to thank the past and current members of the Catalysis Research Group (CRG) in the University of Kwa-Zulu Natal (Westville campus) for the time and input during the group meetings. I especially thank my very good friends Dr. Joel M. Gichumbi, Dr. Mohamed Fadlalla and Ms. Shamla Gounden for their help with the technical aspects as well as their encouragement throughout this study. I also thank my brother in law Mojtaba Darestani Farahani, for his encouragements.

My special thanks go to Mohammad Hassan Alapour (my father in law) for his financial and emotional support and encouragements. I would like to extend my sincere thanks to Mrs. Fattaneh Dorri (my mother in law) and Pouya Alapour (my brother in law) for their supports and encouragement during these years.

At the end and more importantly, I am so grateful to my wife Saba Alapour for her countless encouragement and consistent support and all sacrifices that she has made for me during this study. The accomplishment of this degree was difficult without her. She had many sleepless nights in the lab to accompany me and keep me focused on my research. I believe that I am blessed with having a kind, supportive, strong and respectful wife.

I sing endless praises to God for allowing me to see the end of this, He is forever faithful, loving and gracious, He is a friend that sticks closer than a brother and His name is worthy to be praised.

List of abbreviations

ALD	Atomic Layer Deposition
BET	Brunauer, Emmett and Teller-surface area measurements
C:O ratio	Carbon to oxygen ratio
DH	Dehydrogenation
DF-STEM	Dark Field-Scanning Transmission Electron Microscopy
FID	Flame Ionization Detector
GC	Gas Chromatography
GHSV	Gas Hourly Space Velocity
HVD	High-Valence Dopant
HR-TEM	High Resolution-Transmission Electron Microscopy
ICP-OES	Inductively Coupled Plasma-Optical Emission Spectroscopy
ID	Internal Diameter
ILCS	Impregnated Layer Combustion Synthesis
IR	Infra-Red
LHSV	Liquid Hourly Space Velocity
LVD	Low-Valence Dopant
MS	Mass Spectroscopy
MvK	Mars and van Kervlen.
ODH	Oxidative Dehydrogenation
OMA	Ordered Mesoporous Alumina
PXRD	Powder X-Ray Diffraction
Ref	Reference
RWGS	Reverse Water Gas Shift

SCS	Solution Combustion Synthesis
SEM	Scanning Electron Microscopy
SGCS	Sol-Gel auto Combustion Synthesis
SHS	Self-propagating High temperature Synthesis
SWI	Second Wave Impregnation
SSITKA	Steady-State Isotopic Transient Kinetic Analysis
TCD	Thermal Conductivity Detector
TEM	Transmission Electron Microscopy
TGA	Thermal Gravimetric Analysis
TPD	Temperature Programmed Desorption
TPO	Temperature Programmed Oxidation
TPR	Temperature programmed reduction
UHP	Ultra High Purity
UMxD	Urea Matrix Drying
UV-DRS	Ultraviolet-Diffuse Reflectance Spectroscopy
UV/VIS	Ultraviolet/Visible
XRD	X-Ray Diffraction

Eq. 1

$$\text{Conversion} = \frac{mole\ of\ feed\ in - mole\ of\ feed\ out}{mole\ of\ feed\ in} \times 100$$

Eq. 2

$$\text{Selectivity} = \frac{moles\ of\ carbon\ in\ selected\ product}{Total\ moles\ of\ carbon\ in\ all\ products} \times 100$$

Eq. 3

$$\text{Yield} = \frac{Selectivity\% \times Conversion\%}{100}$$

Chapter one

Introduction

1.1) Background

Nickel has been used extensively in metal based catalysis. It is the fourth most abundant transitional metal on earth and its price is ca. 1/5000 of the price of the gold [1]. The platinum-group metals are amongst the most studied metals. Their low availability, as well as high cost, has limited their applications for large scale processes. Therefore, nickel has gained considerable attention due to its electronic similarity to Pt and Pd, which makes it able to participate in many catalytic reactions [2-4]. In addition, nickel has a high alloying efficiency with all noble and transition metals in different mass ratios that provides a tool for the preparation of versatile catalysts for different applications [1]. Its first application, as a hydrogenation catalyst, led to a Nobel prize in chemistry in 1912. Thereafter, nickel found its place as an active metal catalyst, in particular in hydrocarbon reforming [5-7] and hydrogenation reactions [1]. Nickel can also be used in other catalytic reactions, such as the oxidative dehydrogenation of paraffins [8, 9] and the production of fertilizers [10]. It has also numerous non-catalysis applications, such as in super capacitors, lithium-ion batteries, electrochromic devices, new-generation nano-devices and gas sensors [11-16]. However, pure nickel does not seem to be able to meet the selectivity, activity and stability requirements for wide commercial application of this transitional metal in many industries and requires further modifications [1]. A few general characteristics of nickel are shown in **Figure 1.1**.

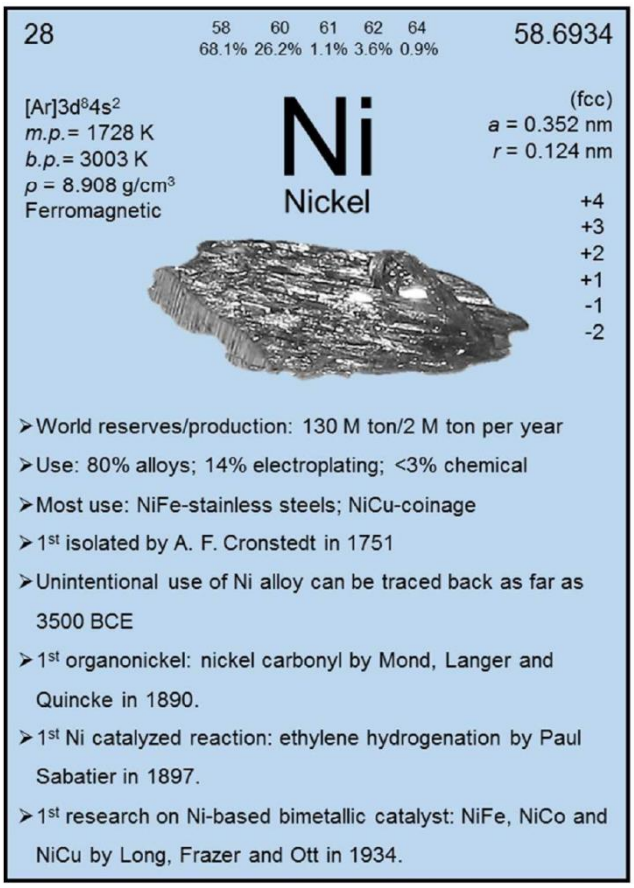

Figure 1.1 The historical background, physical properties and uses of nickel are shown in above fact sheet. Reproduced with permission from ref. 1. Copyright 2016 Royal Society of Chemistry.

1.2) Combustion synthesis of metal oxides

There are different procedures for the synthesis of nickel oxides [17-36]. Amongst them, solution combustion synthesis (SCS) is a relatively new technique that is being used to synthesise metal oxides [35, 36]. This method was first introduced by Kingsley and Patil [37] and has gained considerable attention in recent years (**Figure 1.2**) due to advantages such as easy synthesis, use of inexpensive precursors and providing nano-sized materials with high thermal stability [38-41].

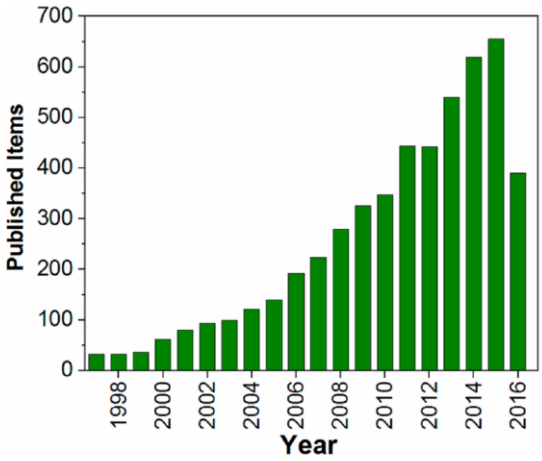

Figure 1.2 Published articles in each year based on the Web of Science database until August 2016. The used keywords were (1) Solution Combustion and (2) Sol-gel Combustion. Reproduced with permission from ref 38. Copyright 2016 American Chemical Society.

The use of an organic fuel is the main characteristic of the SCS, which makes it a self-propagating reaction at the flash point temperature of the used fuel (**Figure 1.3, a**). These fuels act as reducing and, sometimes, chelating agents [42] in the SCS, besides providing the heat of the reaction. In addition, the amount of used water in the solution combustion synthesis has been shown to be highly influential (**Figure 1.3, b**) [42].

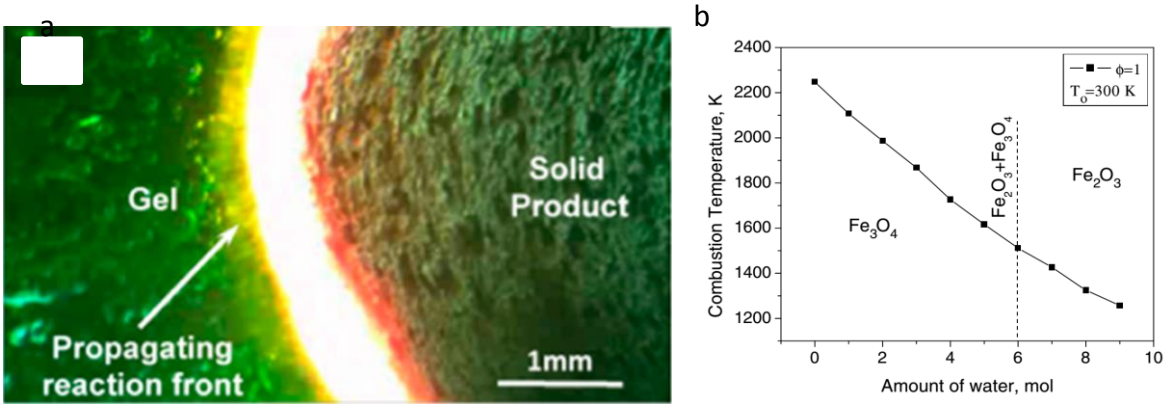

Figure 1.3 a) SCS of nickel oxide using glycine as a fuel. b) Effect of water concentration on the combustion temperature. Panel (a) is reproduced with permission from ref 36. Copyright 2013 American Chemical Society. Panel b is reproduced from ref 42. Copyright 2007 Elsevier.

Each fuel has its own characteristics, such as oxygen/carbon ratio, heat of combustion, decomposition temperature and reducing capability (**Table 1.1**) [43, 44]. Therefore, it can be stated that the used fuel can act as heat generator, reducing and complexing agents, based on the used precursors. The alteration of the aforementioned important parameters seems to have direct impacts on the physicochemical properties of the synthesised materials [38].

Table 1.1 a) Oxygen/Carbon ratio in total combustion reaction versus reducing valency of different organic fuels. [Inset: standard enthalpy of combustion reaction versus fuel reducing valency], b) some properties of common fuels used in combustion synthesis. The figures are reproduced with permission from ref. 43. Copyright 2013 Elsevier. The shown data in Table was obtained from ref 44.

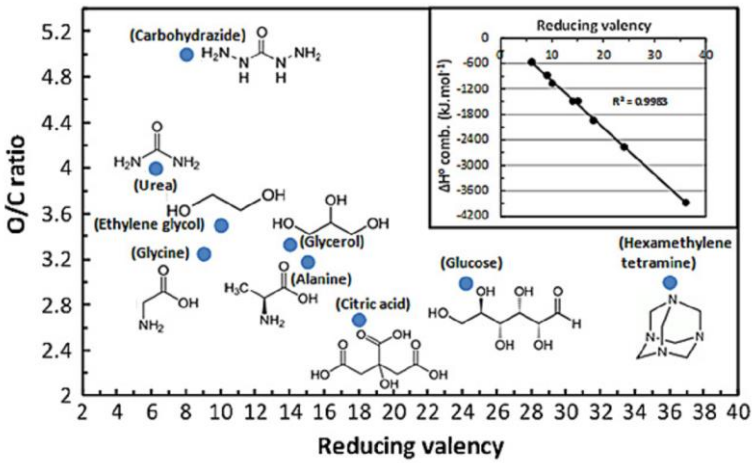

Properties	**Organic fuels**				
Name	**Alanine**	**Glycine**	**Carbohydrazide**	**Urea**	**Citric**
Molecular weight (g.mol^{-1})	80.1	90.1	75.1	60.1	192.1
Heat of combustion (KJ.g^{-1})	18.2	13.0	12.6	10.5	10.2
Decomposition temperature (°C)	314	262	153	135	175

Generally, the increase of fuel/oxidizer ratio results in higher surface area metal oxides due to the release of larger volumes of gases during the combustion synthesis [42]. Furthermore, a

study by Varma and co-workers showed different phases of iron oxides can be formed according to the amount and type of fuels used during the combustion synthesis, which was related at the end to the generated heat, as well as the chelating capability of the used fuels [45].

It is well discussed that the type of the fuel and water concentration can also influence the final concentration of the defect sites, which are involved in catalysis [46]. The engineering of these defect sites is known to modify the redox properties of the materials and seems to be a strong tool for enhancing the catalytic performance in different applications [38, 46]. In addition, Nagaveni *et al.* showed that SCS can be beneficial in terms of modifying the surface acid-base properties [47]. Besides all of the mentioned advantages, combustion techniques are widely used in the synthesis of doped metal oxides with foreign elements, which have made them very attractive for materials preparation for different applications [38, 48]. However, these techniques are also used for the preparation of supported materials [44].

1.2.1) Doped metal oxides

The substitution of dopant atoms in the host lattice of another metal oxide, even in small concentration, can strongly alter the properties of the host oxides, such as transport and electronic properties. It can also change the morphology and lower the phase transition temperature [49]. However, it still remains a challenge to prove (1) the synthesis of a true homogenously "doped" catalyst, and (2) that it is the doped phase that results in the observed catalytic activity [49].

Lanthanum is a low-valence dopant (LVD) for CeO_2, since lanthanum in La_2O_3 has a lower oxidation state than Ce in CeO_2, while lanthanum is a high-valence dopant (HVD) for Ca_2O

following the same principles [49]. LVDs in reducible metal oxides were found to create oxygen vacancies in the lattice of the host oxides. These oxygen vacancies are believed to enhance the activity of oxidation catalysts via the Mars-van Krevelen (MvK) mechanism and to lower the reduction temperature of the host oxides. In contrast to what is explained for LVDs, HVDs are known to reduce the number of oxygen vacancies and create Lewis base sites, which are also applicable in catalytic applications [49]. However, there are some variations from this phenomenon, where the host lattice is of a metal with various common oxidation stations such as vanadium, molybdenum and in some cases nickel [49]. Furthermore, there is considerable uncertainty about substitution in bimetallic mixed oxides, such as spinel and perovskite, since not much data is available for these materials.

Doped nickel oxide is well studied and has been used for the oxidative dehydrogenation (ODH) of ethane and propane. Ti, Ta, W, Zr, Ce, Mo, Sn, Mg, Li, Al, Ga, P and Nb have been studied as dopants in the lattice of NiO [8, 9, 50-69]. However, more focus has been on niobium doped nickel oxide due to its extraordinary performance in the ODH of ethane [9, 52, 56, 60, 61, 64, 67-69]. The NiO has a high concentration of non-stoichiometric oxygen species on the surface [9, 61]. Introduction of Nb seems to reduce the concentration of these species, which are responsible for direct combustion of ethane to CO_2 [9, 61].

A detailed introduction to ODH and common hypotheses of the ODH of paraffin molecules will be discussed in the following sections [9, 61].

1.2.2) Supported metal oxides

Generally bulk metal oxides have low surface areas and large crystallite sizes. Furthermore, these materials as catalysts present low activity and tend to deactivate rapidly due to sintering [70]. These disadvantages can be eliminated by using a suitable support. Widely used supports are generally refractory oxides such as Al_2O_3, SiO_2 and TiO_2 [71]. These materials have high surface area, porosity, mechanical and thermal stability with various pore sizes, and these are known mostly as chemically inert materials [71]. Carbon, zeolite, ordered-mesoporous materials and metal organic frameworks are also gaining more attentions as supports [72].

Precipitation and impregnation are two commercially used synthetic techniques in industry for preparation of supported metal oxides [71]. Both of these methods use the metal precursors (active metal), in most cases an inorganic salt, as a starting point to be deposited onto the support [71]. In precipitation techniques, the growth of metal particles is initiated from a supersaturated solution of the used precursor. The support can form *in situ* (coprecipitation) or can be added to the active metal precursor as a metal oxide (deposition precipitation) (**Scheme 1.1**) [71].

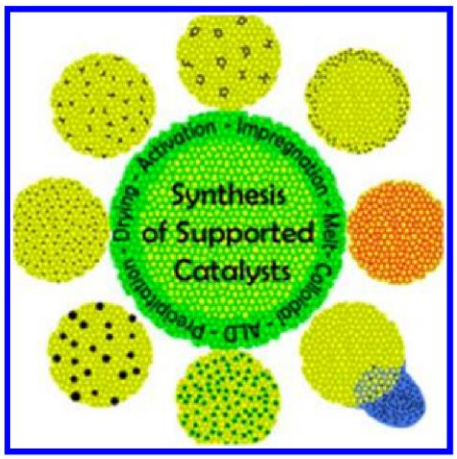

Scheme 1.1 Different techniques for synthesis of supported materials. Reproduced with permission from ref. 71. Copyright 2015 American Chemical Society.

The impregnation "family" includes ion adsorption, ion exchange, impregnation-drying, incipient wetness, melt infiltration, the colloidal route and atomic layer deposition (ALD) (**Scheme 1.1**). Ion adsorption is normally used for the synthesis of supported precious metals, where the precursor molecules selectively adsorb on a specific surface functionally [71]. A similar process occurs in ion exchange, where adsorption takes place through the exchange of ions instead of adsorption on groups and this is normally applied for zeolite supports [71]. The impregnation-drying method is used when a high loading of metal precursor is required. In this method, the washing steps are skipped and the mixture of precursor solution and used support is directly dried (all used precursor can be loaded using this technique) [71]. In incipient wetness impregnation only the pores of the supports are filled with precursor solution, to hinder the deposition on the external surface grain of the supports and also to limit waste. Melt infiltration is only applicable for precursors with low boiling points, where those are melted and directly contacted with the supports, such that capillary action forces adsorb the molten precursors into the pores [71]. Particles can also be formed in solution in the case of the colloidal route and controlled, using stabilizing agents or ligands, after which the formed particles are deposited on the supports [71]. ALD is the loading of the metal precursor in the vapour phase, which is a self-limiting reaction. In this technique produced vapours of precursors pass through the supports and only interact with adsorptive sites and form an atomic layer on top of the support [71].

The SCS method can also be used for the synthesis of supported metal oxides. The urea-matrix drying (UMxD) method is a combination of the impregnation and combustion techniques (using urea as a fuel) [44, 73, 74]. The dehydration of a mixture of metal precursor and oxidic support results in a slurry solution, which will be combusted at certain

temperatures [44, 73, 74]. Furthermore, this method is also applicable for using glycine as a fuel [75]. The surface impregnation combustion technique (combination of sol-gel and combustion) was used by Shi *et al.* to prepare the Co/SiO_2 [76, 77]. Impregnated layer combustion synthesis (ILCS) has been used in combination with SCS, which was called second wave impregnation (SWI) and used to synthesise Pd/CuO, Pd/ZnO and Pd/ZrO_2 materials [78]. However, there are seldom reports of these combustion techniques for the synthesis of supported nickel oxides.

The interaction between the nickel and support varies, with the higher surface area supports optimizing the surface to bulk ratio (the surface that enhances the catalytic activity) and providing different synergies at the interface of the support for new functionalities [70]. Supported nickel oxide on different metal oxides with high surface area such as CeO_2 [79], TiO_2 [80] , SiO_2 [80-83], ZrO_2 [84] and γ-Al_2O_3 [81, 84-88] have been investigated [89]. However, γ-Al_2O_3 has been used more extensively as a support, since it provides a mixture of acidic and basic sites, high surface area, good mechanical strength, low cost and can undergo surface hydration and hydroxylation [90].

Synthesis of NiO/Al_2O_3

There are different procedures for the synthesis of supported nickel oxide catalysts. Co-precipitation, impregnation and physical mixing are the most common methods [91]. However, the aforementioned preparation techniques can result in catalysts which mostly suffer from low activity at low temperature (usually not the case for Ni) and fast deactivation at higher temperatures [92]. To improve the catalytic activity of supported nickel oxide and diminish its drawbacks, solution combustion synthesis (SCS) may be an efficient method for the production of this catalyst.

Dong *et al.* reported the synthesis of nanosheet NiO on alumina tubes using the SCS and ethylene glycol as a fuel (**Figure 1.4**) [93]. Zhao *et al.* in 2012 reported the synthesis of supported nickel oxide on γ-alumina with a trace amount of the $NiAl_2O_4$ phase via SCS [94]. The use of inexpensive precursors in a large-scale synthesis in a short time, providing porous materials, are the advantages of this technique [39-41]. Subsequently, Zeng *et al.* synthesised a catalysts free from the $NiAl_2O_4$ spinel on alumina via modified SCS, where they utilized TiO_2 as a dopant [91]. However, the synthesis of this catalyst via combustion techniques in the absence of any dopant seems to require more investigation.

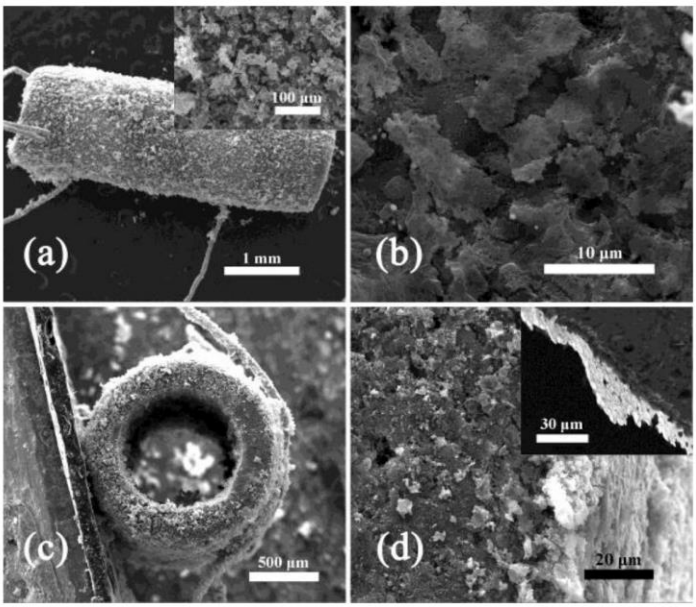

Figure 1.4 (a) and (b) are the overall and typical SEM images of self-grown NiO nanosheets (after SCS) on the alumina tube (the inset in (a) shows the low magnification image of NiO); (c) and (d) are the overall and representative cross-sectional images of the NiO gas sensor (the inset in (d) shows the High-magnification cross-section image of the NiO sensor). Reproduced with permission from ref. 93. Copyright 2015 Royal Society of Chemistry.

1.3) $NiAl_2O_4$ spinel

$NiAl_2O_4$ is a member of the spinel family with a general formula of AB_2O_4 and is known to have a magnetoplumbite like structure [95-97]. Spinel has a cubic lattice with octahedral and tetrahedral sub-lattices (**Figure 1.5**). The normal spinel is formed from bivalent (A) and trivalent metals (B) with the ratio of one to two and those metals occupy the tetrahedral and octahedral sub-lattices, respectively. In an inverse spinel, metal (A) occupies the octahedral sites and half of (B) are placed in tetrahedral sites and generate the general formula of $(B)_{Tet}(AB)_{Oct}O_4$ [98]. However, the random spinel can also form, where A and B are distributed randomly in both sub-lattices [98]. $NiAl_2O_4$ can have different degrees of inversion based on the temperature used for the synthesis [99]. However, the formation of a pure polycrystalline phase of $NiAl_2O_4$ is thermodynamically difficult and requires high temperature (> 800 °C) and sufficient calcination time [25, 100, 101].

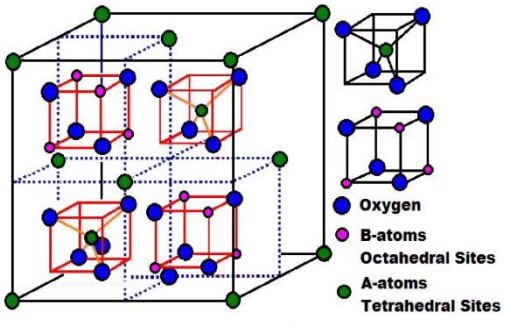

Figure 1.5 General structure of spinel. Reproduced with permission from ref. 113. Copyright 2015 Elsevier.

The $NiAl_2O_4$ spinel is a thermally stable ceramic and has many different catalytic applications in the partial oxidation of methane, methane (steam or dry) reforming [99], oxidative coupling of methane [102], diesel steam reforming [103, 104], tar reforming [105] and tetradecane reforming [106]. The common preparation techniques to synthesis $NiAl_2O_4$

are co-precipitation [97, 107], sol-gel [108], solid state reaction [25], the alkoxide method [109, 110], Pechini [99, 111] and combustion synthesis [112, 113].

The bulk structure of spinel can be reduced at relatively high temperature (~ 900 °C) and, therefore, this phase is viewed as an inactive phase in NiO/Al_2O_3 catalysis applications involving reduced nickel as active sites. However, there is controversy about the last mentioned claim. Nevertheless, $NiAl_2O_4$ can also offer some advantages such as high thermal stability, high metal dispersion and low sintering capability [114-117]. It is well established in the literature that available nickel on the surface of spinel can be reduced at lower temperatures than in the bulk $NiAl_2O_4$ and contributes in the applied catalytic reactions [114-117]. Furthermore, it has been recently proven that the surface of $NiAl_2O_4$ can have a regenerable redox capability that originates from the ability of ionic nickel in this material to migrate between the two sub-lattices [99].

1.4) Catalytic applications of NiO/Al_2O_3

As initially mentioned in this chapter, nickel has versatile catalytic applications. However, the hydrogenation of aldehydes and oxidative dehydrogenation (ODH) of paraffins are chosen as model reactions in this study, which includes catalysis over reduced and oxidized nickel supported on alumina. Therefore, an overview in this section will be provided on these two catalytic systems with specific attention on the nickel atoms (metallic and oxidized form) as active sites.

1.4.1) Aldehyde hydrogenation

Transformation of aldehydes and ketones to the corresponding alcohols has attracted much attention over the years, due to this reaction's laboratory and industrial importance [118,

119]. The produced alcohols can be used as solvents and as raw materials for plasticizers and detergents [120]. Different types of heterogeneous catalysts, containing different transition metals, are used in industry to convert aldehydes to alcohols, while nickel is used more extensively due to its lower cost [121]. Design and production of an active, selective and ecological catalyst with low cost, appear to be the focus at present [122].

The two primary reactions that are involved in the aldehyde hydrogenation are the hydrogenation of aldehyde to form the corresponding alcohol (the desired reaction) and the production of heavy hydrocarbons (the undesired reaction) [123]. The reduced metals were found to be active sites in the desired pathway and disassociation of hydrogen molecules to atomic hydrogen was the rate limiting step [123]. The undesired pathway was found to take place with a slower rate in the case of branched aldehydes and was found to be very substrate dependent and follow the trend:

Conversion of aldehyde:

propanal > hexanal > 2-ethyl-butanal > 2-methyl-pentanal.

Selectivity to heavy hydrocarbons:

propanal > hexanal > 2-methyl-pental > 2-ethyl-butanal.

However, these heavy products are known to form via acid-base catalysed reactions, shown in **Figure 1.6,** which can occur when Al_2O_3 is used as a support [123]. Furthermore, the amount of nickel loading, surface area and morphology, and reducibility of the supported nickel are important parameters that control the rate of hydrogenation and acid-base catalysed reactions, and can be engineered by using different synthetic procedures [123].

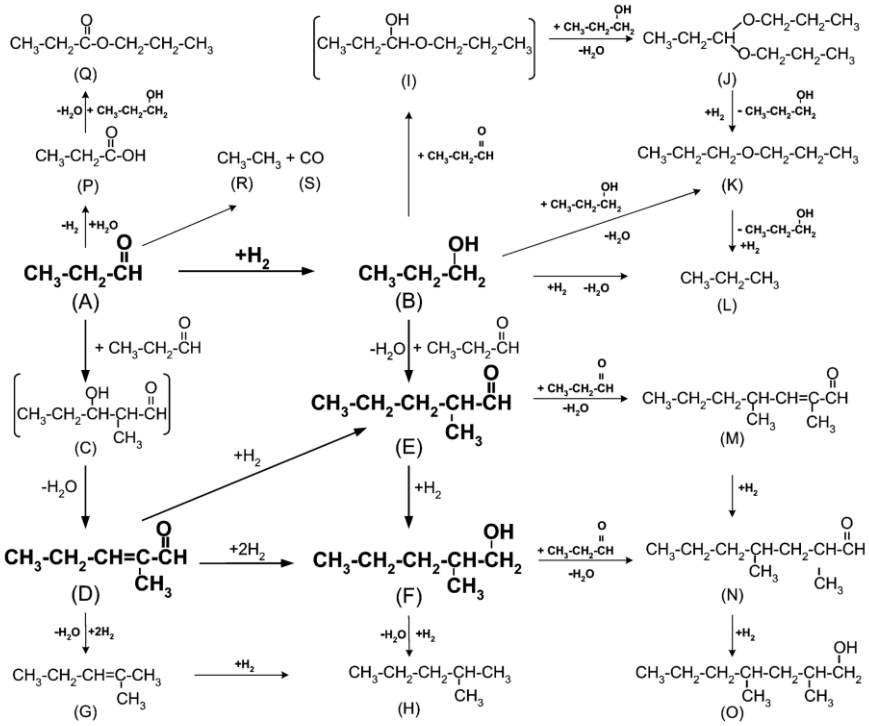

Figure 1.6 The proposed reaction pathways for propanal hydrogenation over NiMoS/ γ-Al_2O_3 catalyst. Reproduced with permission from ref. 123. Copyright 2005 Elsevier.

1.4.2) Oxidative dehydrogenation of paraffin

The manufacturing of liquid fuels from natural gas, coal or biomass created a pool of intermediated-length straight-chain alkanes [124]. Transformation of these low valued chemicals to industrially value-added products such as olefins, aromatics and oxygenates requires extensive research at the current stage [125]. The major applications of medium chain olefins are in the synthesis of alcohols or aldehydes, the production of synthetic lubricants and the production of copolymers with short chain olefins [126]. Short-chain hydrocarbons have been extensively investigated, with an abundance of reported patents and scholarly articles [124]. In contrast, the catalytic conversion of C_7-C_{12} to value added chemicals has not received considerable attention, possibly due to the challenges that accompany their transformation [125].

The dehydrogenation of small chain paraffins and their transformation to the corresponding olefins is a commercial catalytic process in oil refinery industries [127]. The abstraction of a hydrogen atom from the saturated hydrocarbons is the rate limiting step in this reaction and takes place on the reduced metal sites, as for the hydrogenation process [127]. The dehydrogenation (DH) process is normally very selective towards the desired olefin [127]. However, this reaction has some disadvantages, which motivate the scientific communities to look for better alternatives. Thus, this reaction is endothermic and high operating temperatures (> 550 °C) are required [127]. Coking can be counted as the second major disadvantage, which makes the presence of frequent regeneration cycles essential in industrial applications [127]. The third major disadvantage is the low equilibrium conversion, because the produced hydrogen from the dehydrogenation prevents the progress of the reaction and limits the conversion [127]. The equilibrium conversion further is highly dependent on the length of alkane precursor, as well as the temperature of the reaction, as it is shown in **Figure 1.7** [127].

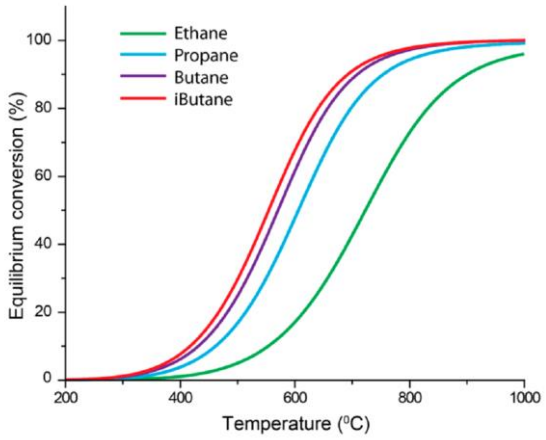

Figure 1.7 The equilibrium conversion in DH of C_2-C_4 paraffins to olefins at 1 bar. Reproduced with permission from ref. 127. Copyright 2014 American Chemical Society.

Oxidative dehydrogenation (ODH) of paraffins seems to be a better alternative than the DH process. This reaction is an exothermic reaction where the equilibrium conversion problem is

eliminated (based on the amount of used oxidant) by the reverse water gas shift reaction (RWGS) through the combustion of the produced hydrogen atoms and subsequent water formation [128]. Metal oxides are known to be the active sites for this reaction [128]. However, the high selectivity towards undesired products like CO_x is the major drawback of this reaction, which is an obstacle for commercialization of this process. Also, the valuable hydrogen is combusted. The nucleophilic oxygen species $(O^{2-})_{latt.}$ (originated from the lattice of metal oxide) are believed to be responsible for selective ODH, which results in the desired products. In contrast, the electrophilic oxygen species (O_2^-, O_2^{2-}, O^-) (formed on the surface of the metal oxide) are responsible for the combustion of the introduced paraffin and CO_x formation [128].

1.5) ODH of paraffins over NiO catalyst

NiO is known as one of the active metals in oxidative dehydrogenation that can operate effectively at relatively low temperature (~ 400 °C). Heracleous and Lemonidou, in 2006, showed that NiO has a high concentration of non-stoichiometric (electrophilic) oxygen species on the surface, which directs the reaction in the undesired direction of high formation of CO_x [9]. Their studies also showed that the introduction of a small amount of Nb in the lattice of NiO could significantly diminish the population of these electrophilic species on the surface and enhance the redox nature of NiO, which lead to a significant enhancement of catalytic performance as it is shown in **Figure 1.8** [9, 61]. They also proved their hypothesis, using transient and steady-state isotopic transient kinetic analysis (SSITKA) with isotopic $^{18}O_2$ [61].

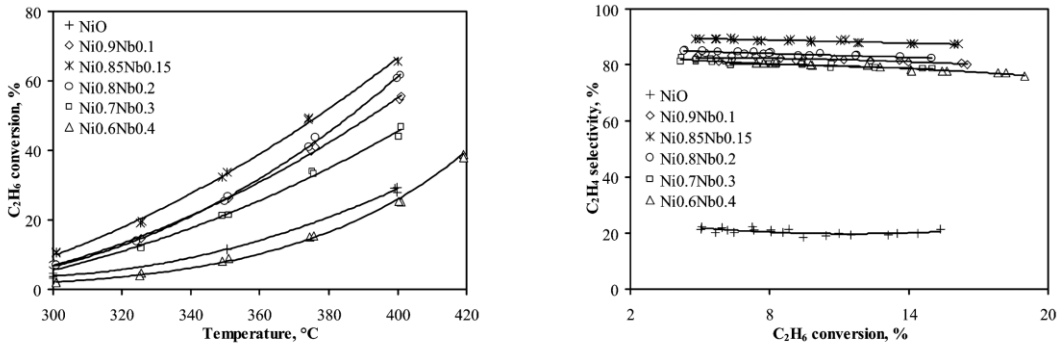

Figure 1.8 (a) Ethane conversion versus temperature (Reaction conditions: *W/F* = 0.54 g s/cm^3, C_2H_6/O_2 = 1/1), (b) Selectivity to ethene in different ethane conversion (Reaction conditions: T=350 °C, C_2H_6/O_2 = 1/1). Reproduced with permission from ref. 9. Copyright 2006 Elsevier.

However, the hypothesis of the original work by Heracleous and Lemonidou was questioned by Millet and co-workers in 2010 [64]. They could prove that added Nb acts as a surface modifier and blocks the accessible sites that contain electrophilic oxygen species [64]. They hypothesised that the O^- with low entropy (originated at high temperature on the surface) is responsible for the selective ODH of ethane and not the $(O^{-2})_{latt.}$ [64]. They used O_2-TPD-MS as a characterization technique and clearly showed the disappearance of O_2^- on the surface, when the Nb was introduced (**Figure 1.9**).

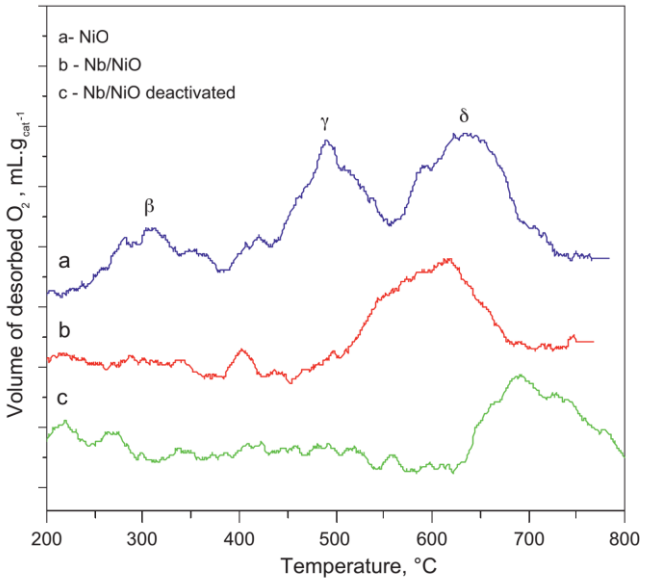

Figure 1.9 O_2-TPD-MS analysis of NiO, Nb/NiO and used Ni/NbO (β= O_2^- on the surface, γ and δ = O^- adsorbed on different site of catalysts). Reproduced with permission from ref. 64. Copyright 2006 Elsevier.

Furthermore, Metiu and co-workers conducted a computational analysis in 2013 to help the better understanding of the ODH of ethane over Nb doped NiO [69]. Based on the experimental facts, Nb ions are mobile at the used calcination temperature, and they will segregate on the surface due to their reaction with O_2 and lower the energy (entropy of mobile Nb on the surface) substantially. Therefore, NbO_2 (LVD) is only expected to substitute the surface Ni. The computational investigations showed that the NbO_2 ion in many ways acts as a LVD and activates the neighbouring and chemisorbed $(O^{-2})_{latt.}$, which results in a surface lattice $(O^{-2})_{latt.}$ involved in the MvK mechanism (**Figure 1.10**).

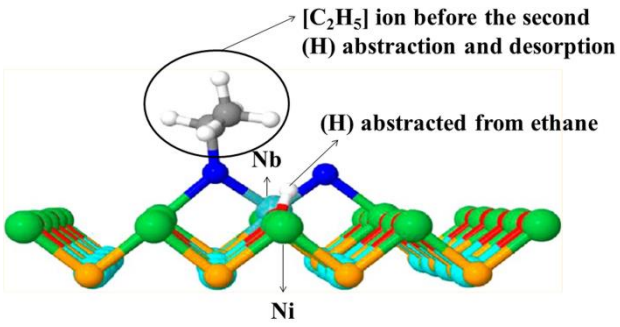

Figure 1.10 DFT computational analysis to probe the possible mechanism of ODH over Nb doped NiO. The hydrogen abstraction from ethane using an oxygen atom from the Nb-O-Ni bond on the surface of Nb doped NiO. Reproduced with permission from ref. 69. Copyright 2013 American Chemical Society.

Finally and very recently, Marcu, Lemonidou and co-workers tried to update their original hypothesis, constructed in 2006, with more detailed experimental analysis [129]. They used an unusual, but strong approach, to characterize the Nb doped NiO. The used an *in situ* electro-conductive analyser and probed the conductivity of these materials under different conditions including the exact reaction conditions [129]. NiO is a p-type semiconductor with many positive holes and Nb introduction was found to decrease the number of these positive holes and reduce the conductivity potential of the NiO. They showed that the $(O^{-2})_{latt}$ which originated from the surface of the catalyst can react with the positive holes and transform to $(O^{-})_{latt}$, which can do the desired ODH reaction [129]. Their experiment may partially explain the two difficult hypotheses, which were made by Millet, Metiu and co-workers [9, 61, 64, 69, 129]. Beside Nb, many other elements were doped or used as supports for NiO, and reports have discussd both the surface and bulk MvK mechanisms over these nickel based catalysts [8, 50, 51, 53, 54, 63, 65, 66].

Zhu *et al.* used "wet" sol-gel and "dry" solid state techniques to synthesise Ta doped NiO catalysts. They showed that the sol-gel resulted in a solid solution and a single phase Ta doped NiO catalyst, while the solid state technique resulted in the formation of a physical mixture of Ta_2O_5 and NiO [51]. The solid solution Ta doped NiO catalyst performed similar to Nb doped NiO [51]. However, the catalyst containing the physical mixture of Ta_2O_5 and NiO enhanced secondary combustion (ethene to CO_x) due to the slow desorption of the formed ethene when the Ta concentration was increased. A direct correlation between the concentration of Ta and the rate of catalyst deactivation was found for all catalysts prepared using both of the aforementioned techniques [51].

Solsona *et al.* synthesised Ni-W-O mixed metal oxides with various W loadings using an evaporation method [50]. They showed that Ni-O sites are active species in the ODH of ethane, and the reduction temperature of NiO shifted to higher temperature when the W loading was increased [50]. The W rich catalyst showed $NiWO_4$ and WO_3 as major phases. The ratio between these two phases was shown to be very important in the ODH performance over these catalysts [50]. However, a high concentration of W enhanced the secondary combustion of the formed ethene due to greater availability of Lewis acidic sites. The selectivity to ethene increased as W loading increased in Ni rich catalysts where NiO and WO_3 were determined as dominant phases. In addition, a weak influence of conversion on the selectivity to ethene was observed over theses catalysts. However, W seems to have a positive impact on the ODH performance over NiO using the same reasons mentioned in the discussion by Nb as Heracleous and Lemonidou (2006) [9, 61] discussed in pervious sections [50]. They also conducted time on line analyses over these catalysts and showed that the conversion decreases in the first 10 hours, but it becomes stable after that for 60 hours [54]. The application of these catalysts in the dehydrogenation of ethane resulted in the formation

of metallic nickel, methane and hydrogen with rapid coking [54]. However, regeneration could completely restore the catalysts [54].

The use of Sn as a promoter seems to improve the ODH (of ethane) performance significantly. The same improvement as for Nb introduction was observed when Sn was introduced into the lattice of NiO [66]. A very low loading of Sn has been shown to increase the surface area of NiO and decrease the crystallite sizes of the catalysts [66]. Sn seems to block the undesired sites of NiO in ODH, as was seen for Nb doped NiO, and minimizes the density of acidic sites that are responsible for the combustion of the formed ethene from the ODH of ethane [66].

The addition of Zr in the lattice of NiO is found to increase the cell parameter of the NiO and also increase the valance of Ni through an electron transfer via the Zr-O-Ni bridge linkage [53]. The authors used the same argument as Savova *et al.* [64], claiming that these two alterations resulted in a higher concentration of O^- (selective oxygen species) on the surface and suppression of O^-_2 (non-selective oxygen species) in the ODH of ethane [53].
Also, the use of phosphorous considerably improved the ODH of ethane over NiO catalysts [8]. The highly dispersed P on the surface of NiO seems to decrease both the concentration and mobility of O^- that are available on the surface lattice of NiO. These changes resulted in lower conversion and better selectivity to ethene (desired product) at the expense of total oxidation selectivity [8].

The increase of porosity in NiO based catalysts seems to enhance the ODH performance [63, 130]. Thus Ni-W-O supported on mesoporous alumina showed improvement in the ODH performance [63]. The use of mesoporous alumina resulted in well dispersed Ni-W-O with

small crystallite size, which contributed to the improved catalytic results over this catalyst when compared to the bulk counterpart [63]. Solsona *et al.* further conducted a study on the ODH of ethane over NiO supported on porous clay and showed that the use of this support improved the catalytic results [130]. This improvement was linked to a higher dispersion of NiO with modified reducibility, which hinders the oxidation of ethane to carbon oxides [130]. They also showed higher distortion of the NiO crystal lattice parameter which resulted in an enhanced selectivity to ethylene, which demonstrates the important role of particle morphology on the selectivity in this material [130]. Consequently, it seems that the application of NiO in the ODH of alkanes has potential, which requires more investigation.

1.6) Motivation for this study

The wide aforementioned application of nickel based materials as well as the interesting chemistry behind this transition metal encouraged the begin of this study. The hydrogenation of aldehydes (octanal in this study) and oxidative dehydrogenation of paraffins (*n*-octane in this study) as model reactions were mainly chosen for the following reasons. Firstly, the hydrogenation of aldehydes is an established commercial process, and the oxidative dehydrogenation of paraffins (in this study *n*-octane) has high potential of commercialization due to its numerous advantages over the traditional dehydrogenation processes. Secondly, the applications of these two model reactions allowed the investigation of the chemistry of nickel in both reduced and oxide forms. The use of different synthetic methods, characterisation techniques and catalytic systems allowed the probing of the NiO/Al_2O_3 based catalysts from the following aspects:

- The synthesis of NiO/Al_2O_3 catalysts with different physicochemical characteristics, such as crystallite size, porosity, phase composition, morphology, redox nature and acid-base sites.

- The role of nickel, involved in the lattice of $NiAl_2O_4$ spinel in both reductive and oxidative reactions.

- The effect of Nb doping in the lattice of $NiAl_2O_4$ spinel on the physicochemical characteristics of these materials, as well as its role in the oxidative activation of *n*-octane.

- The effect of coking, originated from the oxidative activation of *n*-octane over Nb doped $NiAl_2O_4$, on physicochemical characteristics of these catalysts.

- The synthesis of ordered mesoporous alumina and NiO/Al_2O_3 catalysts with different loadings of Nb_2O_5 as an additive.

- The influence of Nb addition on the "confinement effect" between the Al_2O_3 and NiO in materials with similar surface textures and morphologies.

- Application of $NiO\text{-}Nb_2O_5/Al_2O_3$ with ordered mesoporous structures in the oxidative activation of *n*-octane, with the aim of achieving new insight regarding the application of nickel based materials in this catalytic application.

1.7) References

[1] S. De, J. Zhang, R. Luque, N. Yan, Energy Environ. Sci., 9 (2016) 3314-3347.

[2] D. Li, I. Atake, T. Shishido, Y. Oumi, T. Sano, K. Takehira, J. Catal., 250 (2007) 299-312.

[3] D. Li, Y. Nakagawa, K. Tomishige, Appl. Catal., A, 408 (2011) 1-24.

[4] K. Nagaoka, A. Jentys, J.A. Lercher, J. Catal., 229 (2005) 185-196.

[5] C. Jiménez-González, M. Gil-Calvo, B. de Rivas, J.R. González-Velasco, J.I. Gutiérrez-Ortiz, R. López-Fonseca, Ind. Eng. Chem. Res., 55 (2016) 3920-3929.

[6] J.L. Rogers, M.C. Mangarella, A.D. D'Amico, J.R. Gallagher, M.R. Dutzer, E. Stavitski, J.T. Miller, C. Sievers, ACS Catal., 6 (2016) 5873-5886.

[7] B.D. Gould, X. Chen, J.W. Schwank, J. Catal., 250 (2007) 209-221.

[8] S.-B. Ivan, I. Popescu, I. Fechete, F. Garin, V.I. Parvulescu, I.-C. Marcu, Catal. Sci. Tech., 6 (2016) 6953-6964.

[9] E. Heracleous, A.A. Lemonidou, J. Catal., 237 (2006) 162-174.

[10] M. Cifrain, K.V. Kordesch, J. Power Sources, 127 (2004) 234-242.

[11] H.-Y. Wu, H.-W. Wang, Int. J. Electrochem. Sci, 7 (2012) 4405-4417.

[12] M. Ghosh, K. Biswas, A. Sundaresan, C.N.R. Rao, J. Mater. Chem., 16 (2006) 106-111.

[13] L.A. Saghatforoush, M. Hasanzadeh, S. Sanati, R. Mehdizadeh, Bull. Korean Chem. Soc., 33 (2012) 2613-2618.

[14] J.Y. Park, K.S. Ahn, Y.C. Nah, H.S. Shim, Y.E. Sung, J. Sol-Gel Sci. Technol., 31 (2004) 323-328.

[15] M.A. Shah, Nanoscale Res. Lett., 3 (2008) 255-259.

[16] H. Yang, Q. Tao, X. Zhang, A. Tang, J. Ouyang, J. Alloys Compd., 459 (2008) 98-102.

[17] P. Wu, J.H. Sun, Y.Y. Huang, G.F. Gu, D.G. Tong, Mater. Lett., 82 (2012) 191-194.

[18] W. Sun, L. Chen, S. Meng, Y. Wang, H. Li, Y. Han, N. Wei, Mater. Sci. Semicond. Process., 17 (2014) 129-133.

[19] F. Al-Hazmi, T. Al-Harbi, W.E. Mahmoud, Mater. Lett., 86 (2012) 28-30.

[20] W.D. Yu, X.M. Li, X.D. Gao, J. Cryst. Growth, 270 (2004) 92-97.

[21] C. Mahendiran, T. Maiyalagan, K. Scott, A. Gedanken, Mater. Chem. Phys., 128 (2011) 341-347.

[22] M. Salavati-Niasari, M. Entesari, Polyhedron, 33 (2012) 302-309.

[23] R. Bajpai, S. Roy, N. Koratkar, D.S. Misra, Carbon, 56 (2013) 56-63.

[24] Y. Li, M. Cai, J. Rogers, Y. Xu, W. Shen, Mater. Lett., 60 (2006) 750-753.

[25] L. Wu, Y. Wu, H. Wei, Y. Shi, C. Hu, Mater. Lett., 58 (2004) 2700-2703.

[26] S. Ni, T. Li, X. Lv, X. Yang, L. Zhang, Electrochim. Acta, 91 (2013) 267-274.

[27] S.P. Pati, B. Bhushan, A. Basumallick, S. Kumar, D. Das, Mater. Sci. Eng., B, 176 (2011) 1015-1020.

[28] N.G. Cho, I.-S. Hwang, H.-G. Kim, J.-H. Lee, I.-D. Kim, Sens. Actuators, B, 155 (2011) 366-371.

[29] G.J. Kim, X.-F. Guo, J. Phys. Chem. Solids, 71 (2010) 612-615.

[30] Y. Wu, R. Balakrishna, M.V. Reddy, A.S. Nair, B.V.R. Chowdari, S. Ramakrishna, J. Alloys Compd., 517 (2012) 69-74.

[31] G. Bai, H. Dai, J. Deng, Y. Liu, W. Qiu, Z. Zhao, X. Li, H. Yang, Chem. Eng. J., 219 (2013) 200-208.

[32] S. Ren, C. Yang, C. Sun, Y. Hui, Z. Dong, J. Wang, X. Su, Mater. Lett., 80 (2012) 23-25.

[33] S.-W. Choi, J.Y. Park, S.S. Kim, Mater. Chem. Phys., 127 (2011) 16-20.

[34] W.E. Mahmoud, T. Al-Harbi, Superlattices Microstruct., 50 (2011) 21-25.

[35] S. Balamurugan, A.J. Linda Philip, R.S. Vidya, JOSC, 29 (2016) 2207-2212.

[36] K.V. Manukyan, A. Cross, S. Roslyakov, S. Rouvimov, A.S. Rogachev, E.E. Wolf, A.S. Mukasyan, J. Phys. Chem. C, 117 (2013) 24417-24427.

[37] J.J. Kingsley, K.C. Patil, Mater. Lett., 6 (1988) 427-32.

[38] A. Varma, A.S. Mukasyan, A.S. Rogachev, K.V. Manukyan, Chem. Rev., 116 (2016) 14493-14583.

[39] A.S. Prakash, C. Shivakumara, M.S. Hegde, Mater. Sci. Eng., B, 139 (2007) 55-61.

[40] S. Sharma, Z. Hu, P. Zhang, E.W. McFarland, H. Metiu, J. Catal., 278 (2011) 297-309.

[41] S.K. Lathika Devi, K. Sudarsana Kumar, A. Balakrishnan, Mater. Lett., 65 (2011) 35-37.

[42] A.S. Mukasyan, P. Epstein, P. Dinka, Proc. Combust. Inst., 31 (2007) 1789-1795.

[43] C.-C. Hwang, T.-Y. Wu, J. Wan, J.-S. Tsai, Materials Science and Engineering: B, 111 (2004) 49-56.

[44] S.L. González-Cortés, F.E. Imbert, Appl. Catal., A, 452 (2013) 117-131.

[45] K. Deshpande, A. Mukasyan, A. Varma, Chem. Mater., 16 (2004) 4896-4904.

[46] C. Aliotta, L.F. Liotta, V. La Parola, A. Martorana, E.N.S. Muccillo, R. Muccillo, F. Deganello, Appl. Catal., B, 197 (2016) 14-22.

[47] K. Nagaveni, M.S. Hegde, N. Ravishankar, G.N. Subbanna, G. Madras, Langmuir, 20 (2004) 2900-2907.

[48] M.S. Hegde, G. Madras, K.C. Patil, Acc. Chem. Res., 42 (2009) 704-712.

[49] E.W. McFarland, H. Metiu, Chem. Rev., 113 (2013) 4391-4427.

[50] B. Solsona, J.M. López Nieto, P. Concepción, A. Dejoz, F. Ivars, M.I. Vázquez, J. Catal., 280 (2011) 28-39.

[51] H. Zhu, D.C. Rosenfeld, D.H. Anjum, S.S. Sangaru, Y. Saih, S. Ould-Chikh, J.-M. Basset, J. Catal., 329 (2015) 291-306.

[52] H. Zhu, S. Ould-Chikh, D.H. Anjum, M. Sun, G. Biausque, J.-M. Basset, V. Caps, J. Catal., 285 (2012) 292-303.

[53] Y. Wu, J. Gao, Y. He, T. Wu, Appl. Surf. Sci., 258 (2012) 4922-4928.

[54] S. Agouram, A. Dejoz, F. Ivars, I. Vázquez, J.M. López Nieto, B. Solsona, Fuel Process. Technol., 119 (2014) 105-113.

[55] M.O. Guerrero-Pérez, M.A. Bañares, Catal. Today, 142 (2009) 245-251.

[56] Z. Skoufa, E. Heracleous, A.A. Lemonidou, Catal. Today, 192 (2012) 169-176.

[57] B. Farin, C. Swalus, M. Devillers, E.M. Gaigneaux, Catal. Today, 203 (2013) 24-31.

[58] L. Wang, W. Chu, C. Jiang, Y. Liu, J. Wen, Z. Xie, J. Nat. Gas Chem., 21 (2012) 43-48.

[59] J.P. Bortolozzi, T. Weiss, L.B. Gutierrez, M.A. Ulla, Chem. Eng. J., 246 (2014) 343-352.

[60] J. Santander, E. López, A. Diez, M. Dennehy, M. Pedernera, G. Tonetto, Chem. Eng. J., 255 (2014) 185-194.

[61] E. Heracleous, A.A. Lemonidou, J. Catal., 237 (2006) 175-189.

[62] E. Heracleous, A. Delimitis, L. Nalbandian, A.A. Lemonidou, Appl. Catal., A, 325 (2007) 220-226.

[63] B. Solsona, F. Ivars, A. Dejoz, P. Concepción, M.I. Vázquez, J.M. López Nieto, Top. Catal., 52 (2009) 751-757.

[64] B. Savova, S. Loridant, D. Filkova, J.M.M. Millet, Appl. Catal., A, 390 (2010) 148-157.

[65] E. Heracleous, A.A. Lemonidou, J. Catal., 270 (2010) 67-75.

[66] B. Solsona, P. Concepción, B. Demicol, S. Hernández, J.J. Delgado, J.J. Calvino, J.M. López Nieto, J. Catal., 295 (2012) 104-114.

[67] A. Qiao, V.N. Kalevaru, J. Radnik, A. Martin, Catal. Today, 264 (2016) 144-151.

[68] F. Rubio-Marcos, E. Rojas, R. López-Medina, M.O. Guerrero-Pérez, M.A. Bañares, J.F. Fernandez, ChemCatChem, 3 (2011) 1637-1645.

[69] X. Sun, B. Li, H. Metiu, J. Phys. Chem. C, 117 (2013) 23597-23608.

[70] F. Zaera, ChemSusChem, 6 (2013) 1797-1820.

[71] P. Munnik, P.E. de Jongh, K.P. de Jong, Chem. Rev., 115 (2015) 6687-6718.

[72] A. Corma, H. García, F.X. Llabrés i Xamena, Chem. Rev., 110 (2010) 4606-4655.

[73] S.L. González-Cortés, T.-C. Xiao, P.M.F.J. Costa, B. Fontal, M.L.H. Green, Appl. Catal., A, 270 (2004) 209-222.

[74] S.L. González-Cortés, S.M.A. Rodulfo-Baechler, T. Xiao, M.L.H. Green, Catal. Lett., 111 (2006) 57-66.

[75] P. Dinka, A.S. Mukasyan, J. Phys. Chem. B, 109 (2005) 21627-21633.

[76] L. Shi, K. Tao, T. Kawabata, T. Shimamura, X.J. Zhang, N. Tsubaki, ACS Catal., 1 (2011) 1225-1233.

[77] L. Shi, Y. Jin, C. Xing, C. Zeng, T. Kawabata, K. Imai, K. Matsuda, Y. Tan, N. Tsubaki, Appl. Catal., A, 435–436 (2012) 217-224.

[78] A. Kumar, A.S. Mukasyan, E.E. Wolf, Appl. Catal., A, 372 (2010) 175-183.

[79] K. Shimura, K.-i. Shimizu, Green Chem., 14 (2012) 2983-2985.

[80] J. Rynkowski, D. Rajski, I. Szyszka, J.R. Grzechowiak, Catal. Today, 90 (2004) 159-166.

[81] S.R. Kirumakki, B.G. Shpeizer, G.V. Sagar, K.V.R. Chary, A. Clearfield, J. Catal., 242 (2006) 319-331.

[82] J.C. Park, H.J. Lee, J.Y. Kim, K.H. Park, H. Song, J. Phys. Chem. C, 114 (2010) 6381-6388.

[83] A. Ungureanu, B. Dragoi, A. Chirieac, C. Ciotonea, S. Royer, D. Duprez, A.S. Mamede, E. Dumitriu, ACS Appl. Mater. Interfaces, 5 (2013) 3010-3025.

[84] S.A. Nikolaev, D.A. Pichugina, D.F. Mukhamedzyanova, Gold Bull. (Berlin, Ger.), 45 (2012) 221-231.

[85] M. Kang, M.W. Song, T.W. Kim, K.L. Kim, Can. J. Chem. Eng., 80 (2002) 63-70.

[86] X. Meng, H. Cheng, Y. Akiyama, Y. Hao, W. Qiao, Y. Yu, F. Zhao, S.-i. Fujita, M. Arai, J. Catal., 264 (2009) 1-10.

[87] L. Zhang, X. Shu, L. Zhang, Asian J. Chem., 25 (2013) 5071-5075.

[88] X. Wang, H. Yu, D. Hua, S. Zhou, J. Phys. Chem. C, 117 (2013) 7294-7302.

[89] A. Saadi, R. Merabti, Z. Rassoul, M.M. Bettahar, J. Mol. Catal. A: Chem., 253 (2006) 79-85.

[90] G.C. Chase, M.P. Espe, E.A. Evans, R.D. Ramsier, D.H. Reneker, R.W. Tuttle, J. Rapp, Manufacture of metal oxide fibers and nanofibers for decomposing toxic chemicals, University of Akron, USA . 2008, p. 78pp.

[91] Y. Zeng, H. Ma, H. Zhang, W. Ying, D. Fang, Fuel, 137 (2014) 155-163.

[92] R.J. White, R. Luque, V.L. Budarin, J.H. Clark, D.J. Macquarrie, Chem. Soc. Rev., 38 (2009) 481-494.

[93] C. Dong, X. Xiao, G. Chen, H. Guan, Y. Wang, I. Djerdj, RSC Adv., 5 (2015) 4880-4885.

[94] A. Zhao, W. Ying, H. Zhang, H. Ma, D. Fang, Catal. Commun., 17 (2012) 34-38.

[95] R. Collongues, D. Gourier, A. Kahn-Harari, A.M. Lejus, J. Thery, D. Vivien, Annu. Rev. Mater. Sci., 20 (1990) 51-82.

[96] W. Chu, W. Yang, L. Lin, Appl. Catal., A, 235 (2002) 39-45.

[97] T.H. Gardner, J.J. Spivey, E.L. Kugler, A. Campos, J.C. Hissam, A.D. Roy, J. Phys. Chem. C, 114 (2010) 7888-7894.

[98] Z. Boukha, C. Jiménez-González, B. de Rivas, J.R. González-Velasco, J.I. Gutiérrez-Ortiz, R. López-Fonseca, Appl. Catal., B, 158–159 (2014) 190-201.

[99] J.L. Rogers, M.C. Mangarella, A.D. D'Amico, J.R. Gallagher, M.R. Dutzer, E. Stavitski, J.T. Miller, C. Sievers, ACS Catal., 6 (2016) 5873-5886.

[100] H.S.C. O'Neill, W.A. Dollase, C.R. Ross, Phys. Chem. Miner., 18 (1991) 302-319.

[101] C.O. Arean, M.L.R. Martinez, A.M. Arjona, Mater. Chem. Phys., 8 (1983) 443-450.

[102] Y. Kathiraser, W. Thitsartarn, K. Sutthiumporn, S. Kawi, J. Phys. Chem. C, 117 (2013) 8120-8130.

[103] I.E. Achouri, N. Abatzoglou, C. Fauteux-Lefebvre, N. Braidy, Catal. Today, 207 (2013) 13-20.

[104] C. Fauteux-Lefebvre, N. Abatzoglou, N. Braidy, I.E. Achouri, J. Power Sources, 196 (2011) 7673-7680.

[105] D. Li, M. Koike, L. Wang, Y. Nakagawa, Y. Xu, K. Tomishige, ChemSusChem, 7 (2014) 510-522.

[106] T.H. Gardner, D. Shekhawat, D.A. Berry, M.W. Smith, M. Salazar, E.L. Kugler, Appl. Catal., A, 323 (2007) 1-8.

[107] B. Dou, B. Jiang, Y. Song, C. Zhang, C. Wang, H. Chen, B. Du, Y. Xu, Fuel, 166 (2016) 340-346.

[108] N. Salhi, C. Petit, A. Kiennemann, Stud. Surf. Sci. Catal., 174B (2008) 1335-1338.

[109] K. Zhang, G. Zhou, J. Li, T. Cheng, Catal. Commun., 10 (2009) 1816-1820.

[110] M. Machida, K. Eguchi, H. Arai, J. Catal., 120 (1989) 377-386.

[111] J. Deng, M. Cai, W. Sun, X. Liao, W. Chu, X.S. Zhao, ChemSusChem, 6 (2013) 2061-2065.

[112] N.F.P. Ribeiro, R.C.R. Neto, S.F. Moya, M.M.V.M. Souza, M. Schmal, Int. J. Hydrogen Energy, 35 (2010) 11725-11732.

[113] G. Kumar, J. Shah, R.K. Kotnala, V.P. Singh, Sarveena, G. Garg, S.E. Shirsath, K.M. Batoo, M. Singh, Mater. Res. Bull., 63 (2015) 216-225.

[114] I.A.P.S. Murthy, C.S. Swamy, J. Mater. Sci., 28 (1993) 1194-8.

[115] H. Muroyama, R. Nakase, T. Matsui, K. Eguchi, Int. J. Hydrogen Energy, 35 (2010) 1575-1581.

[116] N. Salhi, A. Boulahouache, C. Petit, A. Kiennemann, C. Rabia, Int. J. Hydrogen Energy, 36 (2011) 11433-11439.

[117] R. Lopez-Fonseca, C. Jimenez-Gonzalez, B. de Rivas, J.I. Gutierrez-Ortiz, Appl. Catal., A, 437-438 (2012) 53-62.

[118] J.W. Yang, M.T.H. Fonseca, B. List, Angew. Chem. Int. Ed., 43 (2004) 6660-6662.

[119] B. Chen, U. Dingerdissen, J.G.E. Krauter, H. Rotgerink, K. Mobus, D.J. Ostgard, P. Panster, T.H. Riermeier, S. Seebald, T. Tacke, H. Trauthwein, Appl. Catal., A, 280 (2005) 17-46.

[120] L. Diab, T. Šmejkal, J. Geier, B. Breit, Angew. Chem., 121 (2009) 8166-8170.

[121] G.M. Psofogiannakis, G.E. Froudakis, Chem. Commun., 47 (2011) 7933-7943.

[122] K.R. Kahsar, S. Johnson, D.K. Schwartz, J.W. Medlin, Top. Catal., 57 (2014) 1505-1511.

[123] X. Wang, R.Y. Saleh, U.S. Ozkan, J. Catal., 231 (2005) 20-32.

[124] S. Pradhan, J.K. Bartley, D. Bethell, A.F. Carley, M. Conte, S. Golunski, M.P. House, R.L. Jenkins, R. Lloyd, G.J. Hutchings, Nat Chem, 4 (2012) 134-139.

[125] B. Pillay, M.R. Mathebula, H.B. Friedrich, Appl. Catal., A, 361 (2009) 57-64.

[126] E. Romera, C. Lamotte, P. Bodart, Process for the purification of medium-chain olefins, Fina Research S.A., 1998.

[127] J.J.H.B. Sattler, J. Ruiz-Martinez, E. Santillan-Jimenez, B.M. Weckhuysen, Chem. Rev., 114 (2014) 10613-10653.

[128] C.A. Gärtner, A.C. van Veen, J.A. Lercher, ChemCatChem, 5 (2013) 3196-3217.

[129] I. Popescu, Z. Skoufa, E. Heracleous, A. Lemonidou, I.-C. Marcu, Phys. Chem. Chem. Phys., 17 (2015) 8138-8147.

[130] B. Solsona, P. Concepción, J.L. Nieto, A. Dejoz, J. Cecilia, S. Agouram, M. Soriano, V. Torres, J. Jiménez-Jiménez, E.R. Castellón, Catal. Sci. Tech., 6 (2016) 3419-3429.

Chapter two

A comparative study of NiO/Al_2O_3 catalysts prepared by different combustion techniques for octanal hydrogenation

Abstract

Four catalysts with the molar ratio of Ni : Al (1 : 2) were prepared by solution combustion synthesis (SCS) and sol-gel auto combustion synthesis (SGCS) techniques. Two fuels (urea and oxalyldihydrazide) with distinct O/C (oxygen/carbon) ratios and chelating capability were chosen for investigating the effect of the fuel on the syntheses of these catalysts. All catalysts were fully characterized by PXRD, ICP-OES, TEM, H_2-TPR, pyridine IR, H_2-chemisorption and nitrogen physisorption. Pure NiO/Al_2O_3 (free of spinel) was achieved by application of SGCS and urea as a fuel. Thus, catalysts prepared by urea as a fuel showed high activity for hydrogenation of octanal even under moderate conditions (110 °C). Optimisation showed that the catalyst prepared via SCS using oxalyldihydrazide as a fuel gave the best comparative aldehyde conversion and alcohol selectivity (98 % and 97 %, respectively) albeit at a higher temperature of 150 °C. The catalysts with NiAl2O4 as the dominant phase presented the lowest acidity, likely due to the non-availability of acidic sites of alumina via formation of the spinel, thus making these catalysts highly selective and also offering a slow release of fresh Ni sites.

Keywords: NiO/Al_2O_3; $NiAl_2O_4$; solution combustion; sol-gel auto combustion; hydrogenation.

2.1) Introduction

Solution combustion synthesis (SCS) was shown for the first time by Kingsley and Patil [1]. This technique can be categorized as one member of the self-propagating high temperature synthesis (SHS) family [2]. It has advantages such as the use of inexpensive precursors, large-scale synthesis in a shorter preparation time, providing porous materials and high thermal stability [3-5]. SCS requires a saturated solution of precursors with an organic fuel, which normally combusts close to the ignition temperature of the applied fuel [6]. Sol-Gel Auto Combustion Synthesis (SGCS) is very similar to SCS, except for the removal of water that results in the formation of a gel (slurry) before combustion. This difference in preparation between the two methods affects the final appearance and composition of the materials and possibly their catalytic performance [7]. Both of these techniques are widely used for synthesis of bulk and doped metal oxides [6, 8-13]. Furthermore, it has been shown that the choice of fuel can play a crucial role during the synthesis of the heterogeneous materials prepared [8]. The O/C (oxygen/carbon) ratio and chelating capability of the fuel are two main factors that need to be taken into consideration during the synthesis [6].

The SCS method has also been applied for synthesis of supported materials [6]. The urea-matrix drying technique (UMxD) is a type of SCS merged with a wet impregnation [14-16]. This technique follows the basic principles of combustion synthesis with the only difference being the addition of the oxidic support in the solution and subsequent formation of the slurry. The solution is then combusted, providing the final supported metal oxides [14-16]. Dinka *et al.* demonstrated the same technique using glycine as a fuel [17]. Shi *et al.* reported the synthesis of Co/SiO_2 catalysts by using a surface impregnation combustion technique, which can be considered as a combination of sol-gel combustion and wet impregnation [18, 19]. Kumar *et al.* used Impregnated Layer Combustion Synthesis (ILCS) in combination

with SCS, which was called Second Wave Impregnation (SWI) to synthesise Pd/CuO, Pd/ZnO and Pd/ZrO_2 materials [20]. It may be that supported materials prepared via combustion techniques offer potential advantages for important catalytic applications [3-5].

Transformation of aldehydes (largely produced via hydroformylation) to their corresponding alcohols has attracted much attention over the years, due to this reaction's laboratory and industrial importance [21-23]. The design of active, selective and ecological catalysts with low cost appears to be the focus at present [24]. Nickel oxide has been employed extensively due to its relatively lower cost [25]. Furthermore, supported nickel oxide on different metal oxides with high surface area has been investigated [25-35]. Normally, the interaction between the nickel and support varies, with the higher surface area supports optimizing the surface to bulk ratio (the surface that enhances the catalytic activity) and providing different synergies at the interface of the support [36]. γ-Al_2O_3 has been used more extensively as support, since it provides a high surface area, good mechanical strength and low cost [37]. Co-precipitation, impregnation and physical mixing are the most common techniques for the synthesis of NiO/Al_2O_3 [38]. However, these preparation techniques can result in catalysts which suffer from low activity at low temperature and fast deactivation at higher temperatures in time on line applications [39].

Nickel oxide supported on alumina can be categorized into four different groups, based on its reduction profile. The first of these is α-NiO which has a weak interaction with alumina and is known as a very good precursor for hydrogenation catalysts. β_1- and β_2-NiO bond more strongly with alumina. γ-NiO (found mainly in the bulk $NiAl_2O_4$ spinel phase) has the strongest interaction with alumina and it is thus the most difficult to reduce [40-44], while there are some reports that show the surface of this spinel can be reduced at lower

temperatures [45-48]. In general, the $NiAl_2O_4$ spinel is not known as an active phase for hydrogenation due to its slow reducibility, though this depends somewhat on the application [43, 47]. In addition, Yeng *et al.* also showed that a high nickel loading on the alumina can enhance the catalytic activity of hydrogenation systems [49]. Combustion methods may offer an alternative route to stable catalyst, to overcome this issue due to its discussed advantages.

Synthesis of NiO/Al_2O_3 via combustion synthesis is challenging due to formation of multiple phases in the catalyst mixture [38, 43]. Zhao *et al.* reported the synthesis of supported nickel oxide on γ-alumina with a trace amount of the $NiAl_2O_4$ phase via SCS [43]. Subsequently, Zeng *et al.* synthesised a catalyst free from the $NiAl_2O_4$ spinel on alumina via modified SCS, where they utilized TiO_2 as a dopant [38]. However, the formation of undesired phases or addition of dopants can be counted as disadvantages of their methods.

The recent interesting discoveries in the field of combustion synthesis motivated us to investigate the synthesis of supported nickel oxide on alumina via SCS and SGCS, with the aim of developing an effective synthesis procedure and to explore the influence of the fuel on the synthesis and the particle size of the catalysts. This in turn, allowed an appropriate and detailed understanding of the $NiAl_2O_4$ spinel phase in the presence of NiO for octanal hydrogenation reactions. Octanal was chosen as model substrate because its hydrogenation is a key step in the production of 1-octene from octanal [50]. Furthermore, the formation of by-products such as C_{16} aldol compounds and C_{24} acetal, which are acid catalysed, allow for the probing of acid sites in the catalysts.

2.2) Experimental

2.2.1) General procedure for SCS and SGCS techniques

For SCS, $Ni(NO_3)_2.6H_2O$ (Otto), $Al(NO_3)_3.9H_2O$ (Univar) and the fuel [urea (Unilab) or oxalyldihydrazide (Sigma-Aldrich)] in the correct stoichiometric ratio[51] were dissolved in double distilled water to obtain a saturated solution. Then, the prepared solution was heated in a muffle furnace at 350 °C for 30 minutes to establish the initial ignition. Thereafter, the temperature was ramped up to 500 °C over a period of 270 minutes for annealing and removal of excess carbonic species.

In the case of SGCS, the prepared solution as for SCS was dehydrated with stirring at 90 °C until a thick green gel formed (30-45 minutes, depending on the scale of reaction). The sample was then placed in a muffle furnace following the same heating procedure as for SCS.

2.2.2) Catalyst characterization

Phase identification for each catalyst was made using a Bruker D8 Advance PXRD with a copper radiation source (1.5406 λ). The Retvield refinement analysis was done by loading the .cif files of NiO and $NiAl_2O_4$ in the PANalytical X'Pert HighScore software. This software was then used to optimize the peak shifts, intensities and shapes for each phase and present their population by percent. BET surface area was determined by a Micromeritics Tristar II after degassing the sample at 200 °C overnight in a Micromeritics flow prep 060. The molar ratio between the two elements (*i.e.* nickel and aluminium) was determined via Inductively Coupled Plasma Optical Emission Spectroscopy (ICP-OES) using a Perkin Elmer Precisely Optima 5300DV after the sample was digested in nitric acid using microwave digestion. Hydrogen Temperature Programed Reduction (H_2-TPR) was performed using a Micromeritics 2920 Autochem II Chemisorption Analyser. The metal dispersion and metallic

surface area were determined using a Micromeritics ASAP 2020 chemisorption analyser. A Perkin-Elmer ATR spectrometer was used for pyridine adsorption analysis to probe the acidity of the materials. Prior to analysis, one drop of pyridine was added on 10 mg of catalyst whilst mixing and the sample was left in air for two hours to eliminate the reversibly adsorbed pyridine. The bulk structure of each catalyst was viewed using a Jeol JEM-1010 Transmission Electron Microscope (TEM) and JEM-2100 High Resolution Transmission Electron Microscope (HR-TEM).

2.2.2.1) H_2 chemisorption analysis

The metal dispersion was estimated using a Micromeritics ASAP 2020 Chemisorption analyser. The sample (0.03-0.04 g) was reduced by flow of hydrogen (30 mL/min) for three hours at 600 °C and then flushed at the same temperature and flow rate for 30 minutes with helium. Then, the sample was saturated by passing hydrogen (30 mL/min) through the sample for three hours. The hydrogen uptake was measured using a TCD detector. The metal dispersion is the ratio between the metal on the surface of the support and hydrogen uptake, which was assuming a H_2:Ni chemisorption stoichiometry of 1:1 [52]. Furthermore, the metal dispersion was calculated using the atomic cross sectional area of the metal and the hydrogen uptake [53].

2.2.3) Catalytic testing

Catalytic testing for the hydrogenation reactions was carried out in a continuous flow fixed bed high pressure reactor. The tubular stainless steel reactor tube (grade 316) has a length of 265 mm and an internal diameter of 14 mm. The catalyst bed was placed in the isothermal zone of the reactor tube (volume of 6 mL, pellet sizes 300-600 μm) and was diluted with a double volume of 24 grit carborundum. The same grain size of carborundum was also

packed in the spaces on either side of the bed. The feed used for all reactions consisted of 10 wt.% octanal diluted with octanol to eliminate the effect of the large exotherm associated with the hydrogenation of the neat aldehyde. Octanol was chosen as a diluent since it is the main product of octanal hydrogenation and was found to have no significant influence on the reaction [54]. Prior to each experiment, the catalyst was heated under nitrogen at 200 °C for two hours, followed by reduction using hydrogen at 450 °C overnight. The gas flow rate was adjusted by calibrated nitrogen and hydrogen mass flow meters. A hydrogen pressure of 50 Bar, LHSV of 18 h^{-1} and a temperature ranging from 110 °C to 180 °C were used for all catalytic reactions. The hydrogen to octanal molar ratio was set at 2:1 for all the reactions. The liquid products were collected at regular intervals and analyzed using a Perkin Elmer Clarus 500 GC furnished with a FID using a Petrolite column (50 m length, 200 μm internal diameter). All data points were obtained in duplicate and the mass balance was 100 ± 2 %.

2.3) Results and discussion

The applied labelling system for the reported catalysts describes the composition of the catalyst, which is nickel and alumina, and appears in the label as "NA". The second part of the label carries the data regarding the fuel used for the synthesis of that specific catalyst; "U" for urea and "O" for oxalyldihydrazide. The final part of each label refers to the synthesis procedure where "S" stands for SCS (solution combustion synthesis), and "G" refers to SGCS (sol-gel auto combustion synthesis). For example, NA-U-S represents the NiO/Al_2O_3 catalyst, synthesised using urea as a fuel and SCS as the synthesis technique.

2.3.1) Powder XRD

The molar ratio between nickel and aluminium was kept at 1 : 2 for all four catalysts as shown in **Table 2.1**. The PXRD diffractograms of catalysts prepared with urea presented

broad peaks that illustrate good dispersion of nano-sized nickel oxide particles on the γ-alumina (**Figure 2.1**). The average crystallite size for these catalysts was obtained by employing the Scherrer equation and was found to be less than 2 nm (**Table 2.1**). In contrast, when oxalyldihydrazide was used as the fuel, it yielded poor dispersion (more agglomeration) inferring a larger crystallite size (**Table 2.1**) observed by the sharp peaks in **Figure 2.1**. The greater amount of heat generated during the combustion process from the use of oxalyldihydrazide as fuel seems to be the main cause for this observation.

Table 2.4 Composition, crystal phases and crystallite size for different NiO/Al_2O_3 catalysts.

Catalyst	Ni : Al[b]	NiO : $NiAl_2O_4$[c] (%)	L[d] (nm) (NiO : $NiAl_2O_4$)
NA-U-S[a]	1 : 2	63 : 37	1.9 : 1.9
NA-U-G[a]	1 : 2	100 : 0	1.9 : -[e]
NA-O-S[a]	1 : 2	22 : 78	10.8 : 8.3
NA-O-G[a]	1 : 2	13 : 87	8.3 : 12

a. NA: NiO/Al_2O_3, U: urea, O: oxalyldihydrazide, S: SCS and G: SGCS

b. The molar ratio between to metals according to ICP.

c. The ratio between phases were calculated by application of Rietveld refinement.

d. Average crystallite size from Scherrer equation.

e. The $NiAl_2O_4$ phase is not present.

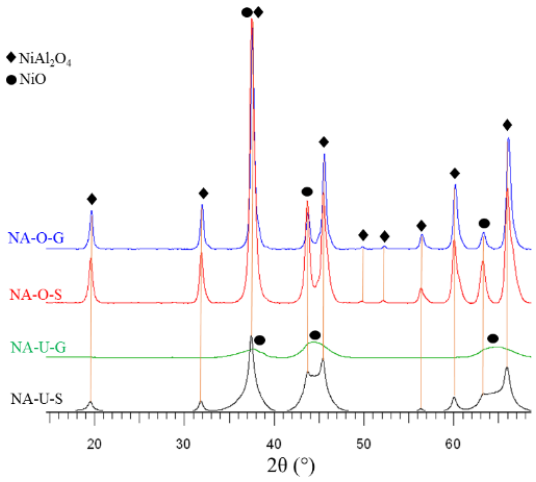

Figure 2.3 PXRD of NiO/Al_2O_3 catalysts.

Usually, SGCS provides higher combustion temperature when compared with SCS due to the lower amounts of water present in the former technique [55]. Therefore, it is typically expected that more $NiAl_2O_4$ should form by using SGCS. Interestingly, the results (**Table 2.1**) do not support this when urea was employed as a fuel, possibly because urea is known to be a good chelating ligand for nickel [6]. It seems that the formation of a urea-nickel complex in the formed gel in the SGCS technique hinders the interaction of nickel with aluminium atoms. Hence, the chelating properties of urea in the absence of water could overcome the higher temperature provided by SGCS, and thus NiO particles supported on Al_2O_3 were obtained, free of the $NiAl_2O_4$ spinel (NA-U-G in **Table 2.1**). However, oxalyldihydrazide gave the expected result and more $NiAl_2O_4$ than free NiO particles was formed when using the SGCS technique (NA-O-G in **Table 2.1**).

2.3.2) Surface area

The BET results were in good agreement with the data obtained from PXRD. BET surface area revealed that the formation of the $NiAl_2O_4$ spinel phase decreased the surface area of the prepared materials (**Table 2.2**) very significantly. Thus, spinel-free NA-U-G had a higher

surface area than NA-U-S with a 37% spinel content, whereas the catalysts prepared using oxalyldihydrazide as the fuel, which had very high spinel content of 78 and 87%, irrespective of the method used, had surface areas that were significantly lower (**Table 2.2**). The higher surface area for NiO on Al_2O_3 synthesised by urea, supports the postulate of well dispersed nickel oxide particles on alumina (**Table 2.2**, NA-U-G). Consequently, the presence of the spinel phase also affected the pore volume and pore diameter, as shown in **Table 2.2**.

Table 2.5 Surface area, pore volume and pore diameter of NiO/Al_2O_3 catalysts.

Catalyst	**BET surface area ($m^2.g^{-1}$)**	**Pore volume ($cm^3.g^{-1}$)**	**Pore diameter (nm)**
NA-U-S	188	0.16	3.4
NA-U-G	218	0.19	3.6
NA-O-S	25	0.11	18
NA-O-G	16	0.05	13.9

2.3.3) Electron microscopy

As illustrated by the TEM images in **Figure 2**, the observed particle sizes of the catalysts are comparable with the calculated crystallite size using the Scherrer equation (**Table 2.1**). Smaller particles were observed for NA-U-S and NA-U-G, while larger particles were observed for the NA-O-S and NA-O-G catalysts.

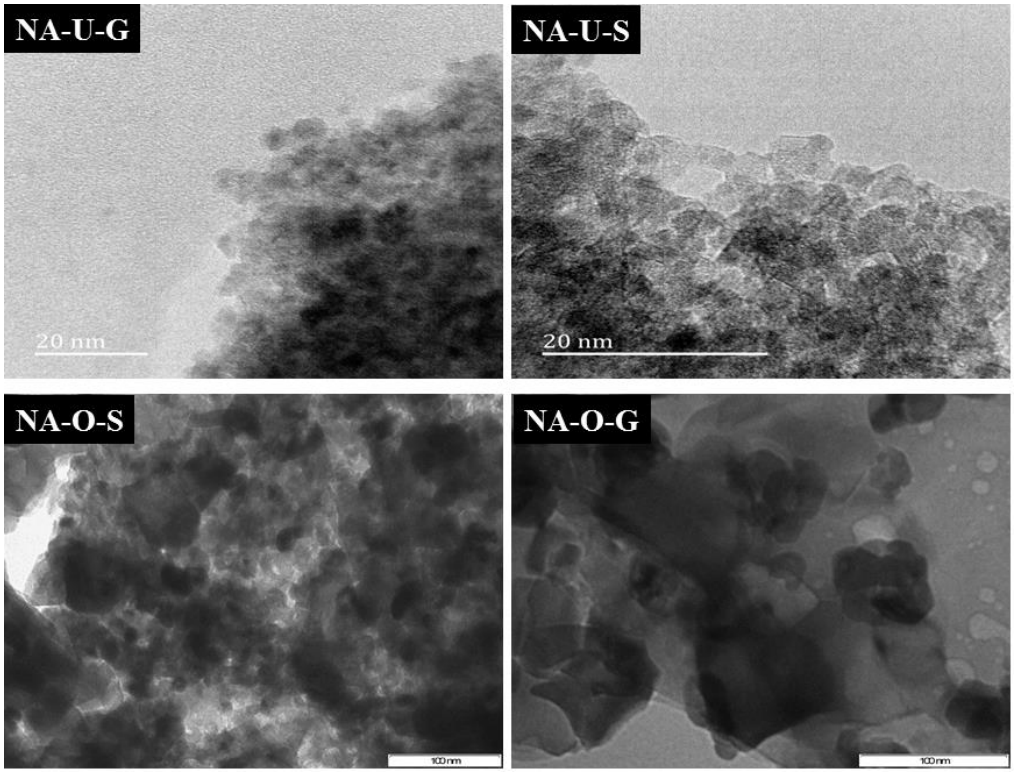

Figure 4.2 TEM images of NiO/Al_2O_3 catalysts.

2.3.4) H_2-TPR, pyridine IR and H_2-Chemisorption

The degrees of reduction and surface acidity of these catalysts were determined by means of H_2-TPR and pyridine IR, respectively. As seen in **Figure 2.3**, which gives the representative reduction peaks, the most intense peak for NA-U-S is assigned to β_2-NiO.[40] This form of nickel oxide is known to bond strongly to alumina. The minor peak at around 400 ºC is due to α-NiO, associated with nickel hydroxide [56], thought to be the more suitable type of NiO phase for hydrogenation due to its weak interaction with the support [40]. A similar H_2-TPR profile to NA-U-S was observed for NA-U-G. Based on reported data, the peak in the temperature range of 500-800 °C can be attributed to the reduction of highly dispersed non-stoichiometric NiO on Al_2O_3 and amorphous nickel aluminate spinel [57]. Therefore, H_2-TPR could not be used definitively to distinguish the available spinel phase present in the NA-U-S catalytic system. The good dispersion, as well as the low crystallinity, in the

catalysts synthesised using urea as the fuel can be related to the lower flame temperature provided by the fuel during the combustion process. Both NA-O-S and NA-O-G present two peaks at 420 ºC and 900 ºC, respectively (**Figure 2.3**). The area under the peak of α-NiO at 420 ºC is clearly larger for NA-O-S compared to NA-O-G which appears to be a semi-quantitative representation of the free NiO and spinel phases present in these systems [41-43, 58]. The peak at about 900 °C is ascribed to $NiAl_2O_4$ (γ-NiO), known to be the most inert phase of nickel oxide for hydrogenation catalysis [41, 42, 44, 58].

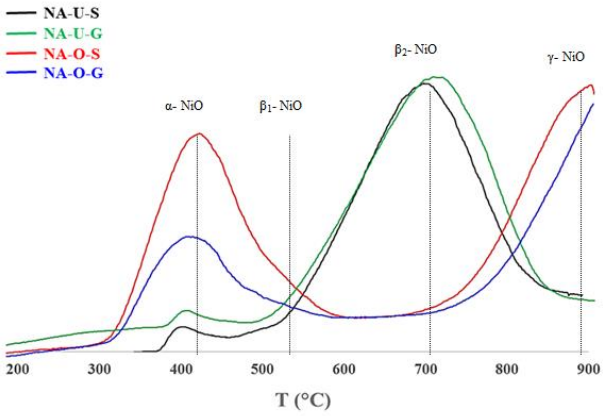

Figure 2.3 H_2-TPR data of NiO/Al_2O_3 catalysts.

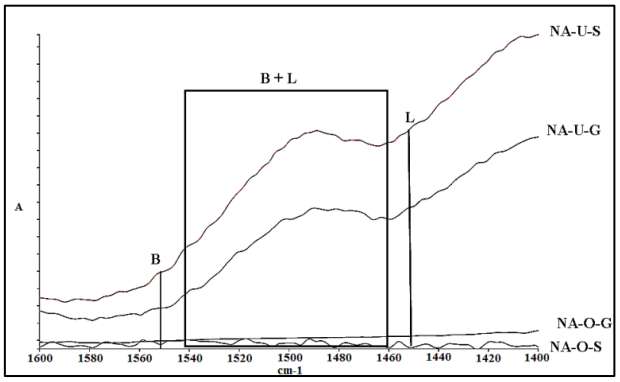

Figure 2.4 Pyridine IR spectra of NiO/Al_2O_3 catalysts.

Pyridine IR of the catalysts prepared via oxalyldihydrazide as a fuel showed surfaces that appear to have a very low density of both Brønsted and Lewis acid sites, while the presence

of Brønsted acid (peak at υ = 1544 cm^{-1}) as well as mixture of Lewis and Brønsted acid (peaks at $\upsilon \sim 1500$ cm^{-1}) sites were established for NA-U-S and NA-U-G, as determined from the data given in **Figure 2.4** [59, 60]. It seems that the lower surface acidity implied for NA-O-S and NA-O-G is likely due to the formation of $NiAl_2O_4$ that block the Brønsted acidic sites of alumina, as suggested by some researchers [61]. Finally, H_2-chemisorption data, shown in **Table 2.3**, indicates that catalysts prepared via urea as a fuel reduce more easily as illustrated by the better dispersion of nickel on the alumina support, whereas more agglomeration is surmised in the case when oxalyldihydrazide is used as fuel. The data obtained during H_2-chemisorption shows good agreement with PXRD and BET results. However, the obtained data for crystalline size from this technique was not comparable with TEM and PXRD data and is not discuss in here, for a number of reasons. Thus, the calculated crystalline size by H_2-chemisorption is referring to the metallic nickel crystalline size while both PXRD and TEM methods are used to measure the NiO crystalline size. Furthermore, this technique may cause agglomeration of the NiO during the analysis, which causes overestimation of the crystalline size. It is also well stablished that the adsorption may be influenced by diffusion limitations and consecutively create error in crystalline size estimation [62].

Table 2.6 H_2-Chemisorption results of NiO/Al_2O_3 catalysts.

Catalyst	**Metal dispersion (%)**	**Metallic surface area ($m^2.g^{-1}$)**
NA-U-S	4.2	9.4
NA-U-G	3.7	8.3
NA-O-S	1.0	2.3
NA-O-G	0.7	1.5

2.3.5) Catalytic results

The catalytic results for all the catalysts tested are shown in **Figures 2.5** and **2.6**. The data in **Figure 2.5** compares the catalysts prepared by SCS and SCGS with the two different fuels. At the lowest temperature tested (110 ºC), the results appear to be clearly influenced by the physical characteristics of the catalysts. NA-U-S and NA-U-G gave a high conversion of octanal (**Figure 2.5**) relative to NA-O-S and NA-O-G. The higher conversion is correlated to the higher metallic surface area and dispersion of the urea synthesised systems compared to NA-O-S and NA-O-G (**Table 2.3**). However, the selectivity towards by-products, which include C_{24} acetal and aldol products, was higher (~ 7%) over these two catalysts, likely due to their higher surface areas as well as the more pronounced surface acidity. NA-O-S gave a higher conversion than NA-O-G, due primarily to a higher metal dispersion and surface area, which is also in keeping with the higher ratio of NiO to the spinel phase observed for the former.

Catalysts synthesised with urea (NA-U-S and NA-U-G) presented similar trends for octanal conversion at 150 ºC as found for these catalysts at 110 ºC (**Figure 2.5**), for the reasons discussed previously. However, NA-O-S now also exhibited high conversion (98 %) at this temperature compared to its performance at 110 ºC. Based on H_2-TPR and the catalytic results at 150 ºC for NA-O-S (**Figures 2.3** and **2.5**), it is clear that the rate of reaction on the metallic Ni (originated from α-NiO, identified by H_2-TPR data) sites increased, whilst at the same time some previously unreduced NiO may have been activated on the surface of the spinel. This effect was not pronounced for NA-O-G, since the conversion only increased slightly.

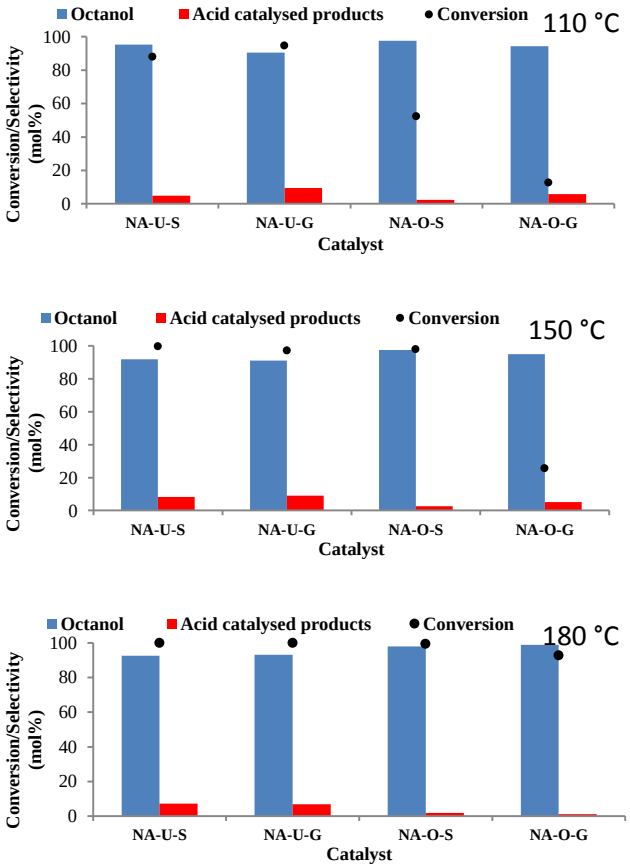

Figure 2.5 Effect of temperature on the selectivity and conversion over NiO/Al_2O_3 catalysts at a LHSV = 18 h^{-1}, pressure = 50 bar, octanal: H_2 ratio of 1:2.

At 180 °C, the conversion is very similar for all the catalysts suggesting lower activation barriers at this temperature. With respect to selectivity, octanol was the dominant product at all temperatures for all the catalysts. However, the acid catalysed products, formed by aldol condensation and acetalisation reactions, increased slightly with an increase in temperature, especially for the catalysts synthesised with urea as fuel. In general, the catalysts synthesised with urea exhibited a higher tendency toward acid catalysed products than the catalysts prepared using oxalyldihydrazide as fuel. This result correlates well with the pyridine IR results, where it is suggested that the presence of $NiAl_2O_4$ in the catalysts, especially those prepared by oxalyldihydrazide as a fuel, gives a lower acidity. These, thus, provide a higher selectivity to octanol and a lower selectivity to the acid catalysed by-products. To establish

the extent of the reduction of the spinel phase during the reaction, a catalyst with high spinel content (> 99.6 %) was tested at 110° C, and the temperature was increased thereafter to 180° C. Subsequently, after several hours of catalytic testing, the temperature was decreased back to 110°C. The result of this experiment is shown in **Figure 2.6**. It can be observed that the octanal conversion increased as expected from 110° C to 180° C, however, when the temperature was lowered again to 110° C, the conversion was higher than when initially tested at 110° C. At the same time the octanol selectivity did not change significantly. This suggests that the presence of the spinel phase, although having a low reduction capability, can possibly provide fresh metallic nickel, likely from defect sites on the spinel surface for catalysts that run for long periods, providing excellent on-line stability in hydrogenation systems.

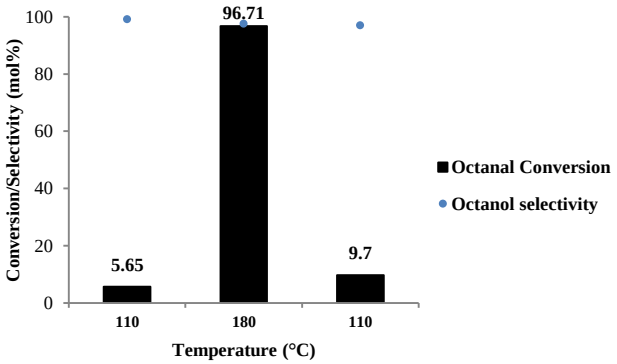

Figure 2.6 Effect of temperature on conversion for high spinel content catalyst.

Scheme 2.1 offers an overview of the reactions occurring and the related surface properties gained, by virtue of the phases present. Ni metallic sites formed by the reduction of NiO, which predominates in the urea synthesised catalysts, show the predicted hydrogenation reaction. At the same time, these systems also show the presence of more acid sites, revealed by the increased selectivity to aldol condensation products and C_{24} acetal. In contrast, the oxalyldihydrazide synthesised catalysts, where the spinel is the dominant phase, show lower

rates when compared to the urea synthesised catalysts (at low temperature) for octanal conversion due to the lower metallic Ni surface area, but improved selectivity to octanol due to the lower density of acid sites which catalyse aldol products and acetal formation.

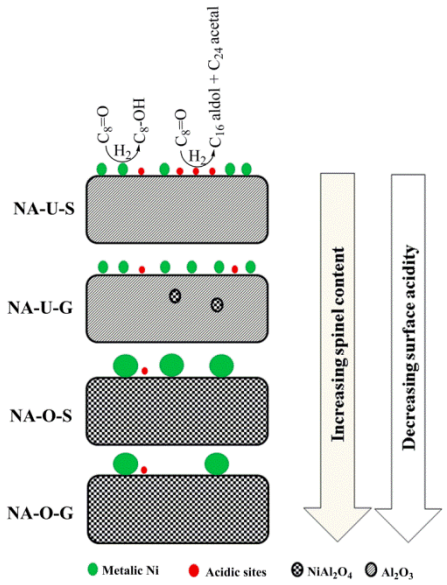

Scheme 2.1 The use of hydrogenation reaction to probe the surface properties of NiO-Al_2O_3 systems.

2.3.6) Used catalyst characterization

The PXRD of the used catalysts is presented in **Figure 2.7**. The intensity of peaks corresponding to the NiO phase decreased and resulted in the detection of trace amounts of metallic nickel as shown in **Figure 2.7**. The catalyst containing pure phase NiO (NA-U-G) clearly does not show the formation of any spinel, while metallic nickel could be detected. This observation suggests that spinel formation might not be the reason for catalyst deactivation (in hydrogenation) in time on line application and deactivation is mainly due to the agglomeration of metallic nickel.

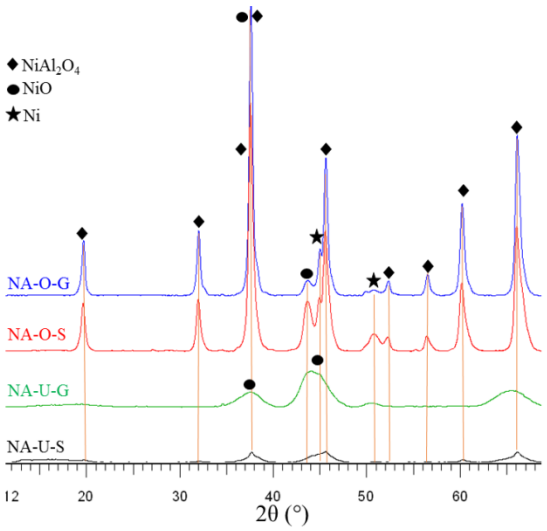

Figure 2.7 PXRD of NiO/Al_2O_3 catalysts.

2.4) Conclusion

Application of urea as a fuel for the synthesis of NiO/Al_2O_3 in both the SCS and SGCS techniques resulted in catalysts with small crystalline size, high surface area and high active metal dispersion, therefore, high activity for the hydrogenation of octanal was observed. However, these catalysts gave some by-products, which can be counted as a disadvantage of using this fuel. SGCS yielded pure NiO/Al_2O_3 (free of $NiAl_2O_4$) material, while the presence of the spinel phase was observed when SCS was chosen for the synthesis of this catalyst.

In contrast, oxalyldihydrazide as a fuel presented lower surface area and larger crystalline size for supported nickel oxide on the alumina and spinel. In addition, the $NiAl_2O_4$ spinel phase was the dominating phase when this fuel was used. However, the small portion of available nickel oxide in this catalyst was found to be α-NiO (from H_2-TPR data), which indicated a good suitability for the hydrogenation of aldehydes. The catalyst prepared with SGCS resulted in lower activity at 110 ºC and 150 ºC than was observed for the catalyst prepared by the SCS method when oxalyldihydrazide was employed as a fuel. Furthermore,

it seems the presence of the $NiAl_2O_4$ spinel phase can block the acidic sites of alumina which enhances the selectivity towards octanol, by suppression of acid catalysed reactions.

Finally, based on the catalytic results at high temperatures, the $NiAl_2O_4$ phase seems to be able to act as a slow generator of metallic nickel atoms required in the hydrogenation reaction, which may improve the catalyst's life-time for industrial applications. Hence, the $NiAl_2O_4$ spinel phase may indeed be of benefit to hydrogenation reactions.

2.5) Acknowledgements

We thank SASOL, the National Research Foundation, South Africa (NRF) and the Technology and Human Resources for Industry Programme (THRIP Grant TP1208035643) for their financial support. We also thank the Electron Microscopy Unit at the University of KwaZulu-Natal (Westville).

2.6) References

[1] J.J. Kingsley, K.C. Patil, Mater. Lett., 6 (1988) 427-32.

[2] K.C. Patil, S.T. Aruna, T. Mimani, Curr. Opin. Solid State Mater. Sci., 6 (2003) 507-512.

[3] A.S. Prakash, C. Shivakumara, M.S. Hegde, Mat. Sci. Eng. B., 139 (2007) 55-61.

[4] S. Sharma, Z. Hu, P. Zhang, E.W. McFarland, H. Metiu, J. Catal., 278 (2011) 297-309.

[5] S.K. Lathika Devi, K. Sudarsana Kumar, A. Balakrishnan, Mater. Lett., 65 (2011) 35-37.

[6] S.L. Gonzalez-Cortes, F.E. Imbert, Appl. Catal., A, 452 (2013) 117-131.

[7] A.S. Mukasyan, P. Epstein, P. Dinka, Proc. Combust. Inst., 31 (2007) 1789-1795.

[8] C. Aliotta, L.F. Liotta, V. La Parola, A. Martorana, E.N.S. Muccillo, R. Muccillo, F. Deganello, Appl. Catal., B., 197 (2016) 14-22

[9] Z.X. Yue, J. Zhou, L.T. Li, H.G. Zhang, Z.L. Gui, J. Magn. Magn. Mater., 208 (2000) 55-60.

[10] Q. Xiao, Z. Si, Z. Yu, G. Qiu, Mater. Sci. Eng., B, 137 (2007) 189-194.

[11] P.K. Roy, J. Bera, J. Mater. Process. Technol., 197 (2008) 279-283.

[12] B.G. Toksha, S.E. Shirsath, M.L. Mane, S.M. Patange, S.S. Jadhav, K.M. Jadhav, J. Phys. Chem. C, 115 (2011) 20905-20912.

[13] T. Cwele, N. Mahadevaiah, S. Singh, H.B. Friedrich, Appl. Catal., B, 182 (2016) 1-14.

[14] S.L. Gonzalez-Cortes, T.-C. Xiao, P.M.F.J. Costa, B. Fontal, M.L.H. Green, Appl. Catal., A, 270 (2004) 209-222.

[15] S.L. Gonzalez-Cortes, T.-C. Xiao, T.-W. Lin, M.L.H. Green, Appl. Catal., A, 302 (2006) 264-273.

[16] D. Jiao, Y. Ma, F. Cao, Particuology, 10 (2012) 468-474.

[17] P. Dinka, A.S. Mukasyan, J. Phys. Chem. B, 109 (2005) 21627-21633.

[18] L. Shi, K. Tao, T. Kawabata, T. Shimamura, X.J. Zhang, N. Tsubaki, ACS Catal., 1 (2011) 1225-1233.

[19] L. Shi, Y. Jin, C. Xing, C. Zeng, T. Kawabata, K. Imai, K. Matsuda, Y. Tan, N. Tsubaki, Appl. Catal., A, 435-436 (2012) 217-224.

[20] A. Kumar, A.S. Mukasyan, E.E. Wolf, Appl. Catal., A, 372 (2010) 175-183.

[21] J.W. Yang, M.T.H. Fonseca, B. List, Angew. Chem. Int. Ed., 43 (2004) 6660-6662.

[22] B. Chen, U. Dingerdissen, J.G.E. Krauter, H. Rotgerink, K. Mobus, D.J. Ostgard, P. Panster, T.H. Riermeier, S. Seebald, T. Tacke, H. Trauthwein, Appl. Catal., A, 280 (2005) 17-46.

[23] J. Valand, A.S. Mahomed, S. Singh, H.B. Friedrich, J. Porous Mater., 23 (2016) 175-183.

[24] K.R. Kahsar, S. Johnson, D.K. Schwartz, J.W. Medlin, Top. Catal., 57 (2014) 1505-1511.

[25] J.C. Park, H.J. Lee, J.Y. Kim, K.H. Park, H. Song, J. Phys. Chem. C, 114 (2010) 6381-6388.

[26] M. Kang, M.W. Song, T.W. Kim, K.L. Kim, Can. J. Chem. Eng., 80 (2002) 63-70.

[27] J. Rynkowski, D. Rajski, I. Szyszka, J.R. Grzechowiak, Catal. Today, 90 (2004) 159-166.

[28] S.R. Kirumakki, B.G. Shpeizer, G.V. Sagar, K.V.R. Chary, A. Clearfield, J. Catal., 242 (2006) 319-331.

[29] A. Saadi, R. Merabti, Z. Rassoul, M.M. Bettahar, J. Mol. Catal. A: Chem., 253 (2006) 79-85.

[30] X. Meng, H. Cheng, Y. Akiyama, Y. Hao, W. Qiao, Y. Yu, F. Zhao, S.-i. Fujita, M. Arai, J. Catal., 264 (2009) 1-10.

[31] K. Shimura, K.-i. Shimizu, Green Chem., 14 (2012) 2983-2985.

[32] S.A. Nikolaev, D.A. Pichugina, D.F. Mukhamedzyanova, Gold Bull. (Berlin, Ger.), 45 (2012) 221-231.

[33] A. Ungureanu, B. Dragoi, A. Chirieac, C. Ciotonea, S. Royer, D. Duprez, A.S. Mamede, E. Dumitriu, ACS Appl. Mater. Interfaces, 5 (2013) 3010-3025.

[34] L. Zhang, X. Shu, L. Zhang, Asian J. Chem., 25 (2013) 5071-5075.

[35] X. Wang, H. Yu, D. Hua, S. Zhou, J. Phys. Chem. C, 117 (2013) 7294-7302.

[36] F. Zaera, ChemSusChem, 6 (2013) 1797-1820.

[37] G.C. Chase, M.P. Espe, E.A. Evans, R.D. Ramsier, D.H. Reneker, R.W. Tuttle, J. Rapp, Manufacture of metal oxide fibers and nanofibers for decomposing toxic chemicals, University of Akron, USA . 2008, p. 78.

[38] Y. Zeng, H. Ma, H. Zhang, W. Ying, D. Fang, Fuel, 137 (2014) 155-163.

[39] R.J. White, R. Luque, V.L. Budarin, J.H. Clark, D.J. Macquarrie, Chem. Soc. Rev., 38 (2009) 481-494.

[40] J. Zhang, H. Xu, X. Jin, Q. Ge, W. Li, Appl. Catal., A, 290 (2005) 87-96.

[41] K.Y. Koo, H.-S. Roh, Y.T. Seo, D.J. Seo, W.L. Yoon, S. Bin Park, Int. J. Hydrogen Energy, 33 (2008) 2036-2043.

[42] X. Zou, X. Wang, L. Li, K. Shen, X. Lu, W. Ding, Int. J. Hydrogen Energy, 35 (2010) 12191-12200.

[43] A. Zhao, W. Ying, H. Zhang, H. Ma, D. Fang, Catal. Commun., 17 (2012) 34-38.

[44] Y. Kathiraser, W. Thitsartarn, K. Sutthiumporn, S. Kawi, J. Phys. Chem. C, 117 (2013) 8120-8130.

[45] I.A.P.S. Murthy, C.S. Swamy, J. Mater. Sci., 28 (1993) 1194-8.

[46] H. Muroyama, R. Nakase, T. Matsui, K. Eguchi, Int. J. Hydrogen Energy, 35 (2010) 1575-1581.

[47] N. Salhi, A. Boulahouache, C. Petit, A. Kiennemann, C. Rabia, Int. J. Hydrogen Energy, 36 (2011) 11433-11439.

[48] R. Lopez-Fonseca, C. Jimenez-Gonzalez, B. de Rivas, J.I. Gutierrez-Ortiz, Appl. Catal., A, 437-438 (2012) 53-62.

[49] R. Yang, X. Li, J. Wu, X. Zhang, Z. Zhang, Y. Cheng, J. Guo, Appl. Catal., A, 368 (2009) 105-112.

[50] M. Kelly, Octene-1 by Sasol Heptene-1 Hydroformylation Technology, 2014. https://www.ihs.com/products/SRICReport-PEPReview2014-12-Octene-1bySasolHeptene-1HydroformylationTechnology.html., Access date: 15th of March 2017,

[51] K.C. Patil, Chemistry of Nanocrystalline Oxide Materials: Combustion Synthesis, Properties and Applications, World Scientific2008.

[52] M.A. Nygren, P.E.M. Siegbahn, J. Phys. Chem., 96 (1992) 7579-84.

[53] J. Zhang, H. Wang, A.K. Dalai, Appl. Catal., A, 339 (2008) 121-129.

[54] T. Chetty, H.B. Friedrich, V.D.B.C. Dasireddy, A. Govender, P.J. Mohlala, W. Barnard, ChemCatChem, 6 (2014) 2384-2393.

[55] A.S. Mukasyan, P. Epstein, P. Dinka, Proc. Combust. Inst., 31 (2007) 1789-1795.

[56] M. Tan, X. Wang, X. Wang, X. Zou, W. Ding, X. Lu, J. Catal., 329 (2015) 151-166.

[57] M.C. Sánchez-Sánchez, R.M. Navarro, J.L.G. Fierro, Int. J. Hydrogen Energy, 32 (2007) 1462-1471.

[58] J. Yang, X. Wang, L. Li, K. Shen, X. Lu, W. Ding, Appl. Catal., B, 96 (2010) 232-237.

[59] B. Chakraborty, B. Viswanathan, Catal. Today, 49 (1999) 253-260.

[60] S.D. Kim, S.C. Baek, Y.-J. Lee, K.-W. Jun, M.J. Kim, I.S. Yoo, Appl. Catal., A, 309 (2006) 139-143.

[61] Z. Boukha, C. Jimenez-Gonzalez, B. de Rivas, J. Ramon Gonzalez-Velasco, J. Ignacio Gutierrez-Ortiz, R. Lopez-Fonseca, Appl. Catal., B, 158 (2014) 190-201.

[62] C.R. Adams, H.A. Benesi, R.M. Curtis, R.G. Meisenheimer, J. Catal., 1 (1962) 336-44.

Chapter three

Oxidative dehydrogenation of *n*-octane over niobium doped $NiAl_2O_4$: A novel example of beneficial coking in catalysis over spinel base catalyst

Abstract

Four catalysts with different doping concentration of niobium were prepared using Sol-Gel auto Combustion Synthesis (SGCS). The compositions of these spinels were confirmed using ICP-OES and the change in their electronic profile (upon Nb doping) was established using UV-DRS. All four as-prepared catalysts before and after reaction, were characterized using PXRD and nitrogen physisorption analysis. The morphologies of these catalysts were viewed using TEM and SEM. The redox nature of these catalysts was investigated with H_2-TPR and O_2-TPO with reduction/oxidation/reduction sequences. All above characterizations showed the partial substitution of Nb in the $NiAl_2O_4$ spinel lattice and $NiNb_2O_6$. Furthermore, Nb appears to preferentially occupy the octahedral sites of the spinel. This occupancy resulted in modification of nickel migration, electronic profile, redox properties and surface textures. These catalysts were used for oxidative dehydrogenation of *n*-octane under anaerobic conditions. The catalytic results supported the characterization data and also revealed the role of Nb in the modification of acidic sites. The characterization of the used catalysts and *in situ* XRD analysis showed the positive role of a low quantity of coking of these catalysts. The coke formation was found to facilitate the nickel migration from octahedral to tetrahedral sites and results in a smaller crystallite size of $NiAl_2O_4$ spinel, which seems to be positively involved during the catalytic reactions.

3.1) Introduction

The manufacturing of liquid fuels from natural gas, coal or biomass has created a pool of intermediated-length straight-chain alkanes [1]. Transformation of these low valued chemicals to industrially value-added products such as olefins, aromatics and oxygenates requires extensive research at the current stage [2]. The major application of medium chain length olefins are in the synthesis of alcohols or aldehydes, the production of synthetic lubricants and the production of copolymers with short chain olefins [3]. Short-chain hydrocarbons have been investigated extensively, and there are many patents and scholarly articles on the topic [1]. In contrast, the catalytic conversion of C_7-C_{12} chain length chemicals to value-added chemicals has not received considerable attention, possibly due to the present challenges that affect their transformation [2].

The dehydrogenation (DH) of short-chain hydrocarbons (C_2-C_4) is a commercial procedure for the production of ethylene, propylene, butylenes and 1, 3-butadiene [4]. Disadvantages of the DH process, such as low equilibrium conversion, coke formation and the process being endothermic have motivated researchers to investigate alternatives [4]. Oxidative dehydrogenation (ODH) seems to be a good alternative, however, the formation of cracked products and CO_x are the main obstacles that prevent the ODH process from being industrially practicable [4, 5]. Molybdenum, vanadium and nickel oxides based catalysts are amongst the most investigated metal oxides for the ODH of paraffins [5-8]. Furthermore, DH and ODH processes have been applied extensively for the activation of paraffins [4-6, 9, 10].

Pure phase NiO is known to provide poor ODH results and normally results in direct combustion of the used paraffin in the reaction stream [11]. The non-stoichiometric (electrophilic) oxygen species are known as active sites for the combustion, which seem to

have a high concentration on the surface of pure NiO catalysts. Use of supports [12, 13], (high valance) dopants [14-16] and phosphorus [17, 18] seems to improve the catalytic results over the Ni based catalysts, which follow the Mars and Van Krevelen (MvK) mechanism. Thus, doping NiO with Al showed an enhanced selectivity towards the formation of ethene from ethane [19, 20]. Lemonidou and co-workers showed that the formation of $NiAl_2O_4$ (together with the NiO phase) decreased the amount of desorbed oxygen species (electrophilic) and therefore increased the selectivity to ethene, while the conversion was decreased [19].

Nickel aluminate is a member of the spinel family with the general formula of AB_2O_4 and is known to have a magnetoplumbite-like structure [21-23]. Preparation techniques to synthesis $NiAl_2O_4$ include co-precipitation [23, 24], sol-gel [25], solid state reaction [26], alkoxide method [27, 28], Pechini [29, 30] and combustion synthesis [31, 32]. $NiAl_2O_4$ had been used for the partial oxidation of methane, methane (steam or dry) reforming [29], oxidative coupling of methane [33], diesel steam reforming [34, 35], tar reforming [36] and tetradecane reforming [37]. This bimetallic oxide has been structurally probed and it seems that there is no common conclusion about the level of inversion in $NiAl_2O_4$ [29]. Accordingly, nickel can occupy any of tetrahedral or octahedral sites and form inverse or normal spinel, respectively, or occupy both sub-lattices giving a random spinel [38]. The level of inversion seems to be highly influenced by the preparation technique and the temperature of synthesis [26, 39, 40]. Furthermore, the migration of the nickel between two sub-lattices or to the $NiAl_2O_4$ surface is well stablished and seems to be highly dependent on catalytic reaction conditions [29].

Substitution of dopant atoms (even in small quantities) in the lattice of a host oxide can have profound influences on the properties of the host, such as morphology changes, change in

electronic and transport properties and lower transition temperature, which are important parameters in heterogonous catalysis [41]. Nb has been found to be one of the best dopants for Ni based catalysts [6, 11, 42, 43]. To the best of our knowledge, no doped $NiAl_2O_4$ has been explored in the oxidative dehydrogenation of paraffins. Material based studies on doped $NiAl_2O_4$ showed some significant changes, such as ion migration upon the occupancy of foreign metals and changes in the lattice constant [40, 44].

Coke formation in ODH (especially under anaerobic conditions) is expected. The coke can cover the surface and deactivate the catalyst during the paraffin activation [4]. However, exceptions are known to the above mentioned phenomena, and there are some examples of beneficial coking, where catalytic reactions were enhanced due to coke formation [45-47]. The reported reasons for profitable coking are deposited coke that acts as active sites, the selective deactivation of non-selective catalytic sites and the participation of the formed coke in the catalytic reactions [48]. Interestingly, $NiAl_2O_4$ is found to be active in catalytic reactions which normally suffer from the coke formation, and minimizes coke deposition [33, 35]. However, there is no detailed explanation for this behaviour and more investigations seem to be required.

To explore the effect of doping in the $NiAl_2O_4$ spinel, four catalysts with different Nb loading were synthesised using Sol-Gel auto Combustion Synthesis (SGCS). Characterization showed the partial substitution of doped Nb into the spinel lattice. Then, these catalysts were used for the ODH of *n*-octane. Finally, the characterization of the used catalysts and the comparison with the fresh catalysts helped us propose the positive impacts of coke formation over these catalysts.

3.2) Experimental

3.2.1) Materials

The metal precursors used in the synthesis, $Ni(NO_3)_2.6H_2O$ (ACS reagent grade), $Al(NO_3)_3.9H_2O$ (ACS reagent grade) and ammonium niobium oxalate [$C_4H_4NNbO_9.xH_2O$] (99.99% trace metals basis), were used as received from Sigma-Aldrich. Oxalyldihydrazine was freshly synthesised using a reported method.[49] De-ionized water was used throughout the synthesis. *n*-Octane (>98%) was purchased from Alfa Aesar. Synthetic air (UHP) and nitrogen (UHP) were supplied from zero air and N_2 generators (Peak Scientific), respectively, for catalytic testing. Hydrogen (base line), Argon (base line) and Helium (base line) were purchased from Afrox for GC analyses in this study. 10% H_2/Ar and 10% O_2/Ar (Afrox) were used in the TPR-TPO-TPR analysis.

3.2.2) SGCS synthesis of nickel aluminate catalysts

The stoichiometric amounts of each precursor (including fuel) were weighed and mixed in water. The solution was stirred at 80 °C on a heater stirrer until all used starting materials were fully dissolved and dehydrated and resulted in the formation of a thick gel. The formed gel was left in a muffle furnace (set at 400 °C) under static flow of air for 30 min for ignition, followed by a temperature ramp up to 500 °C and this temperature was held for one extra hour. The resultant material was crushed over 10 min and calcined at 1000 °C under flow of air for 4.5 h. To insure good homogeneity of the catalyst and to prevent the formation of NiO, the sample was crushed every 1.5 h with a mortar and pestel over 10 min during the calcination at 1000 °C. The final colour of the catalyst was sky blue.

Since the aim of this study was to synthesis of $NiAl_2O_4$ spinel with Nb as a dopant, the atomic ratio between Al and Ni was kept at approximately 2:1. Nb substitution (with Al or Ni) was calculated based on the charge balance and the final molecular formula of spinel (AB_2O_4). Therefore, the four catalysts for this study are $NiAl_2O_{4\pm\delta}$, $Ni_{0.98}Al_2Nb_{0.02}O_{4\pm\delta}$, $Ni_{0.97}Al_{1.97}Nb_{0.06}O_{4\pm\delta}$ and $Ni_{0.95}Al_{1.95}Nb_{0.1}O_{4\pm\delta}$, labelled as SP, SP-0.02 Nb, SP-0.06 Nb and SP-0.10 Nb throughout this study.

3.2.3) Oxidative dehydrogenation of *n*-octane

A continuous-flow fixed-bed reactor (in vertical flow mode) was used for catalytic testing. The catalyst particles were loaded in the middle of the isothermal zone in a stainless steel tube (10 mm ID and 200 mm length). The voids were filled using carborundum (40 gritt, Polychem) to minimize the contribution of homogeneous gas phase reactions [50]. Fresh catalyst, 0.5 ml (~0.45 g) with a particle size of 300-600 μm diluted with the same volume of carborundum (to eliminate mass transfer limitations), was used for each set of data. All reactions were carried out in the range of 450-550 °C at 50 °C intervals. The molar ratio of carbon to oxygen (C : O) was set at 8 : 1 with a Gas Hour Space Velocity (GHSV) of 12 000 h^{-1}. Air was used as a source of oxygen and nitrogen as an inert gas and diluent. The flow rates of *n*-octane, air and nitrogen were adjusted to set the GHSV. The concentration of *n*-octane in the reactant steam was 11%. The flow rate of nitrogen and air were controlled using two separate mass flow controllers (Bronkhorst) and *n*-octane was pumped (series II HPLC pump) into the heated reactor line (140 °C) to ensure that *n*-octane is in the gas phase.

All products were analysed offline by using a gas syringe and gas chromatography (GC). H_2, CO and CO_2 were analysed using a PerkinElmer Clarus 400 GC equipped with a TCD detector and PLOT 1010 column with argon as a carrier gas. Unreacted oxygen was

quantified using a PerkinElmer Clarus 500 GC equipped with a TCD and PLOT 5A with helium as a carrier gas. The light products in the gas phase were analysed using a Shimadzu 2121 GC with FID detector and capillary column. H_2 and N_2 were used as carrier gas in this GC. The collected liquid products in the catch-pot were analysed by the aforementioned Shimadzu GC. All reported reactions have a 100±1 % carbon balances and all reported results are the average of at least two runs under steady state conditions.

3.2.4) Physicochemical characterization

Powder X-Ray diffraction (Bruker D8 Advance) with a copper radiation source (λ=1.5406 nm) in 2theta range of 10-70 with total number of scans of 4222 and scan rate of 0.5 s/scan was used to analyse the phase composition of the synthesised materials. The bulk composition of the synthesised spinel was confirmed with Inductively Coupled Plasma-Optical Emission Spectroscopy using a PerkinElmer Precisely Optima 5300DV, after the sample was digested in H_2SO_4 (98%, Merck). BET-surface area measurements were done using a Micromeritics Tristar II. Samples were degassed under a flow of N_2 at 200 °C with a Micromeritics flow prep 060 overnight prior to each BET analysis. UV-DRS spectra were collected using a PerkinElmer (Lambda 35, UV/VIS Spectrometer) that was equipped with Labsphere reflectance spectroscopy accessories. TGA was done using a TA instrument (SDT Q600) under positive flow of air. Temperature programmed reduction/oxidation/reduction was carried out using a Micromeritics 2920 Autochem II analyser using methods reported elsewhere [51]. The catalyst morphology was viewed using a Ziess Ultra plus Scanning Electron Microscope (SEM). The bulk structures of the catalysts were viewed using a Jeol JEM-1010 Transmission Electron Microscope. A Jeol JEM-2100 High Resolution-Transmission Electron Microscope (HR-TEM) was used (in dark field-scanning transition electron microscope [DF-STEM] mode) for elemental distribution analysis (mapping).

3.3) Results and discussions

3.3.1) XRD and ICP

Based on our previous report, sol-gel auto combustion using oxalyldihdrazide facilitates the synthesis of $NiAl_2O_4$ [32]. However, high calcination temperature (~1000 °C) is required for the synthesis of pure phase $NiAl_2O_4$ [29]. The targeted elemental compositions were achieved and confirmed using ICP (**Table 3.1**). The PXRD data of the prepared catalysts are shown in **Figure 3.1a**. The absence of any nickel oxide phase was confirmed by XRD for all four catalysts. The XRD pattern of SP and SP-0.02 Nb showed only the peaks of spinel (**Figure 3.1a)**. Nevertheless, the formation of the $NiNb_2O_6$ phase was detected when higher concentrations of Nb precursors were used during the synthesis of SP-0.06 Nb and SP-0.10 Nb (**Figure 3.1a)**. This phase belongs to the columbite family and is known to be inert under oxidative dehydrogenation reaction conditions [52, 53]. In addition, the high intensity of peaks in the XRD diffractograms suggest a high degree of crystallinity for these catalysts, which is driven by the high temperature treatment during the synthesis. The calculated average crystallite sizes of the spinel, using the Scherrer equation, for all catalysts showed an increase in crystallite size with introduction of niobium (**Table 3.1**), except SP-0.06 Nb.

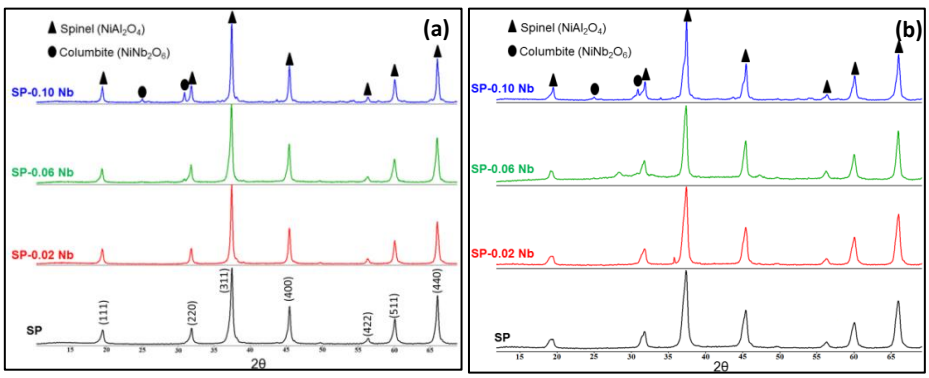

Figure 3.1 PXRD patterns of (a) as prepared catalysts, (b) used catalysts.

No change in the peak positions of the fresh and used catalysts is observed, which is a strong proof for the thermal stability of these materials under the reaction condition (after 50 h). Surprisingly, the intensity of all the spinel peaks had decreased after the reactions. This implies smaller crystallite sizes for the used catalysts compared to what was observed for the fresh catalysts. The crystallite sizes for the used catalysts are tabulated in **Table 3.1**. Generally, the crystallite sizes increased with Nb content for the materials. Further studies on the XRD patterns of these catalysts were required to probe the possibility of Nb substitution into the spinel cubic lattice.

Table 3.1 Elemental and phase compositions of as prepared catalysts

Catalyst	**Ni**[a]	**Nb**[a]	**L**[b] **(nm)**	
			Fresh	**Used**
SP	1.00	-	22.9	12.00
SP-0.02 Nb	0.98	0.02	29.4	12.6
SP-0.06 Nb	0.97	0.06	25.1	15.6
SP-0.10 Nb	0.95	0.10	31.8	21.5

a. The atomic % according to ICP.

b. Average crystallite size of $NiAl_2O_4$ estimated using Scherrer equation.

According to the reports, the planes (220) and (422) are sensitive to cation distribution in the tetrahedral sub lattice of the cubic spinel [40, 44, 54]. Normally, an increase in intensities of the peaks corresponding to these planes suggests the acceptance of substitution in the tetrahedral sites, otherwise the octahedral site was the host for the foreign element [40, 44, 54]. As it is shown in **Figure 3.2**, the intensities of both peaks decreased when 0.02 atomic % nickel was substituted with niobium in SP-0.02 Nb, indicating the replacement of nickel in

the octahedral sub-lattice in this molecule. However, different behaviour was observed when the substitution was designed in a way as to replace both aluminium and nickel. The data, in **Figure 3.2**, shows that substitution can take place in both sub-lattices based on the available ionic vacancies in the spinel structure. However, the formation of $NiNb_2O_5$ shows that the substitution of Nb in the spinel lattice is partial. The exact same trend of substitution in the sub-lattices was observed for the used catalysts, suggesting the retention of the original structures. However, nickel ions seem to have migrated from the octahedral to the tetrahedral sites, since the intensities of both planes were consistently higher than what was observed for the fresh catalysts. This shows that levels of inversion for the under study spinels decrease during the catalytic reactions.

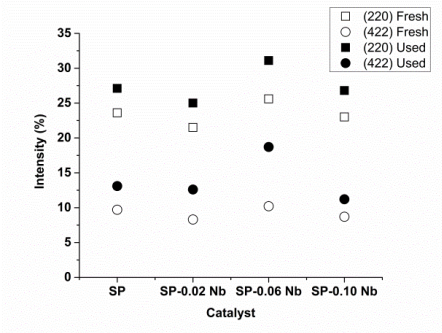

Figure 3.2 The change in intensities of plane (220) and (422) in the fresh and used catalysts. (The intensity of the peak with an *hkl* value of (311) was used as a reference in each diffractogram)

3.3.2) UV-DRS analysis

The UV-DRS spectra were obtained to further investigate the coordination of Ni^{2+} in these catalysts. The bands at 716 nm and 640 nm are due to the nickel in octahedral and tetrahedral sub lattices of spinel, respectively [33, 55]. The low concentration of introduced Nb in SP-0.02 Nb seems to replace the Ni^{2+} in octahedral positions and motivate the migration of Ni^{2+} in octahedral sites to the tetrahedral sites, since the intensities of the peaks at 716 nm and 640

nm in the UV spectrum of SP-0.02 Nb are respectively, lower and higher than for SP (**Figure 3.3**). However, niobium in SP-0.06 Nb seems to replace both Al^{3+} and Ni^{2+} ions in the octahedral and tetrahedral sub-lattices and results in smaller peaks for both sites, than in the other catalysts (**Figure 3.3**). The highest concentration of Nb doping (and lowest molar ratio of Ni^{2+}) in SP-0.10 Nb showed the lowest Ni^{2+} concentration in octahedral sites, while tetrahedrally coordinated Ni^{2+} occupancy was similar to that of the undoped spinel (**Figure 3.3**).

Thus, the UV-DRS and XRD data suggest Nb prefers to be octahedrally coordinated and motivates the Ni^{2+} migration, if any ionic vacancies are present in the tetrahedral sub lattice (based on molar ratio between Ni and Al). However, partial substitution can only be discussed, since peaks corresponding to the columbite phase were observed in the XRD diffractograms (**Figure 3.1**).

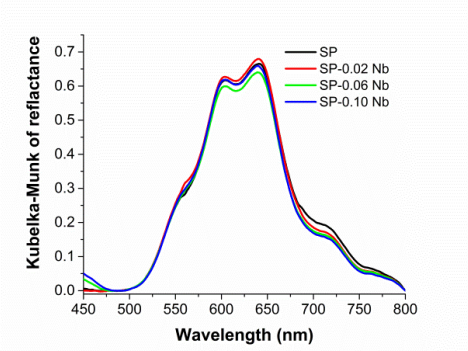

Figure 3.3 UV-DRS data of SP-x Nb catalsts (x: 0, 0.02, 0.06 and 0.10).

3.3.3) Nitrogen physisorption analysis

The BET surface areas and pore volume of the catalysts decreased with addition of niobium. However, no regular trend was observed in the change of pore diameter for the different catalysts. The nitrogen physisorption measurements of the used catalysts generally showed higher surface area, pore volume and pore diameter than the fresh catalysts. The different between the physical properties of the fresh and used catalysts is large for SP-0.02 Nb and the

difference becomes smaller as the concentration of the niobium phase increases in the catalyst mixtures.

Table 3.2 Surface area, pore volume and pore diameter of SP-x Nb catalysts (x: 0.0-0.1).

Catalyst	BET surface area ($m^2.g^{-1}$)		Pore volume ($cm^3.g^{-1}$)		Pore diameter (nm)	
	Fresh	Used	Fresh	Used	Fresh	Used
SP	17	22	0.04	0.10	10.4	17.7
SP-0.02 Nb	13	15	0.03	0.08	8.2	19.9
SP-0.06 Nb	11	12	0.02	0.05	8.5	17.9
SP-0.10 Nb	8	8	0.01	0.01	8.3	6.6

3.3.4) TEM and SEM analysis

These catalysts showed hexagonal and spherical morphology as shown in **Figure 3.4** (a). Both $NiAl_2O_4$ and $NiNb_2O_6$ have this morphology and hence they cannot be separately identified [52]. To investigate the distribution of all three elements in these catalysts, EDX mapping analysis was done in DF-STEM mode using HR-TEM. Formation of $NiAl_2O_4$ always results in a good dispersion of nickel. In addition, no clusters containing Nb have detected in SP-0.06 Nb [**Figure 3.4** (b)], even where some $NiNb_2O_6$ was detected as the extra phase in the PXRD (**Figure 3.1**). This shows both of $NiAl_2O_4$ and $NiNb_2O_6$ phases positively contributed to the observed high dispersion for these catalysts. SEM images showed sponge shaped morphology and introduction of niobium seems to diminish the size of these spongy particles (**Figure 3.5**).

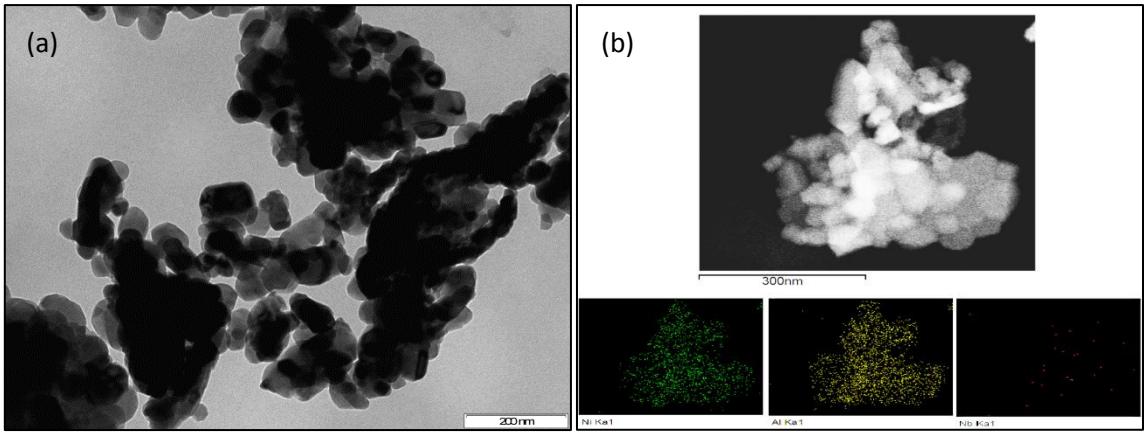

Figure 3.4 (a) General TEM image of the as prepared catalysts. (b) Mapping analysis of Sp-0.06 Nb using HR-TEM (DF-STEM mode).

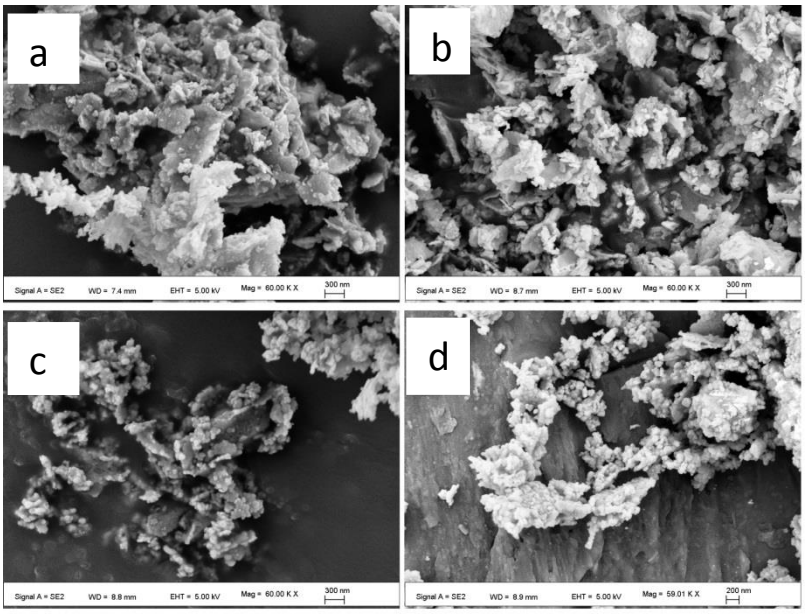

Figure 3.5 SEM images of SP-x Nb catalysts [x: a) 0.00,b) 0.02, c) 0.06 and d) 0.10].

3.3.5) H_2-TPR data

H_2-TPR analysis was performed to further investigate the effect of Nb doping on the redox properties of the catalysts. The complete reduction of bulk $NiAl_2O_4$ requires a high temperature (>900 °C) as shown in **Figure 3.6**, which is in a good agreement with the

reported values [29, 56, 57]. Deconvolution of the spinel peaks was performed based on the Gaussian model for qualitative investigation purposes.

A small peak at ~ 300 °C was observed for all catalysts, which is attributed to the reduction of nickel oxide on the surface of bulk spinel [29]. In addition, the SP catalyst presented a very small peak at 423 °C, which is attributed to a small quantity of the NiO phase (without any interaction with spinel surface) that could not be detected by XRD and other characterization techniques used in this study [58]. As seen from the deconvolution in **Figure 3.6**, two peaks are assigned to the spinel reduction for all catalysts. Based on the available literature, most of the cubic spinel lattice contains the ions in the octahedral sub-lattice and these have a greater chance of exposure on the surface of materials [59]. Therefore, it can be postulated that the first reduction peak of spinel ($SP_{[oct]}$) is related to the available nickel on the octahedral sites, while the second is corresponding the nickel ion in tetrahedral sites ($SP_{[tet]}$). The SP and SP-0.10 Nb showed very similar temperatures for $SP_{[oct]}$ and $SP_{[tet]}$, with a smaller reduction peak for $SP_{[oct]}$ than for SP-0.10 Nb as the only difference, which is strongly supported by XRD and UV-DRS data (**Figures 3.2** and **3.3**). The reduction temperature of $SP_{[oct]}$ becomes smaller and moved to higher temperature in SP-0.02 Nb than observed for SP which suggests a lower population of nickel ions in octahedral sites for this catalyst. The shift of the $SP_{[oct]}$ peak in SP-0.06 Nb to higher temperature followed the same trend as seen for SP-0.02 Nb. However, the peak positions of $SP_{[oct]}$ and $SP_{[tet]}$ were almost the same. XRD and UV-DRS data (**Figure 3.1** and **3.2)** support this observation and indicate the use of nickel for the formation of the columbite resulted in a decrease of nickel content in both sub lattices.

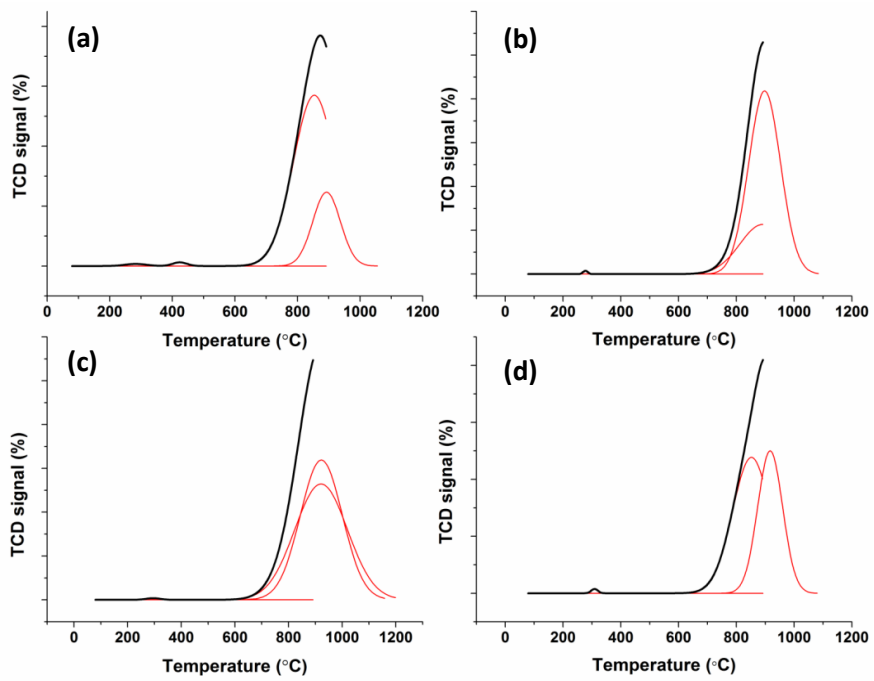

Figure 3.6 The first H_2-TPR analysis of SP-x Nb (x: **(a)**: 0, **(b)**: 0.02, **(c)**: 0.06 and **(d)**: 0.10).

The catalysts were reoxidised using oxygen as oxidant. It is well established that nickel atoms in the metallic state leave the lattice of spinel. Each type of generated metallic nickel atom will result in a different type of nickel oxide, and the second TPR can be viewed as a good technique to identify these species. As shown in **Figure 3.7**, three different types of NiO were identified after the reduction of the catalysts for the second time. The total peak area for two of the three formed nickel oxides decreases as the concentration of Nb increases in these catalysts. Based on XRD, UV-DRS and the first TPR data, SP-0.10 Nb has higher concentration of octahedrally coordinated nickel in the cubic spinel lattice (compared to the tetrahedral sites) than SP-0.06 Nb. In addition, the peak areas of $SP_{[oct]}$ decrease as the Nb content of these catalysts increases, suggesting that the presence of nickel in the octahedral sites diminished by addition of Nb. This discussion is well supported by the trend of peak intensities at 716 nm in the UV-DRS data in **Figure 3.3**.

Based on literature, the first reduction peak (~ 190 °C) in the second TPR data can be assigned to the reduction of Ni^{3+} [58]. This peak was only observed in SP and SP-0.02 Nb, which suggests that Ni^{3+} species possibly originated from the sites with octahedral coordination. In addition, the peaks at ~230 °C and 350 °C are assigned to the different crystallite sizes of NiO with no interaction with the support [58]. It is also well accepted that the NiO peak at temperatures below 400 °C originated from octahedral coordination, while the higher temperature peak is corresponding to tetrahedrally coordinated NiO supported on alumina [60]. Therefore, the observed peak at 550 °C is attributed to large particles of nickel oxide supported on alumina with tetrahedral coordination [58, 60]. This data agrees with the aforementioned characterization techniques and suggests that the available atomic nickel in tetrahedral sites of spinel are more difficult to be reduce and have a lower contribution to reduction in catalytic reactions.

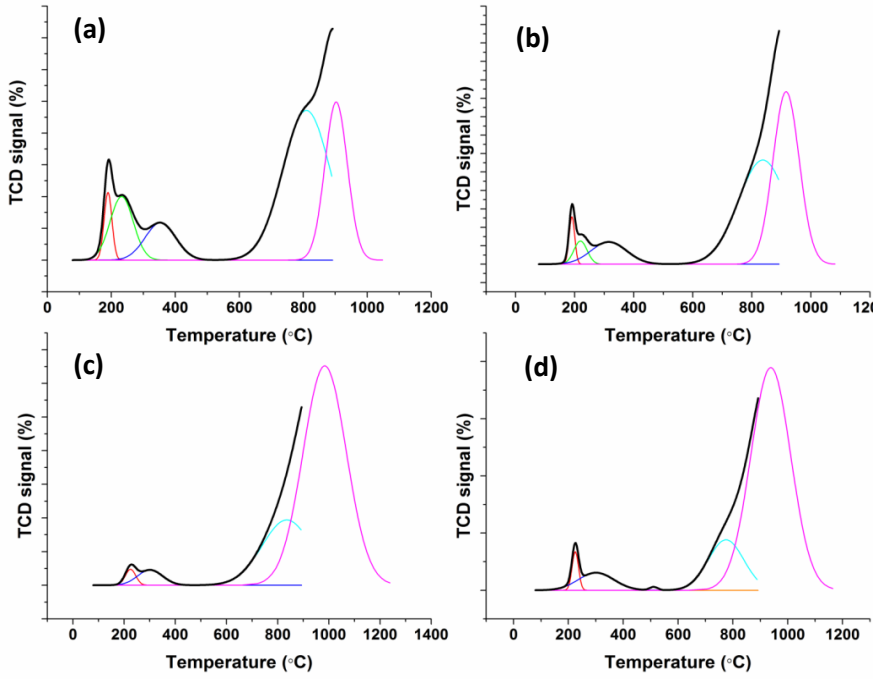

Figure 3.7 The second H_2-TPR analysis of SP-x Nb (x: **(a)**: 0, **(b)**: 0.02, **(c)**: 0.06 and **(d)**: 0.10).

3.3.6) Catalytic data

3.3.6.1) n-octane conversion:

A carbon to oxygen ratio (8:1) was chosen for this study because it seems that anaerobic conditions are more suitable for the ODH of medium chain paraffins [61]. The under study spinel based catalysts showed relatively good conversions under the chosen operating conditions (**Figure 3.8**). This suggests that the available nickel atoms on the surface of the spinel follow a redox cycle, which has been well established in the recent literature [29]. Therefore, a partial reduction of the spinel peak in H_2-TPR can be considered in each cycle, and following a number of these cycles, this seems to result in a lowering of the onset temperature of the reduction peak for this phase (**Figure 3.7** and **3.8**). Hence, higher reaction temperatures (450-550 °C) were considered for these catalysts due to possible advantage of a redox nature of nickel on the spinel surface. At 450 °C and 500 °C, the activities of these catalysts seem to decrease upon increasing the amount of niobium as a dopant. This behaviour seems to be driven by the decrease in the surface area (**Table 3.2)** or introduction of Nb in the octahedral sub-lattice of spinel and its subsequent effects on reduction temperatures (**Figure 3.6**). The catalysts containing the highest concentration of Nb atoms showed the lowest activity at 550 °C. The $NiNb_2O_6$ seems to be an inert phase (from the redox aspect) in ODH under the chosen reaction conditions. The detected NiO phase in the SP catalyst (based on the first H_2-TPR) in **Figure 3.6** seems to not contribute much to the activity, based on the activity data, and more investigations are required to discover the possible reason(s).

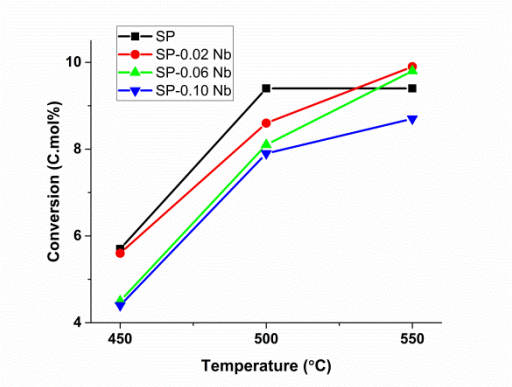

Figure 3.8 Catalytic conversion of *n*-octane over SP-x Nb (x: 0, 0.02, 0.06 and 0.10) catalysts. (Reaction conditions: C : O = (8 : 1), GHSV = 12000 h^{-1}, Concentration of *n*-octane in the feed = 11%)

3.3.6.2) Selectivity to different products:

The selectivity towards octene isomers generally increased with increasing Nb doping, at all temperatures. However, the selectivity over octene in SP-0.02 Nb was higher than over SP-0.06 Nb, suggesting that a high concentration of nickel ions in octahedral sub-lattices, compared to the tetrahedral sub-lattices, results in an increase in direct combustion of the feed and CO_2 formation. However, elevating the reaction temperature seems to have a negative impact on the selectivity towards octenes, suggesting the consecutive cracking and combustion of the primary products to secondary products (aromatics, cracked and CO_x) at high temperatures.

With the exception of SP-0.06 Nb, the selectivity towards aromatics decreased as the Nb content of these catalysts increased, which suggests that the majority of Nb in these catalysts is involved in the $NiNb_2O_6$ lattice and does not contribute to the catalytic role of the spinel phase. This trend shows the important role of physical surface characteristics, such as surface area, pore volume and diameter in catalytic conversion of octene isomers to aromatics. For instance, there is a direct correlation between pore volume and selectivity to aromatics.

However, the concentration of active sites (nickel in our case) in the pores is also important. Therefore, SP-0.06 Nb showed the lowest selectivity towards aromatics, which was expected from the UV-DRS and XRD data (**Figures 3.2** and **3.3**) for this catalyst, showing the maximum doping of Nb in both octahedral and tetrahedral sub lattices. In addition, the possible formed Ni^{3+} in trace quantities (**Figure 3.7**) can also be counted as possible active sites to facilitate the aromatics formation. Furthermore, the increase of the temperature positively affects the aromatics formation over the two least active catalysts (SP-0.06 Nb and SP-0.10 Nb). However, the most active catalysts showed a high propensity to crack the formed aromatics when the temperate was increased to 550 °C from 500 °C.

Olefin cracking is highly dependent on the surface acidity of the catalyst [4]. The catalytic data suggests the lowest selectivity to cracked products was obtained over SP-0.02 Nb, whereas SP showed the highest selectivity. This suggest that the substitution of $Ni_{[Oct]}$ sites with Nb resulted in lower selectivity towards cracked products, however, the contributions of $NiNb_2O_6$ on the surface acidity and area, as well as doping created a complex set of results for interpretation of this catalytic data, which is out of the scope of the current study.

The selectivity towards CO_x seems to exactly follow the order of Nb substitution in the octahedral and tetrahedral sites as determined by XRD (**Figure 3.2**), UV-DRS (**Figure 3.3**) and H_2-TPR (**Figure 3.5**) analyses. The two catalysts containing similar $Ni_{[Oct]}/Ni_{(Tet)}$ ratios, SP and SP-0.10 Nb showed very similar selectivity to CO_x, while the catalyst with low nickel occupation in both sites (SP-0.06 Nb) and low oxygen vacancies (due to high loading of Nb as a High Valance Dopant [HVD]) seems to accelerate the CO_x formation. However, the low concentration of Nb in SP-0.02 Nb seems to be beneficial for minimizing selectivity to CO_x, possibly due to a balance between $Ni_{[Oct]}/Ni_{(Tet)}$ which thus facilitate the Ni migration

between the two sub-lattices. This migration in bivalent poly-metal oxides seems to be highly dependent on oxygen or ionic vacancies in their lattices, which seems to be tuned in $NiAl_2O_4$ by addition of Nb.

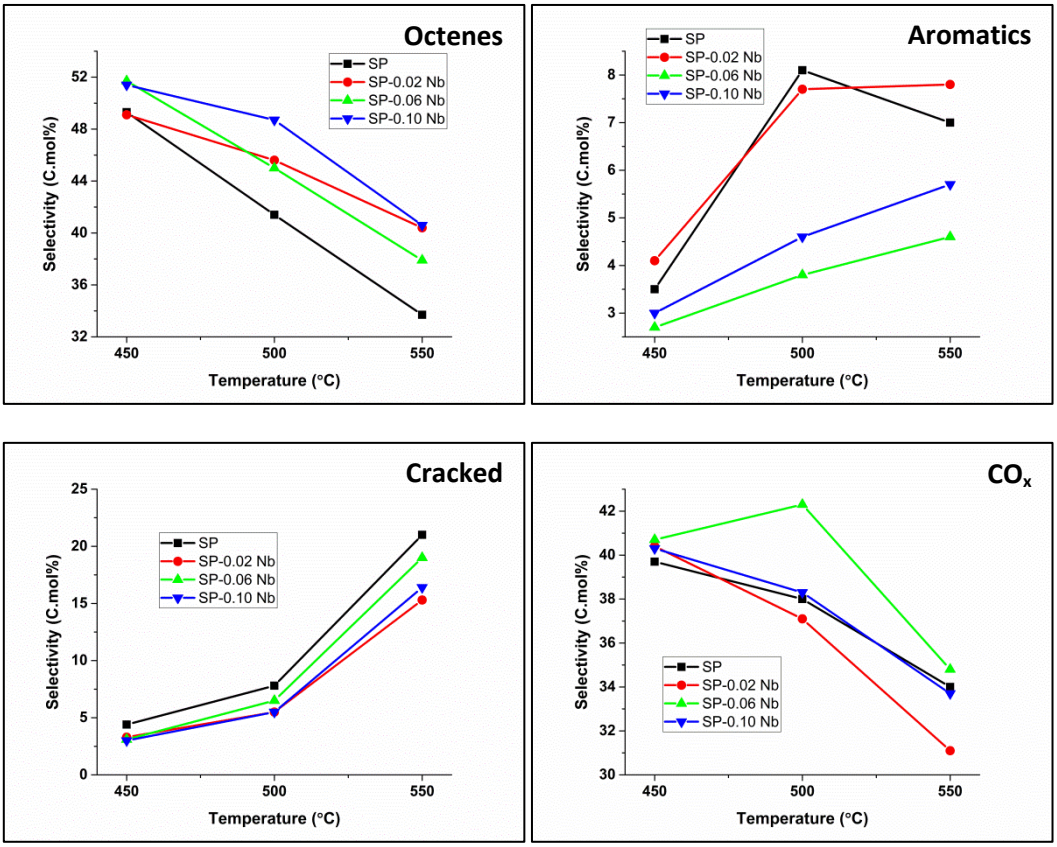

Figure 3.9 Catalytic selectivity to different products of SP-x Nb (x: 0, 0.02, 0.06 and 0.10). (Reaction conditions: C : O = (8 : 1), GHSV = 12000 h^{-1}, Concentration of *n*-octane in the feed = 11%)

The selectivity to aromatic products could provide evidence for the reaction pathways in this system. It seems high temperature (550 °C) is required to form o-xylene over all catalysts (**Figure 3.10**). Ethylbenzene seems to be the dominant aromatic over SP, while catalysts containing Nb seem to give styrene as the dominant aromatic over all temperature ranges, indicating that Nb accelerates the acid-base catalysed reactions (**Figure 3.10**). Catalysts with

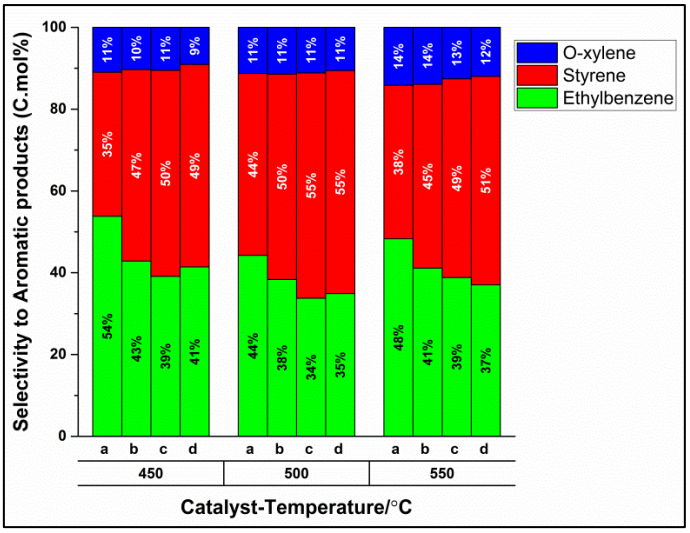

Figure 3.10 Selectivity towards different aromatic products; a) SP, b) SP-0.02 Nb, c) SP-0.06 Nb and d) SP-0.10 Nb. (Reaction conditions: C : O = (8 : 1), GHSV = 12000 h^{-1}, Concentration of *n*-octane in the feed = 11%)

a combination of the acidic and basic sites are believed to be suitable for transformation of ethylbenzene to styrene [62]. However, a volcano type of behaviour was observed in selectivity to styrene over all catalysts at the different temperatures, suggesting the participation of non-oxidative dehydrogenation (DH) (to form ethylbenzene from octene) over these catalysts (**Figure 3.10**), which was in agreement with an increase in the detection of hydrogen (data available in Appendix). The breakdown of selectivity to different octene isomers, CO and CO_2 also can be found in the Appendix. In addition, a calculation of produced H_2 from the products formed and detected H_2 shows (**Appendix 3.3)** that ODH is dominant over all catalysts and Nb introduction further suppresses the already minor dehydrogenation pathway existing for SP and promotes the ODH pathway.

3.3.7) Coke analysis

Slight coke formation in the unsteady state was expected, since a somewhat anaerobic condition C:O (8:1) was chosen for this catalytic testing. To determine the catalyst stability and to estimate the possible coking, all catalysts were subjected to a time-on-stream analysis at 500 °C. After reaching steady state, (no change in the activity and selectivity observed) the catalysts were run for a further 48 h, showing the stability of these catalysts in time on line applications. The reactor was switched off after 48 hours and the catalysts were cooled down under nitrogen and subjected to coke analysis.

The TGA data showed mass losses of 4%, 2%, 2% and 1.5% for the used SP, SP-0.02 Nb, SP-0.06 Nb and SP-0.10 Nb catalysts, respectively (**Appendix 3.4**). The data in **Figure 3.11** shows the different types of coke formed on the surface of these catalysts. SP showed two different types of coke that could be removed at 462 °C (soft coke) and 596 °C (hard coke), respectively (**Figure 3.11**). However, the small peak of hard coke for this catalyst seems to be the coke formed on the available NiO phase detected by H_2-TPR (**Figure 3.6**) in this catalyst, since this peak was absent for the others (**Figure 3.11**). The peak corresponding to the soft coke moved slightly to higher temperature with decrease in the peak area upon introduction of Nb in the catalysts. This trend suggests that Nb introduction increases the acidity of the catalysts (coke on stronger acidic sites need higher temperature to be removed) [63] and the amount of coke seems to be directly dependent on the surface area (which can be due to doped spinel or excess columbite phase) of the catalysts. However, other characterization data of the used catalysts showed decrease in the crystallite sizes, increase in surface areas and nickel migration between the two sub-lattices of the cubic spinel catalysts during the catalytic testing. Coke formation, the redox cycle and heat treatment during the catalytic tests are only possible causes for the aforementioned changes in the catalysts, such as change in Ni distribution between two sub-lattices of the spinel, change in BET surface

area and slight change of crystallite sizes when fresh and used catalysts were compared. Thus, *in situ* XRD study on the SP-0.02 Nb was done in an attempt to discover the main parameter for these changes.

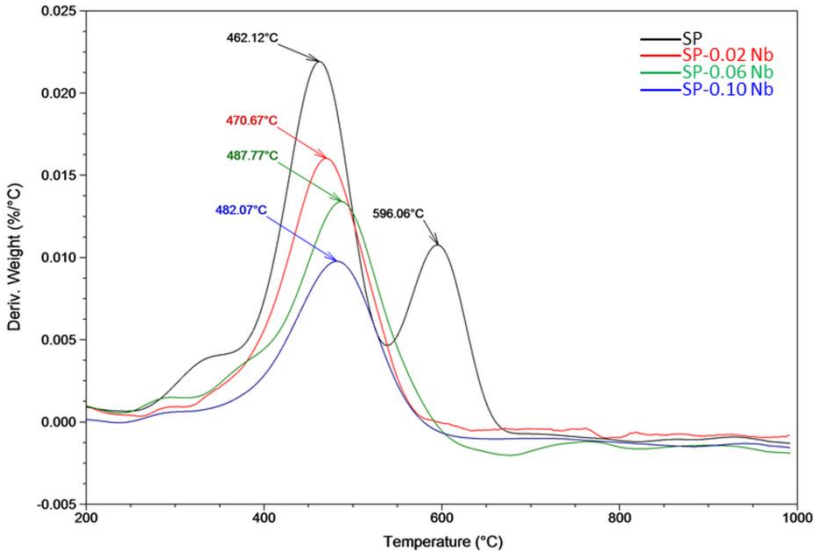

Figure 3.11 TGA analysis of the used SP-x Nb (x: 0, 0.02, 0.06 and 0.10) under flow of air.

The *in situ* XRD data of fresh SP-0.02 Nb under reduction and oxidation conditions from 100-600 °C is available in **Appendix 3.5**. This data suggests no nickel migration or crystallite size change when redox cycles at various temperatures were examined. This observation implies the positive impact of low levels coking on the $NiAl_2O_4$ spinel and shows why many reports discuss the coke resistivity of this spinel in different catalytic applications [29, 34, 35, 64].

The above discussion suggests that coke formation facilitates the nickel migration to the surface by capturing the migrated Ni ion and enhancing the catalytic activity and reducing the crystallite sizes of the catalysts, which resulted in $NiAl_2O_4$ with higher surface area and smaller crystallite size compared to the fresh catalysts. In addition, the TEM image of used

SP-0.02 Nb was compared to the fresh one. This comparison shows the presence of very small crystals (4-5 nm), which are absent in the fresh catalyst. The lattice fringes of these small crystals were comparable with the calculated d spacing value from the XRD (**Figure 3.12**). However, the d spacing in the observed small crystals of the used catalyst (0.2094 nm) is slightly higher than the fresh catalyst (0.2013 nm), which proves that the peak broadening is the result of the appearance of these small crystals after the catalytic testing.

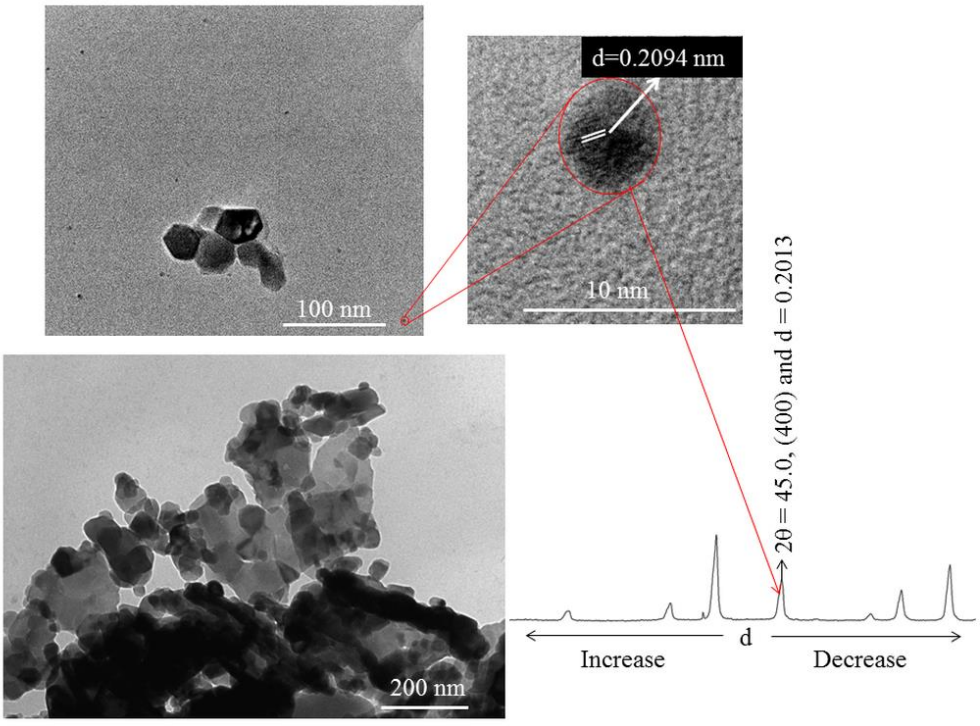

Figure 3.12 The comparison of the (a) used and the (b) fresh SP-0.02 Nb. The lattice fringe (d spacing) of the small crystal (appeared after the testing) of the used SP-0.02 Nb was measured using HR-TEM (c) and compared to the d spacing value obtained from PXRD.

3.4) Conclusion

The niobium seems to preferably replace the nickel in the octahedral sub-lattice of spinel. This dopant was also found to be able to replace both Al^{3+} and Ni^{2+}, possibly due to similar ionic radii. This occupancy resulted in modification of nickel migration, electronic profile,

redox properties and surface textures. The addition of niobium also was found to decrease the redox capability of $NiAl_2O_4$ and increase the density of the acidic sites in each catalyst. Generally, the crystallite sizes and degree of inversion of spinel were reduced when the used catalysts were compared to the as-prepared catalysts. The slight coking of the catalysts (under somewhat anaerobic conditions) was found to facilitate the migration of nickel from octahedral to tetrahedral sites, which was accompanied with the reduction of the crystallite sizes when used and fresh catalysts were compared.

3.5) Acknowledgments

We thank SASOL and the National Research Foundation, South Africa (NRF) for their financial supports. We also thank the Electron Microscopy Unit at the University of KwaZulu-Natal (Westville campus).

3.6) References

[1] S. Pradhan, J.K. Bartley, D. Bethell, A.F. Carley, M. Conte, S. Golunski, M.P. House, R.L. Jenkins, R. Lloyd, G.J. Hutchings, Nat. Chem., 4 (2012) 134-139.

[2] B. Pillay, M.R. Mathebula, H.B. Friedrich, Appl. Catal., A, 361 (2009) 57-64.

[3] E. Romera, C. Lamotte, P. Bodart, Process for the purification of medium-chain olefins, Fina Research S.A., 1998.

[4] J.J.H.B. Sattler, J. Ruiz-Martinez, E. Santillan-Jimenez, B.M. Weckhuysen, Chem. Rev., 114 (2014) 10613-10653.

[5] C.A. Carrero, R. Schlögl, I.E. Wachs, R. Schomaecker, ACS Catal., 4 (2014) 3357-3380.

[6] C.A. Gärtner, A.C. van Veen, J.A. Lercher, ChemCatChem, 5 (2013) 3196-3217.

[7] M.I. Fadlalla, H.B. Friedrich, Catal. Sci. Tech., 4 (2014) 4378-4385.

[8] J. Chetty, V.D.B.C. Dasireddy, S. Singh, H.B. Friedrich, React. Kinet. Mech. Cat., 120 (2017) 307-321.

[9] F. Cavani, N. Ballarini, A. Cericola, Catal. Today, 127 (2007) 113-131.

[10] R. Grabowski, Catal. Rev., 48 (2006) 199-268.

[11] E. Heracleous, A.A. Lemonidou, J. Catal., 237 (2006) 162-174.

[12] L. Smoláková, M. Kout, E. Koudelková, L. Čapek, Ind. Eng. Chem. Res., 54 (2015) 12730-12740.

[13] J.P. Bortolozzi, E.D. Banús, N.L. Courtalón, M.A. Ulla, V.G. Milt, E.E. Miró, Catal. Today, 273 (2016) 252-258.

[14] H. Zhu, D.C. Rosenfeld, D.H. Anjum, V. Caps, J.-M. Basset, ChemSusChem, 8 (2015) 1254-1263.

[15] X. Sun, B. Li, H. Metiu, J. Phys. Chem. C, 117 (2013) 23597-23608.

[16] J.-M. Basset, H. Zhu, D.C. Rosenfeld, P. Laveille, Solid-state synthesis of nickel oxide-based oxidative dehydrogenation catalysts for alkene manufacture from alkanes, Dow Global Technologies LLC, USA . 2016, p. 19pp.

[17] S.-B. Ivan, I. Popescu, I. Fechete, F. Garin, V.I. Parvulescu, I.-C. Marcu, Catal. Sci. Tech., 6 (2016) 6953-6964.

[18] W. Weng, M. Davies, G. Whiting, B. Solsona, C.J. Kiely, A.F. Carley, S.H. Taylor, Phys. Chem. Chem. Phys., 13 (2011) 17395-17404.

[19] Z. Skoufa, G. Xantri, E. Heracleous, A.A. Lemonidou, Appl. Catal., A, 471 (2014) 107-117.

[20] L. Smoláková, Š. Botková, L. Čapek, P. Priecel, A. Sołtysek, M. Kout, L. Matějová, Chinese J. Catal., 34 (2013) 1905-1913.

[21] R. Collongues, D. Gourier, A. Kahn-Harari, A.M. Lejus, J. Thery, D. Vivien, Annu. Rev. Mater. Sci., 20 (1990) 51-82.

[22] W. Chu, W. Yang, L. Lin, Appl. Catal., A, 235 (2002) 39-45.

[23] T.H. Gardner, J.J. Spivey, E.L. Kugler, A. Campos, J.C. Hissam, A.D. Roy, J. Phys. Chem. C, 114 (2010) 7888-7894.

[24] B. Dou, B. Jiang, Y. Song, C. Zhang, C. Wang, H. Chen, B. Du, Y. Xu, Fuel, 166 (2016) 340-346.

[25] N. Salhi, C. Petit, A. Kiennemann, Stud. Surf. Sci. Catal., 174B (2008) 1335-1338.

[26] Y.S. Han, J.B. Li, X.S. Ning, B. Chi, J. Am. Ceram. Soc., 87 (2004) 1347-1349.

[27] K. Zhang, G. Zhou, J. Li, T. Cheng, Catal. Commun., 10 (2009) 1816-1820.

[28] M. Machida, K. Eguchi, H. Arai, J. Catal., 120 (1989) 377-386.

[29] J.L. Rogers, M.C. Mangarella, A.D. D'Amico, J.R. Gallagher, M.R. Dutzer, E. Stavitski, J.T. Miller, C. Sievers, ACS Catal., 6 (2016) 5873-5886.

[30] J. Deng, M. Cai, W. Sun, X. Liao, W. Chu, X.S. Zhao, ChemSusChem, 6 (2013) 2061-2065.

[31] N.F.P. Ribeiro, R.C.R. Neto, S.F. Moya, M.M.V.M. Souza, M. Schmal, Int. J. Hydrogen Energy, 35 (2010) 11725-11732.

[32] M.D. Farahani, J. Valand, A.S. Mahomed, H.B. Friedrich, Catal. Lett., 146 (2016) 2441-2449.

[33] Y. Kathiraser, W. Thitsartarn, K. Sutthiumporn, S. Kawi, J. Phys. Chem. C, 117 (2013) 8120-8130.

[34] I.E. Achouri, N. Abatzoglou, C. Fauteux-Lefebvre, N. Braidy, Catal. Today, 207 (2013) 13-20.

[35] C. Fauteux-Lefebvre, N. Abatzoglou, N. Braidy, I.E. Achouri, J. Power Sources, 196 (2011) 7673-7680.

[36] D. Li, M. Koike, L. Wang, Y. Nakagawa, Y. Xu, K. Tomishige, ChemSusChem, 7 (2014) 510-522.

[37] T.H. Gardner, D. Shekhawat, D.A. Berry, M.W. Smith, M. Salazar, E.L. Kugler, Appl. Catal., A, 323 (2007) 1-8.

[38] Z. Boukha, C. Jiménez-González, B. de Rivas, J.R. González-Velasco, J.I. Gutiérrez-Ortiz, R. López-Fonseca, Appl. Catal., B, 158–159 (2014) 190-201.

[39] H.S.C. O'Neill, W.A. Dollase, C.R. Ross, Phys. Chem. Miner., 18 (1991) 302-319.

[40] C.O. Arean, M.L.R. Martinez, A.M. Arjona, Mater. Chem. Phys., 8 (1983) 443-450.

[41] E.W. McFarland, H. Metiu, Chem. Rev., 113 (2013) 4391-4427.

[42] X. Sun, B. Li, H. Metiu, J. Phys. Chem. C, 117 (2013) 23597-23608.

[43] I. Popescu, Z. Skoufa, E. Heracleous, A. Lemonidou, I.-C. Marcu, Phys. Chem. Chem. Phys., 17 (2015) 8138-8147.

[44] C.O. Augustin, K. Hema, L.J. Berchmans, R. Kalai Selvan, R. Saraswathi, Phys. Status Solidi a, 202 (2005) 1017-1024.

[45] D. Teschner, E. Vass, M. Hävecker, S. Zafeiratos, P. Schnörch, H. Sauer, A. Knop-Gericke, R. Schlögl, M. Chamam, A. Wootsch, A.S. Canning, J.J. Gamman, S.D. Jackson, J. McGregor, L.F. Gladden, J. Catal., 242 (2006) 26-37.

[46] J. McGregor, Z. Huang, E.P.J. Parrott, J.A. Zeitler, K.L. Nguyen, J.M. Rawson, A. Carley, T.W. Hansen, J.-P. Tessonnier, D.S. Su, D. Teschner, E.M. Vass, A. Knop-Gericke, R. Schlögl, L.F. Gladden, J. Catal., 269 (2010) 329-339.

[47] S. Gomez Sanz, L. McMillan, J. McGregor, J.A. Zeitler, N. Al-Yassir, S. Al-Khattaf, L.F. Gladden, Catal. Sci. Tech., 5 (2015) 3782-3797.

[48] C.H. Collett, J. McGregor, Catal. Sci. Tech., 6 (2016) 363-378.

[49] A. Koch, A. Phukan, O.B. Chanu, A. Kumar, R.A. Lal, J. Mol. Struct., 1060 (2014) 119-130.

[50] H.B. Friedrich, A.S. Mahomed, Appl. Catal., A, 347 (2008) 11-22.

[51] V.D.B.C. Dasireddy, S. Singh, H.B. Friedrich, Appl. Catal., A, 421–422 (2012) 58-69.

[52] S. Lei, C. Wang, D. Guo, X. Gao, D. Cheng, J. Zhou, B. Cheng, Y. Xiao, RSC Adv., 4 (2014) 52740-52748.

[53] B. Savova, S. Loridant, D. Filkova, J.M.M. Millet, Appl. Catal., A, 390 (2010) 148-157.

[54] B.P. Ladgaonkar, A.S. Vaingankar, Mater. Chem. Phys., 56 (1998) 280-283.

[55] P. Priecel, D. Kubička, L. Čapek, Z. Bastl, P. Ryšánek, Appl. Catal., A, 397 (2011) 127-137.

[56] C. Jiménez-González, Z. Boukha, B. de Rivas, J.R. González-Velasco, J.I. Gutiérrez-Ortiz, R. López-Fonseca, Energy & Fuels, 28 (2014) 7109-7121.

[57] L. Zhou, Y. Guo, J.M. Basset, H. Kameyama, Chem. Commun., 51 (2015) 12044-12047.

[58] S.R. Kirumakki, B.G. Shpeizer, G.V. Sagar, K.V.R. Chary, A. Clearfield, J. Catal., 242 (2006) 319-331.

[59] J.P. Jacobs, A. Maltha, J.G.H. Reintjes, J. Drimal, V. Ponec, H.H. Brongersma, J. Catal., 147 (1994) 294-300.

[60] C. Li, Y.-W. Chen, Thermochim. Acta, 256 (1995) 457-465.

[61] J. Zhang, X. Liu, R. Blume, A. Zhang, R. Schlögl, D.S. Su, Science, 322 (2008) 73-77.

[62] W. Weiss, D. Zscherpel, R. Schlögl, Catal. Lett., 52 (1998) 215-220.

[63] K. Nakajima, Y. Baba, R. Noma, M. Kitano, J. N. Kondo, S. Hayashi, M. Hara, J. Am. Chem. Soc., 133 (2011) 4224-4227.

[64] N. Salhi, A. Boulahouache, C. Petit, A. Kiennemann, C. Rabia, Int. J. Hydrogen Energy, 36 (2011) 11433-11439.

Chapter four

Niobium, as a modifier of the "confinement effect", in ordered mesoporous $NiO\text{-}Al_2O_3$ catalysts with nanorod morphology, used for activation of *n*-octane

Abstract

Four catalysts with different loading of Nb with the general formula of 25 wt% [$NiO\text{-}Nb_2O_5$]/Al_2O_3 were prepared via glycol-thermal synthesis. These nano-composites were characterised using powder and *in situ* XRD, N_2-physisorption analysis, NH_3-TPD, SEM, TEM and HR-TEM techniques. The formation of ordered mesoporous nano-composites with nanorod like morphology was shown using glycol-thermal technique. In addition, the synthesis of template free ordered mesoporous alumina (OMA) can be achieved using glycol-thermal technique. The materials were investigated as catalysts for the oxidative dehydrogenation of *n*-octane. The catalytic and characterization data suggest the presence of a strong "confinement effect" between NiO and the mesoporous structure of Al_2O_3 in the absence of Nb , whereas the addition of Nb was shown to weaken the $NiO\text{-}Al_2O_3$ interactions and subsequently the "confinement effect". This change in the chemical nature of nickel on each catalysts and added acidity via addition of Nb, in the presence of similar surface textures for all catalysts gave, different catalytic results, which gave insight on the ODH system over nickel based catalysts. The lattice oxygen, $O^{-2}{}_{latt.}$, with high entropy, radical reactions (originated from Nb_2O_5 sites), available electrophilic oxygen species (especially at high temperatures) and high acidity of the catalysts (with high Nb loading) were found to accelerate the pathway that results in CO_x formation from *n*-octane.

4.1) Introduction

The dehydrogenation (DH) of paraffins and their transformation to olefins is a commercially established technique [1]. This reaction has the advantage of high selectivity towards the olefins [1]. However, drawbacks of this process are its being endothermic, coke formation and the low equilibrium conversion [1]. Therefore, high operating temperatures and frequent catalyst regenerations are required to have a constant production output in time on line process [1]. The need for an efficient replacement for the DH process has motived researchers in the field to conduct a wide spectrum of investigations on the oxidative dehydrogenation (ODH) of paraffins. The ODH is an exothermic reaction, which makes it operable at lower temperatures than the temperature in DH [2-4]. Coke formation is normally minimal in ODH reactions and the reverse water gas shift reaction (RWGS) decreases the limiting role of the equilibrium conversion in DH [4]. However, the major disadvantage of this reaction is a high production of carbon containing greenhouse gases such as CO_2, CO and CH_4, which prevents it from achieving commercialization [2-4].

The oxidative dehydrogenation (ODH) of short-chain paraffins to olefins has been widely discussed in a large body of patents, technical articles and reviews [2-6]. In contrast, less attention has been paid to the ODH of medium-chain paraffins, mainly due to the complex analysis of the catalysts and the formed products [5, 7-14]. However, a large quantity of these medium-chain paraffins arises from the production of liquid fuels from coal, biomass and natural gas [5, 7]. Furthermore, the produced medium-chain alkenes are gaining considerable importance for the production of alcohols or aldehydes, synthetic lubricants and as co-polymers with short-chain olefins [15].

Transition metal oxides are known as the right tools for the ODH of paraffins [3, 4, 6]. Amongst them, nickel oxide based catalysts have attracted attention due to their capabilities of activating paraffins at relatively low temperatures [4]. Non-modified bulk nickel oxide seems to facilitate the deep oxidation of the introduced paraffin and results in high selectivity towards CO_x [16, 17]. However, most of the doped NiO catalysts showed enhanced ODH catalytic activity [16-20]. The surface of the bulk NiO catalyst seems to have a high concentration of non-stoichiometric oxygen species (electrophilic) that are known to be responsible for the direct combustion of the paraffins [16, 17]. Generally, supported or doped NiO seems to have an efficient Mars van Krevelen (MvK) type mechanism compared to the bulk nickel oxide, and suppresses the formation of electrophilic oxygen species on the surface of NiO [21]. There are different schools of thought about this positive impact on the ODH over the doped or supported NiO.

The elements Nb [16-18, 22-32], Ta [21, 33], W [20, 34-36], Zr [37, 38], Mo [39], Ce [37, 40-42], Mg [21], Al [21, 37, 43, 44], Ga [21], Ti [20, 21], Sn [20, 37, 45, 46], Co [47], P [19, 24], Bi [48], and La [37] have been investigated as dopants in recent years and showed to improve the catalytic activity of NiO in the ODH of paraffins. Furthermore, the use of different supports [41, 47-54] and even physical mixing with the doped metal (followed by calcination) [20, 30, 55] seem to improve the catalytic performance. The physicochemical characteristics and catalytic performance of doped nickel oxide are not only affected by the type of dopant, but also the used synthetic techniques to prepare these catalysts [20]. However, the hypotheses behind the promotional effect of introduced dopants are still controversial and, therefore, more investigations are required.

The studies done by Heracleous and Lemonidou (in 2006) seem to be one of the first detailed investigations in the application NiO for the ODH of ethane [16, 17]. The reduction of non-stoichiometric oxygen species on the surface of the catalyst and an enhanced MvK mechanism upon the addition of Nb as a dopant was concluded from their work. They showed that $O^{-2}_{latt.}$, originated from the lattice of NiO is responsible for the selective ODH reaction [16, 17]. However, Millet and co-workers (in 2010) questioned the original hypothesis by using O_2-TPD-MS and showed that O^- species (electrophilic), which are strongly bonded to the surface of Nb doped NiO, are responsible for ODH [23]. Metiu and co-workers (in 2013), using a computational approach, could prove that NbO_2 ions in many ways act as a low valence dopant (LVD) and activate the neighbouring and chemisorbed $O^-_{2\,latt.}$, which almost supports both of the aforementioned studies by proposing that the surface lattice is involved in the MvK mechanism [27]. Marcu, Lemonidou and co-workers (in 2015) conducted an *in situ* electro-conductive analysis, since NiO is a P-type semiconductor, and updated their original hypothesis [29]. According to their study, $O^{-2}_{latt.}$ reacts with the positive holes of Nb doped NiO and results in the formation of $O^-_{latt.}$, which can selectively abstract the hydrogen from the ethane and form ethene [29]. Very recently, Basset and co-workers prepared doped NiO using different dopants and concluded that the incorporation of foreign metals in the NiO and formation of a solid solution results in a decrease of positive holes. These positive holes are charge carriers in the NiO lattice and lowering their formation suppresses the formation of electrophilic oxygen species, which are believed to be the sites for the direct combustion of the paraffins [20, 55].

On the other hand, an increase of porosity seems to enhance ODH activity and this can be provided by porous supports containing alumina [41, 43, 44, 47, 48, 53, 56]. These mesoporous materials have attracted considerable attention in catalysis among other types of

porous material. Mesoporous materials provide advantages such as high surface areas with large pore volumes, which generally enhance the performance of materials in terms of energy and power density, stability and life-time [57, 58]. Most of the common procedures for the synthesis of ordered mesoporous materials require the use of expensive templates. However, the available template free methods for preparation of mesoporous materials result in disordered mesoporous materials, with high crystallinity and low stability in catalytic applications [57, 58]. The work done by Yuan *et al.* and modified by Morris *et al.,* are among the best techniques for the preparation of ordered mesoporous Al_2O_3 (OMA) [59, 60]. However, these pioneering works and more complicated synthesis techniques of OMA require the use of different expensive templates. To the best of our knowledge, there is no template free synthesis for the preparation of OMA and the introduction of a template free technique is a point of great interest, since the high costs of the templates can be avoided.

The above discussion motivated us to conduct a study on 25 wt% [Ni and Nb (in oxide forms)] with 75 wt% Al_2O_3 as the major matrix and to conduct the synthesis *in situ* using a glycol thermal method. This preparation technique gave us four ordered mesoporous catalysts with different Nb and Ni loading and almost similar physical textures, which is helpful for probing only chemical characteristics of these materials. The interactions between Nb and Ni were analysed using different characterization techniques and linked to the catalysis application. Finally, the mentioned hypotheses were investigated on the *n*-octane system to gain more insight into the ODH of paraffins using nickel based catalysts.

4.2) Experimental

4.2.1) Materials

$Ni(NO_3)_2.6H_2O$ (ACS reagent grade), $Al(NO_3)_3.9H_2O$ (ACS reagent grade) and $C_4H_4NNbO_9.xH_2O$ (99.99% trace metals basis) were purchased from Sigma-Aldrich and freshly used. Ammonia solution (25%) was used to adjust the pH during the synthesis. De-ionized water was used for all steps of the synthesis. For catalytic testing, synthetic air (UHP) and nitrogen (UHP) were produced in-house using Peak Scientific generators and *n*-octane with the assay of >98% was purchased from Alfa Aesar. Argon, helium and hydrogen cylinders (instrumental grade) were purchased from Afrox and used for GC analysis. 5% NH_3/He was used for the NH_3-TPD experiment.

4.2.2) Glycol-thermal synthesis of 25% (NiO-Nb_2O_5)/Al_2O_3

The required amount of Ni, Nb and Al salts were weighed and dissolved in 500 ml water with stirring. Then, ammonia solution was added to adjust the pH to nine, which resulted in the formation of a precipitate. The solution was allowed to stir for a few extra minutes to insure that the precipitation was complete and there was no metallic ion left in the solution. The precipitate was filtered off under vacuum. The precipitate was washed three times using water. The formed, wet precipitate was transferred from the Buchner funnel to a Parr reactor vessel, followed by addition of 200 ml of ethylene glycol. Then, the vessel was loaded in a Parr reactor and the temperature was set at 200 °C and rotation speed of 300 rpm. The reaction was carried out overnight and the maximum self-generated pressure was between 130-150 psi (depending on the ratio between the used precursors). Thereafter, the formed thick gel was transferred and washed with water, using a vacuum filter to remove any unreacted ethylene glycol. The thick gel was left under an IR lamp (power = 200 W)

overnight. Finally, the formed hard solid was crushed using a mortal and pestel and calcined under flow of air at 450 °C for six hours.

4.2.3) Oxidative dehydrogenation of *n*-octane

The catalytic testing was performed in a continuous flow fixed bed reactor (in vertical flow mode). A stainless steel tube with the 10 mm ID and 200 mm length was used as a reactor tube while the catalysts particles were loaded in the isothermal zone. To eliminate the occurrence of homogenous gas phase reaction, the voids were filled with carborundum (40 gritt, Polychem). 0.4 ml (~0.3 g) of fresh catalyst with the particle size of 300-600 μm was mixed with the same volume of carborundum in the catalyst bed. All reactions were carried out in the range of 360-440 °C at 40 °C intervals. Nitrogen used as an inert gas, air was used as a source of oxygen and *n*-octane was the chosen paraffin for this study. To maintaine the GHSV and vary the C:O ratio, the ratio between the air and nitrogen was adjusted. The concentration of *n*-octane in the reactant steam was 7%.

4.2.4) Physicochemical characterization

A powder X-Ray diffractometer (Bruker D8 Advance) equipped with a copper radiation source (λ = 1.5406 nm) was used to analyse the phase composition of the prepared materials. The redox properties of the materials were investigated using an *in situ* XRD Anton Paar XRK 900 reaction chamber. The bulk composition of synthesised composites were confirmed with Inductively Coupled Plasma-Optical Emission Spectroscopy using a PerkinElmer Precisely Optima 5300DV, after the sample was digested in H_2SO_4 (98%, Merck). Nitrogen physisorption measurements were done using a Micromeritics Tristar II. Samples were degassed under flow of N_2 at 200 °C with a Micromeritics flow prep 060 overnight prior to each BET analysis. The catalyst morphology was viewed using a Ziess

Ultra plus Scanning Electron Microscope (SEM). The bulk structures of the catalysts were viewed using a Jeol JEM-2100, while a High Resolution-Transmission Electron Microscope (HR-TEM) was used (in STEM mode) to determine the elemental distribution (mapping).

4.3) Results and discussion

4.3.1) PXRD

Figure 4.1 shows the PXRD diffractograms of the studied catalysts. All catalysts showed very broad peaks, which is an indication of the small crystallite sizes for all phases. This observation suggests a high dispersion of the loaded metal oxides. Three phases were detected in the NiAl Catalyst, NiO, Al_2O_3 and $NiAl_2O_4$. The small intensity of the $NiAl_2O_4$ spinel phase implied its formation in this catalyst with an amorphous texture in a small quantity. Normally, the formation of this phase is thermodynamically difficult and it seems to present larger crystallite sizes than NiO in NiO-Al_2O_3 systems [61]. 2Ni1Nb showed approximately the same characteristics as NiAl, with the smaller intensity for NiO peaks as the only difference. This small difference was expected, since a lower loading of NiO was targeted during the synthesis. 1Ni2NbAl did not follow this trend and showed a larger crystallite size of NiO, using Al_2O_3 peaks as reference. Finally, NbAl showed the loading of Nb_2O_5 on Al_2O_3 with very small crystallite sizes (by comparing the broadness of Nb_2O_5 peaks to the present peak of Al_2O_3 in this catalyst), which was expected since niobium ammonium oxalate was used during the synthesis [16, 23]. The PXRD pattern of the blank Al_2O_3 prepared with this technique is available in appendix (**Appendix 4.1**). Overall, the PXRD data shows that highly dispersed metal oxides with small crystallite sizes can be obtained using the glycol-thermal synthesis, which are known as catalytically interesting materials in different applications.

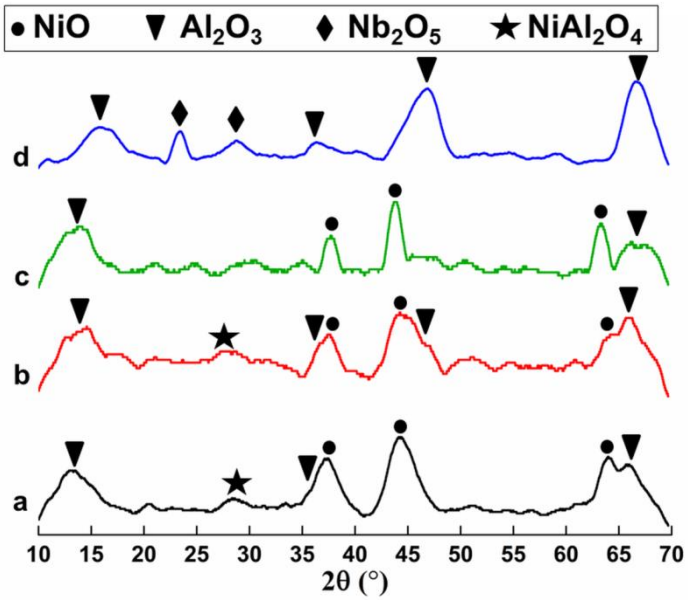

Figure 4.1 The PXRD of Ni(3-x)Nb(x)Al (X= 3, 2, 1, 0). a) NiAl, b) 2Ni1NbAl, c) 1Ni2NbAl and d) NbAl.

4.3.2) ICP and N_2 physisorption analysis

ICP results (**Table 4.1**) show that the targeted elemental compositions for these catalysts were achieved. The nitrogen physisorption analysis was performed to further investigate the surface texture of these catalysts. These materials have high surface areas, which could be expected from the PXRD data (**Figure 4.1**) since broad peaks (indication of small crystallite sizes) were observed. The addition of niobium increased the surface areas of the prepared catalysts. Thus, the lowest BET surface area was found for NiAl (235 m^2/g) and the highest for NbAl (349 m^2/g), as shown in **Table 4.1**. NiAl and 2Ni1NbAl showed lower surface areas than the blank alumina synthesised using the glycol-thermal technique, which can be due to formation of $NiAl_2O_4$ spinel in these catalysts [61]. Furthermore, the formation of the amorphous Nb_2O_5 using ammonium niobium oxalate as a precursor seems to positively influence the surface area, which is in good agreement with other reports [16, 23]. Generally, the pore diameters decreased upon the addition of Nb (**Table 4.1**), which is well within the

expected trend of observed BET surface area. However, the pore volumes did not change considerably when the Nb concentration was varied, except in the case for 1Ni2NbAl that had values close to pure alumina synthesised using this technique (**Table 4.1**).

Table 4.1. The BET surface areas, pore volumes, average pore sizes and elemental compositions for all catalysts.

Catalyst	BET surface area (m^2/g)	Pore volume (cm^3/g)	Average pore diameter (nm)	Compostion (wt%)[a]
				$NiO/NiO+Nb_2O_5$
NiAl	235	0.44	7.5	-
2Ni1NbAl	287	0.45	6.4	2.04/3
1Ni2NbAl	337	0.54	6.4	1.14/3
NbAl	349	0.45	5.2	-
Al	296	0.6	6.8	-

a. Calculated using ICP.

Figure 4.2 a displays the nitrogen adsorption-desorption isotherms of all catalysts. All materials show type IV isotherms with H1 hysteresis loops, which are characteristics of mesoporous materials [60]. These isotherms show steep capillary condensation steps that are evidence for uniformity of mesoporous in these catalysts. Amongst them, the isotherm for 1Ni2NbAl shows the greater condensation step, which is indicative of larger primary mesoporous. Regardless, the uniformity of these primary mesoporous seems to be similar, since comparable hysteresis loops are observed for these catalysts. The pore size distributions (PSDs) for all catalysts are shown in **Figure 4.2 b**. The observed sharp peaks in the range of 9-10 nm confirm the isotherms discussion and the synthesis of mesoporous materials with narrow PSDs. The isotherm and PSD for the blank alumina, synthesised using the glycol-thermal technique, are shown in **Figure 4.2**. Thus far, this characterization

technique confirms the synthesis of template free ordered mesoporous alumina (OMA), using the glycol-thermal methods [60].

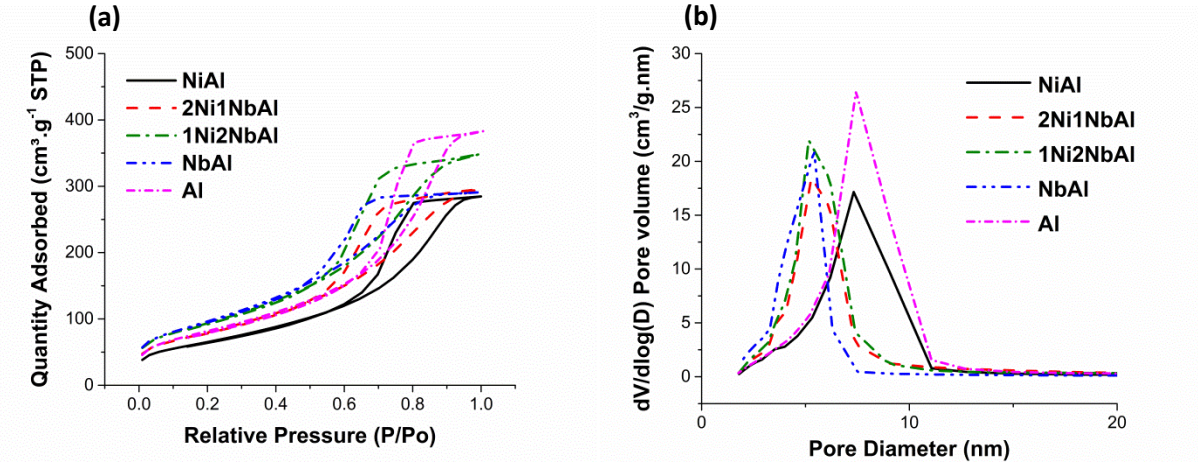

Figure 4.2 (a) Nitrogen adsorption-desorption isotherms of all catalysts. (b) Pore size distributions for all catalysts.

4.3.3) TEM

TEM images of all catalyst are shown in **Figure 4.3**, which show a nanorod like morphology with random length and width. However, NbAl showed shorter nanorods than the other catalysts. In some of these images porous alumina was also detected in small quantity. The observed unified mesoporous structures for these catalysts seem to originate from the gap between the nanorods. This mesoporousity seems to be the dominant and the primary reason for the observed steep isotherms for these catalysts and the existing porous alumina seems to make a low contribution to the porosity of these materials. Therefore, the randomly porous alumina could not be detected using the isotherms. Furthermore, it can be postulated that the available inter-particles forces are responsible for the existing mesoporous structures in all catalysts, like what can be achieved using the hard template techniques for the preparation of these materials [57, 60]. The TEM image of blank alumina, synthesised with this technique, is available in the appendix (**Appendix 4.3**)

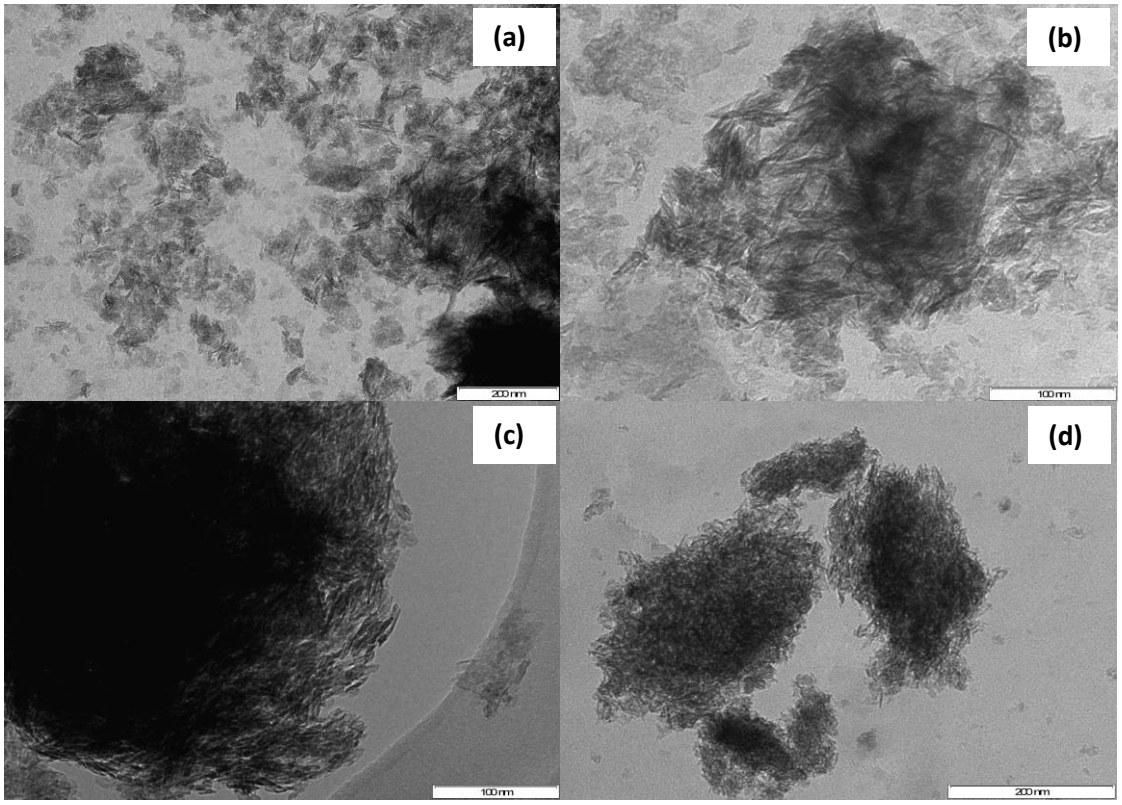

Figure 4.3 TEM images of all catalysts. a) NiAl, b) 2Ni1NbAl, c) 1Ni2NbAl and d) NbAl.

4.3.4) HR-TEM

To further investigate the composition of the nanorods, line scan analysis of a single nanorod was done using HR-TEM and the images and spectra are shown in **Figure 4.4**. All three elements are present in a single scanned nanorod as can be seen in **Figure 4.4**. This image (**Figure 4 4**) and the PXRD data (**Figure 4.1**) suggest that the nano-sized crystallites of all three oxides are orientated in a very close contact to form a single nanorod.

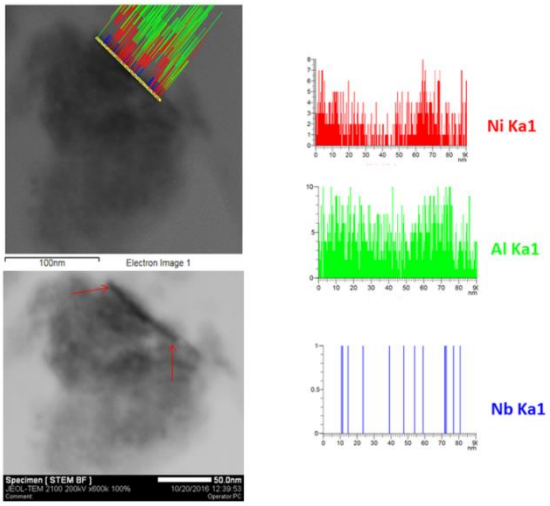

Figure 4.4 Line scan of a single nanorod using HR-TEM in STEM mode (bright field) of 2Ni1NbAl. (The smaller nanorods are present, but could not be viewed due to the lower obtained resolution when the scanning mode of the HR-TEM was used).

Figure 4.5 shows the elemental mapping of NiAl and 2Ni1NbAl. Both nickel and niobium seem to be highly dispersed over alumina. In addition, this observation shows the presence of interactions between these metals and alumina. The mapping results of 1Ni2NbAl are shown in **Figure 4.6.** The small particles of nickel oxide seem to form the nanorods. However, the nanorods (mainly containing nickel oxide) showed low concentration of alumina and a trace quantity of niobium (**Figure 4.6a**.). In addition, the mapping of another group of nanorods at a different site showed alumina and niobium oxides as major components, while nickel was detected in trace quantity (**Figure 4.6b**). This suggests, niobium prefers to interact with alumina and weakens the interaction between nickel and alumina.

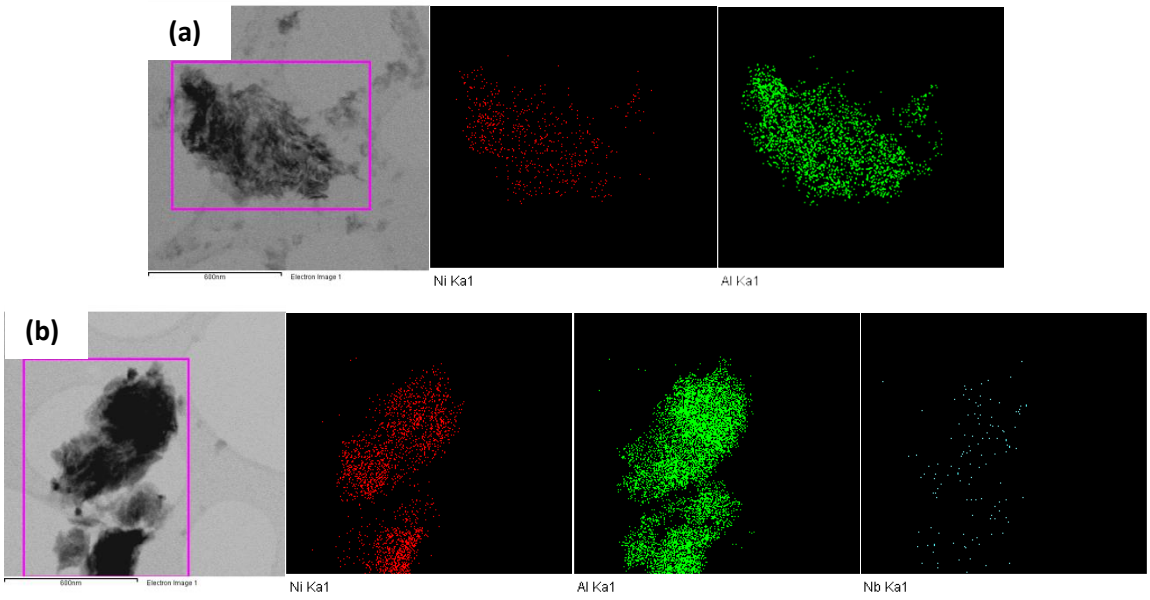

Figure 4.5 The elemental mapping of (a) NiAl and (b) 2Ni1NbAl, using HR-TEM (bright field in STEM mode).

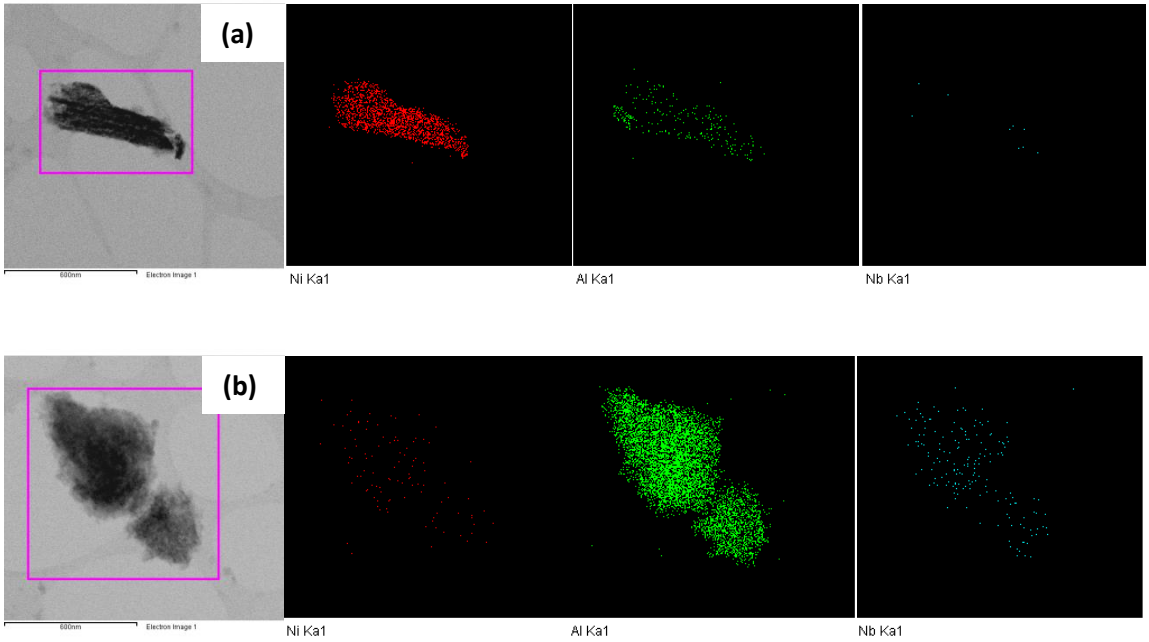

Figure 4.6 The elemental mapping of 1Ni2NbAl, using HR-TEM (bright field in STEM mode). (a) site with high nickel content, (b) site with low nickel content.

4.3.5) SEM

The SEM images of all catalysts are shown in **Figure 4.7**. The presence of the nanorods in all catalysts could also be detected using this characterization technique. Based on the obtained SEM images, NbAl showed smaller nanorods than the other catalysts, which is in a good agreement with the images viewed using TEM (**Figure 4.3**). Furthermore, this technique allowed us to observe the nanorods from different directions, which was not possible using the TEM. These SEM images further support the hypothesis of origination of mesoporous from the gaps between the nanorods. The SEM image of blank alumina, synthesised with this technique is in the appendix (**Appendix 4.4**).

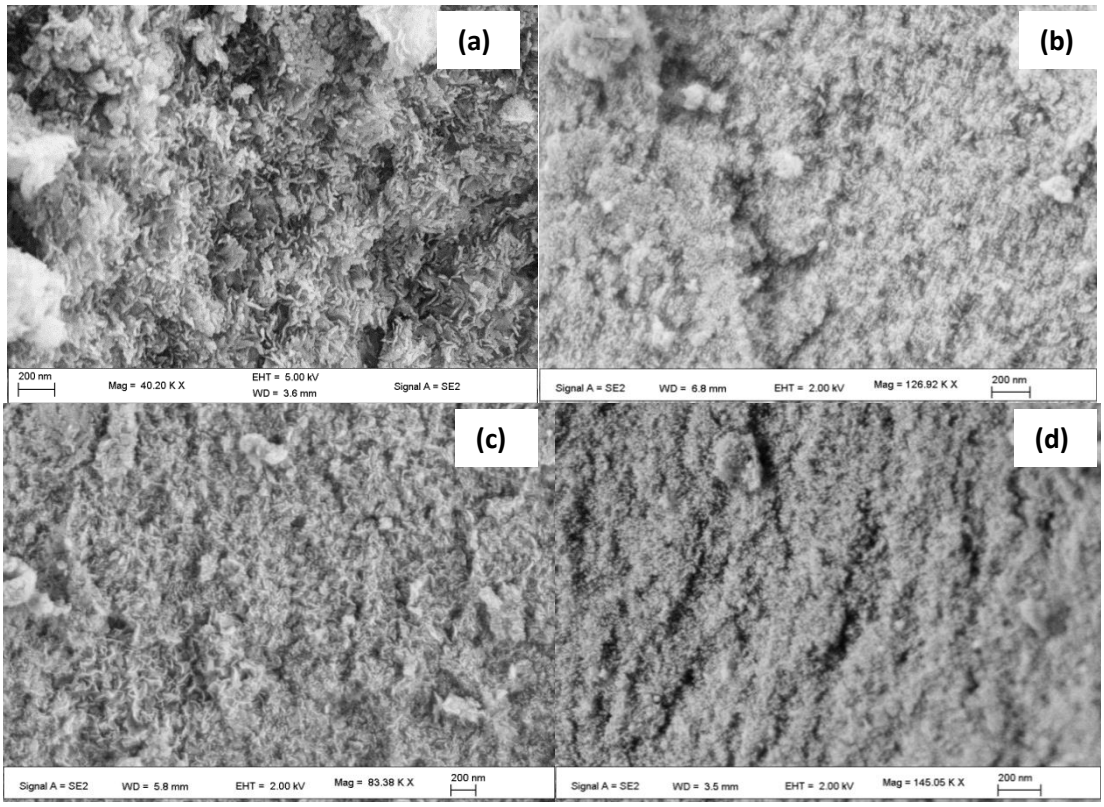

Figure 4.7 TEM images of all catalysts. a) NiAl, b) 2Ni1NbAl, c) 1Ni2NbAl and d) NbAl.

4.3.6) Investigation of the control catalyst

Thus, according to the shown characterization, nanorod-like morphology OMA catalysts containing different amounts of NiO and Nb_2O_5 could be achieved using the glycol-thermal synthesis technique. However, two key questions still remain unanswered. First, what is the main reason for the formation of nanorod morphology? Second, what is the main parameter in controlling the porosity that results in the ordered mesoporous structures in these nano-composites?

To answer these two questions, a nano-composite with the elemental composition of NiO = 87.6 wt%, Nb_2O_5 = 6.2 wt% and Al_2O_3 = 6.2 wt% (confirmed by ICP) was synthesised using the glycol-thermal technique. This nano-composite was characterized using PXRD, N_2-physisorption, TEM and SEM which are shown in **Appendix 4.5**. **Appendix 4.5 c** and **d** show the presence of nanorod-like morphology for this material. This observation clearly shows that the formation of nanorods originated from the synthetic technique. In addition, the nitrogen adsorption-desorption isotherm of this sample shows a type IV isotherm with a H1 type hysteresis loop, which are the indicative of mesoporous structure. However, the "non-steep" capillary condensation step of this nano-composite reveals that this sample has irregular mesoporous structure. Therefore, the second question can be answered by stating that the mesoporousity seems to also originate from the glycol-thermal synthesis. However, the presence of alumina appears to be necessary for the synthesis of ordered mesoporous materials in this study.

4.3.7) In situ XRD

To investigate the redox properties of available nickel oxides in these catalysts, an *in situ* XRD analysis of three nickel containing catalysts was conducted and the results are shown in **Figure 4.8**. The reduction of NiO in NiAl started slowly at 550 °C (**Figure. 4.8a**). This slow reduction at relatively high temperatures and the considerable quantity of unreduced NiO remaining, even at 600 °C, indicates the presence of a strong interaction between nickel and aluminium oxide. These strongly bonded NiO/Al_2O_3 catalysts are known to be β_1, β_2 or γ ($NiAl_2O_4$ spinel) types of NiO, which are categorized based on their reduction temperatures [62-65]. However, low quantity of formed reduced nickel has a high tendency to oxidise back to NiO at 100-250 °C (**Figure 4.8a**). The second reduction (of regenerated NiO) was conducted to further investigate the occurrence of NiO agglomeration, resulting from the redox cycle in this catalyst. As can be seen in **Figure 4.8a**, the reduction of regenerated NiO has shifted to a lower temperature (500 °C) when was compared to the first reduction step. This observation shows NiO in NiAl has the potential of slow agglomeration when following the redox cycles.

The addition of Nb in 2Ni1Nb resulted in some interesting changes in the redox properties of these catalysts (**Figure 4.8b)**. The first reduction of NiO species in this catalyst is slightly shifted towards higher temperature (600 °C) upon the addition of Nb. This might be due to lower nickel loading in this catalyst, which resulted in a better dispersion of nickel particles with stronger interaction with the Al_2O_3 . The re-oxidation step showed the same behaviour as was seen for NiAl (**Figure 4.8b)**. The second reduction of the re-oxidised 2Ni1NbAl started at 450 °C. Thus, a large change in the reduction temperatures between the first and second cycles with ΔT = 150 °C was observed, while this change was smaller (ΔT = 50 °C) for the NiAl catalyst (**Figure 4.8a)**. This considerable change in the reduction temperatures of these two catalysts suggests the regenerated NiO in 2Ni1NbAl has weaker interaction with

alumina than in NiAl after the re-oxidation step and the rate of NiO agglomeration is higher in this catalyst compared to NiAl as these catalysts follow further redox cycles.

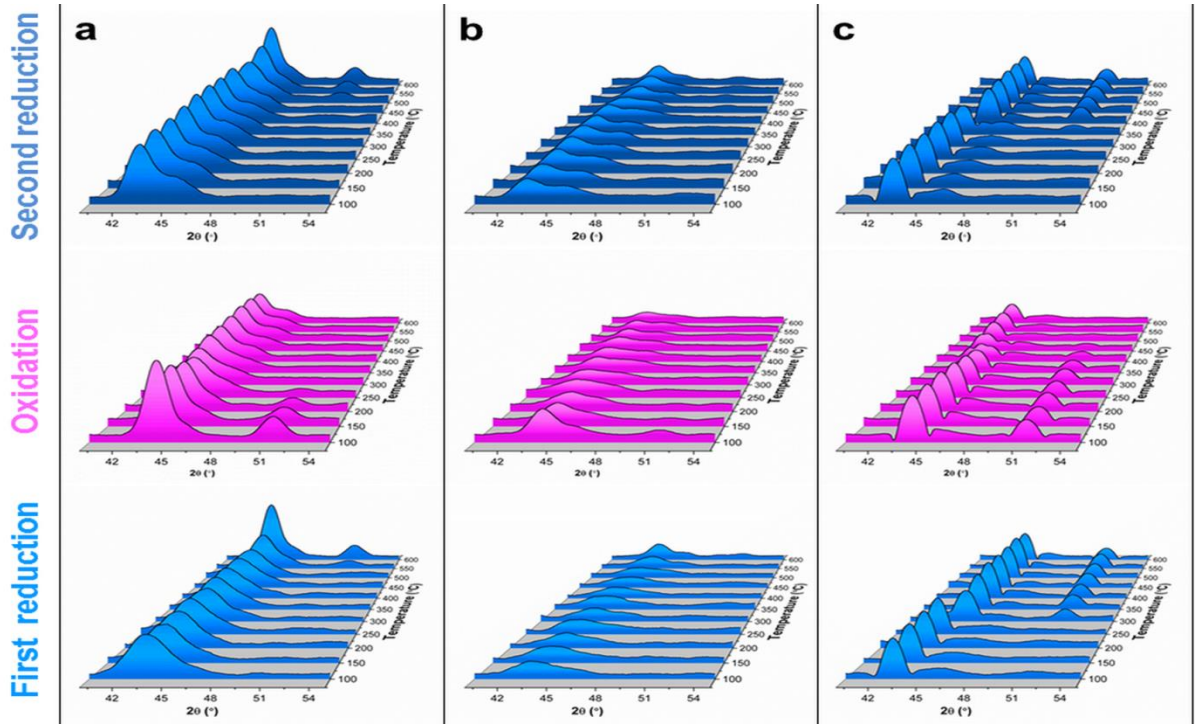

Figure 4.8 The *in situ* XRD analysis of nickel containing catalysts. a) NiAl, b) 2Ni1NbAl and c) 1Ni2NbAl. The catalysts were first reduced in the first step, then oxidised followed by the second reduction. Temperature range = 100-600 °C. The peak representing NiO has a 2θ value of 44°, while metallic Ni has two peaks with 2θ values of 46° and 53°.

1Ni2NbAl showed very different redox behaviour to what was observed for NiAl and 2Ni1NbAl. The available NiO in this catalyst seems to have no interaction with alumina and behaves as bulk NiO with the low reduction temperature of 300 °C (**Figure 4.8c**) [17, 25, 33]. All available NiO seems to be reduced at once as the temperature reaches to 300 °C, while a broader reduction range was observed in the cases of NiAl and 2Ni1NbAl. Furthermore, the oxidation step occurs in the temperature range of 300-450 °C. This

behaviour is also in a good agreement with the redox nature of bulk nickel oxides, where the larger crystals of NiO are more difficult to reduce than the smaller ones where no interaction with supports is present [17, 25, 33].

The characterisation data suggest the presence of "the confinement effect" between mesoporous structure of Al_2O_3 and NiO in NiAl and 2Ni1NbAl catalysts [66-68]. This was expected, since the discussed data in **Figure 4.4** clearly show that a single nanorod has all three used metal oxides. Therefore, the reduction temperature of NiO has shifted to higher temperature for these catalysts and agglomeration resulted in the lower reduction temperature for the second cycle. Nb is found to decrease the contribution of the confinement effect as the temperature of the second reduction was much lower than the first reduction when it is compared to the NiAl catalyst. Finally, the *in situ* XRD results for 1Ni2NbAl suggest the confinement effect is totally absent when a high concentration of Nb is introduced in the synthesis of this nano-composite. Therefore, the available nickel in 1Ni2NbAl displayed known characteristics for bulk NiO.

4.3.8) NH_3-TPD

The surface acidity data are shown in **Table 4.2**. The introduction of niobium has increased the total acidity of the catalysts, which is in a good agreement with other reports [16, 26, 69]. However, the presence of nickel, even in small quantity (1Ni2NbAl), is seen to suppress the presence of acidic sites when compared to NbAl (**Table 4.2**). Comparing the weak acidic sites (α) to strong acidic sites (β) allowed us to investigate the influence of the "confinement effect" on the acidity of these catalysts. 2Ni1NbAl showed slightly higher total acidity than NiAl. However, the addition of Nb in the presence of the "confinement effect" seems to

convert some of strong acidic sites to weak ones. In addition, further addition of Nb (1Ni2NbAl) and absence of the "confinement effect" seems to only increase the density of strong acidic sites when compared to NiAl (**Tabel 2**). Finally, the density of both, weak and strong, acidic sites increased when only niobium was loaded on alumina (NbAl).

Table 4.2 Acidity of all catalysts measured, using NH_3-TPD.

Catalyst	Weak acidic sites (α^a) (mmol $NH_3.g^{-1}$)	Strong acidic sites (β^b) (mmol $NH_3.g^{-1}$)	Total acidity (mmol $NH_3.g^{-1}$)
NiAl	0.16	0.45	0.61
2Ni1NbAl	0.30	0.34	0.64
1Ni2NbAl	0.16	0.65	0.81
NbAl	0.71	1.20	1.91

a. The desorbed ammonia at below 500 °C
b. The desorbed ammonia at above 500 °C

4.3.9) Catalytic results

These catalysts were tested in ODH of *n*-octane at different temperatures and the conversion results are shown in **Figure 4.9**. The catalyst containing the highest NiO loading and no niobium additive (NiAl) was found to give the lowest conversion amongst all catalysts at different temperatures (**Figure 4.9**). According to *in situ* XRD data, the confinement effect negatively influenced the redox properties of this catalyst and subsequently compromised the *n*-octane and oxygen conversion when it was used in this ODH application (**Figure 4.9**).

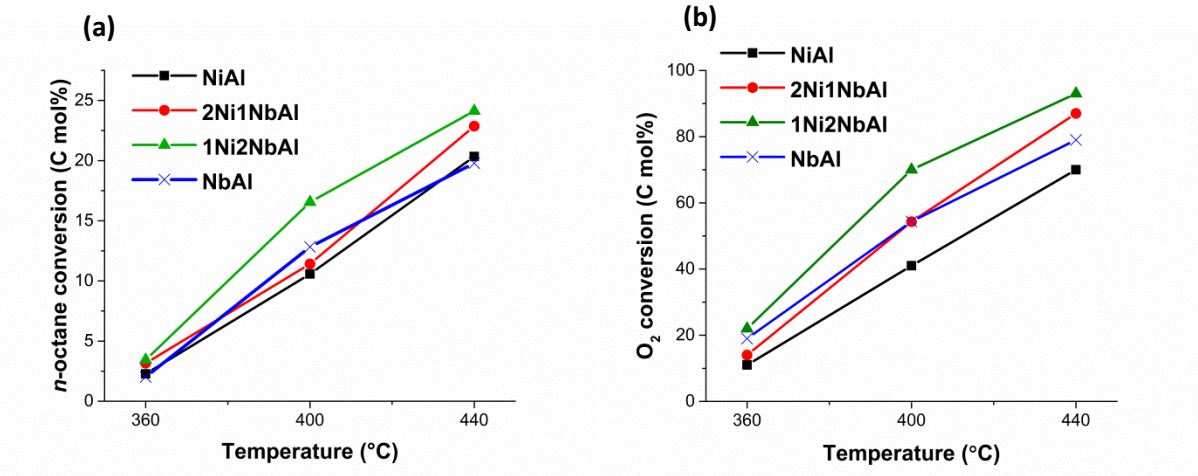

Figure 4.9 a) *n*-octane conversion and b) oxygen conversion in ODH of *n*-octane over all catalysts. Reaction conditions: C:O = 8:4, GHSV = 16000 h^{-1} and concentration of *n*-octane in the feed:= 7%.

2Ni1NbAl was more active than NiAl and the conversion increased with increasing temperature. Based on *in situ* XRD data (**Figure 4.8b**), the confinement effect for this catalyst is weaker at temperatures above 400 °C due to changes induces by the redox cycles, which improved the redox properties of this catalyst and enhanced the conversion (**Figure 4.9**).

1Ni2NbAl was the most active catalyst at all tested temperatures (**Figure 4.9**). This activity was expected since *in situ* XRD data proved the similarity of NiO in this catalyst to bulk NiO, which follows the redox cycles at relatively low temperatures. However, the conversion was limited at 440 °C by the absence of sufficient oxygen in the reaction steam (**Figure 4.9b**).

NbAl also showed moderate activity at all three different temperatures. Based on previous reports, on Nb_2O_5, this catalyst cannot follow the redox cycles at the chosen reaction conditions [16, 26]. Therefore, these conversion values are possibly due to radical [70] and acid-base (**Table 4.2**) catalysed reactions over this high surface area mesoporous catalyst. The oxygen conversions (**Figure 4.9 b**) well match the obtained trend for *n*-octane conversions.

Figure 4.10 shows the selectivity to the different formed products in the ODH of *n*-octane at different temperatures. NiAl showed the highest selectivity to octene isomers at all temperatures (**Figure 4.10a**). The selectivity to octene decreased as the temperature increased, which may imply the conversion of the formed octene to other, secondary, products. The selectivity to aromatics increased at higher temperatures (**Figure 4.10b**), which suggests the further dehydrogenation of the formed octenes and their aromatization requires higher temperatures. The selectivity towards cracked products (**Figure 4.10c**) has a volcano shape for this catalyst at three different temperatures. This trend suggests that 400 °C is not sufficiently hot to convert the cracked products to CO_x, while 440 °C seems to further crack the cracked products and produce CO_x (**Figure 4.10 c and d**).

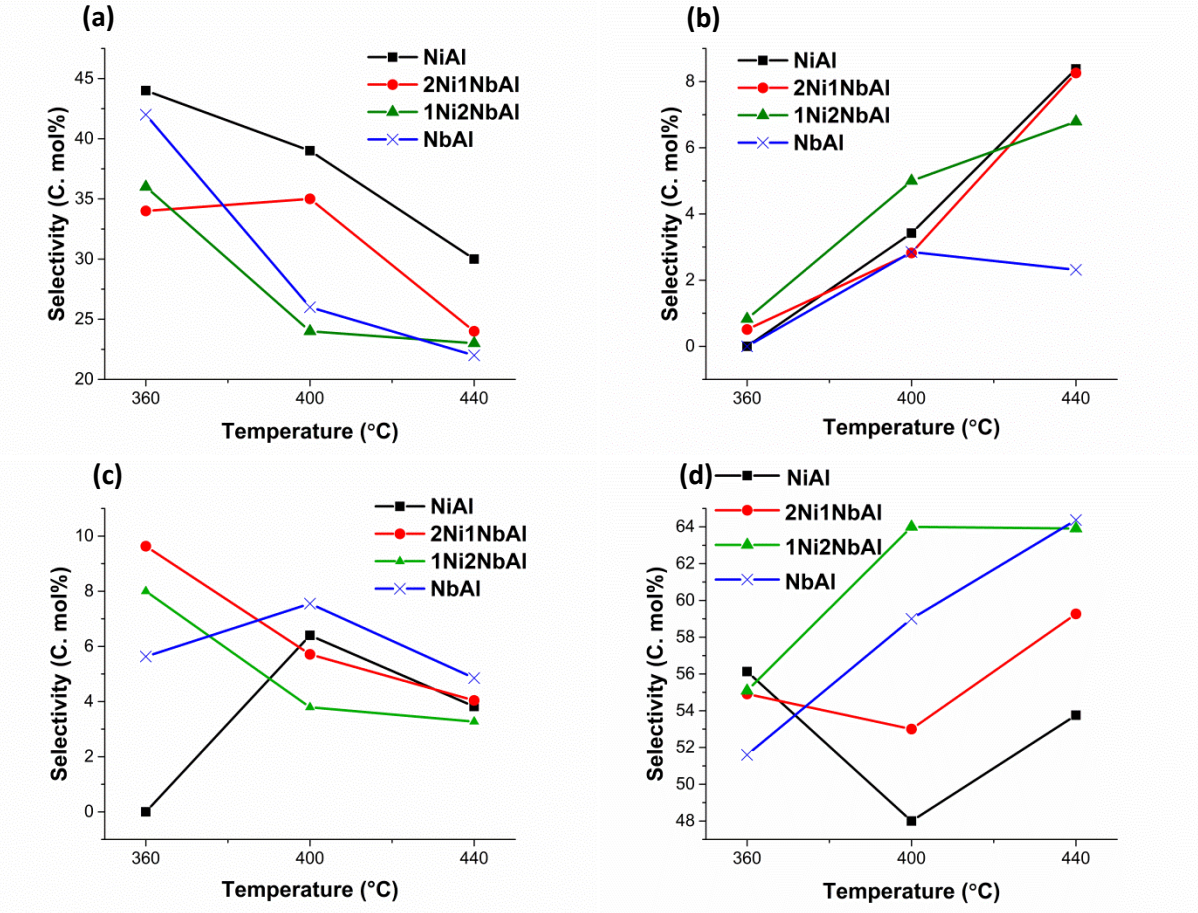

Figure 4.10 a) Selectivity to octene isomers, b) selectivity to different aromatics, c) selectivity to cracked products and d) selectivity to CO_x in ODH of *n*-octane over all catalysts. Reaction conditions: C:O = 8:4, GHSV = 16000 h^{-1} and concentration of *n*-octane in the feed = 7%.

The selectivity to octene decreased when Nb was introduced, as is shown for 2Ni1NbAl in **Figure 4.10a**. However, this selectivity stayed almost the same when the temperature was changed from 360 °C to 400 °C, while the conversion increased almost 8% (**Figure 4.10a**). The constant selectivity at two different temperatures shows that the rate of reaction on the same active site only is increased, and this temperature change did not manipulate the nature of existing active sites at 360 °C. However, the increase of temperature to 440 °C changes

these sites and activates them towards cracked products, aromatics and CO_x formation. The same increase in selectivity to aromatics was observed with increasing temperature as was seen for NiAl (**Figure 4.10b**). Interestingly, increasing the temperature from 360 °C to 400 °C resulted in lower selectivity to cracked products, and CO_x (**Figure 4.10 c** and **d**). The activation of desired active sites (or nucleophilic oxygen species) for the ODH reaction at this temperature might be the reason for this change, which was different from the observed behaviour for NiAl, but often observed in various ODH systems for medium-chain paraffins [5, 10]. Regardless, the temperature change to 440 °C from 400 °C resulted in cracking and combustion of the formed alkenes, as was observed in the case of NiAl.

1Ni2NbAl gave the lowest selectivity to octenes at all temperatures. A large drop in selectivity to octenes can be seen in **Figure 4.10a** when the temperature was changed from 360 °C to 400 °C. This result was expected, since the conversion between these temperatures showed a large increase and a sharp reduction at approximately this temperature was observed in the *in situ* XRD data for this catalyst (**Figure 4.8c**). However, the selectivity did not change much after 400 °C, suggesting the occurrence of only one reduction step in this catalyst, as indeed is seen in the *in situ* XRD data (**Figure 4.8c**). Generally, the selectivity to aromatics increased with increasing temperature, as was observed for the two other nickel containing catalysts (**Figure 4.10b**). The selectivity to cracked products and CO_x increased as the temperature was increased from 360 °C to 400 °C and stayed almost the same between 400 °C and 440 °C (**Figure 4.10 c** and **d**). This behaviour suggests a contribution of this phase change to acid catalysed and combustion reactions. In addition, the increase in conversion and the general maintenance of selectivity toward different products between 400 °C to 440 °C suggests that temperature only affects the reaction rate without modifying the active sites for different reactions involved in this catalytic system.

NbAl showed a consistent drop in selectivity to octenes as the temperature was increased (**Figure 4.10 a**). The opposite trend was observed for CO_x selectivity (**Figure 4.10 d**). The selectivity to aromatics increased initially, when the temperature was increased from 360 °C to 400 °C, but decreased when the temperature was increased further to 440 °C (**Figure 4.10 b**). Almost the same trend was observed for cracked products (**Figure 4.10 c**). According to NH_3-TPD data (**Table 4.2**) and the available literature on Nb, the addition of this element generally increases the density of acidic sites, which seem to strongly contribute to cracking of the formed alkenes and in this case, even more stable products like aromatics [4]. Based on available literature, NbAl is not capable of presenting redox behaviour at these conditions, and the acid catalysed reactions and operating temperatures seem to play the main roles in this case [16, 26].

The cracking of ethylbenzene and styrene normally results in the formation of benzene, which is shown in **Table 4.3**. Generally, the selectivity towards benzene (**Table 4.3**) matches well with the observed trend of total acidity over these catalysts (**Table 4.2**). In addition, selectivities to CO and CO_2 are shown in **Table 4.3**. CO is known to originate from the extreme cracking and oxygen insertion of the formed hydrocarbons during reactions (**Table 4.3**). However, CO_2 is believed to have two sources of the formation, the extreme cracking and oxygen insertion and direct combustion of the introduced feed [2]. Therefore, discovering the link between the obtained characterisation and catalytic data is complex, especially when effects of increased conversion and the surface texture are present.

Table 4.3 Selectivity to CO_2, CO and benzene over all catalysts.

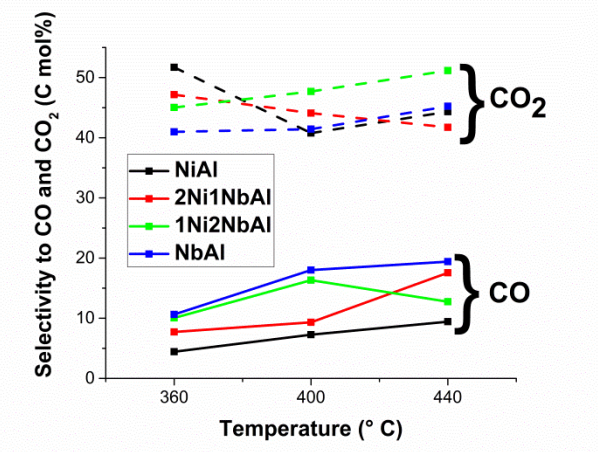

	Selectivity to benzene (C mol%)		
Catalyst	**360 °C**	**400 °C**	**440 °C**
NiAl	0	1	2
2Ni1NbAl	0	1	3
1Ni2NbAl	0	2	2
NbAl	0	4	6

The shown catalytic data for temperature optimization (**Figure 4.9** and 4.**10** and **Table 4.3**) provided valuable data about the different important parameters involved in the oxidation of *n*-octane over these catalysts, such as phase change and acid catalysed reactions. However, a closer look was required to discover more about the existing catalytic reactions in these materials. Therefore, the detailed breakdown of formed products over each catalyst is shown in **Figure 4.11**. The formed different products were compared based on yields to minimize the contribution of conversion to selectivity. In addition, the data were divided by the BET surface areas of the relevant catalysts to compare them on the same bases.

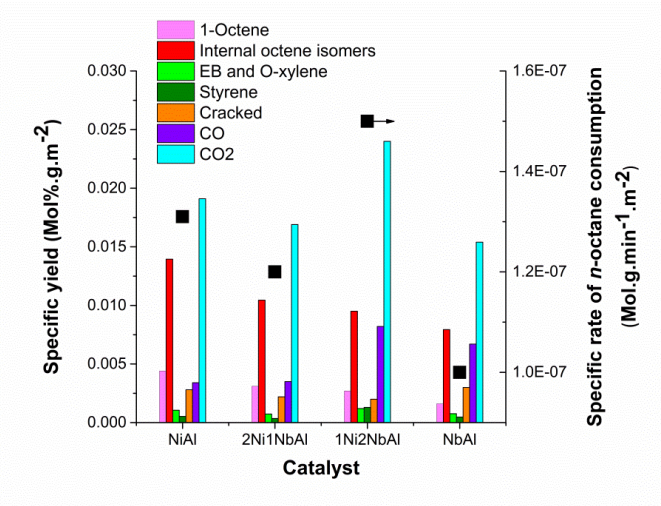

Figure 4.11 Specific catalytic data for oxidation of *n*-octane over all catalysts. (The yields and the rates of reactions are divided by the BET surface areas of the relevant catalysts). Reaction conditions: C:O = 8:4, GHSV = 16000 h^{-1}, temperature = 400 °C and concentration of *n*-octane in the feed= 7%.

The addition of Nb seems to decrease the rate of reaction, except for 1Ni2NbAl where nickel showed similar chemistry as bulk NiO (**Figure 4.11**). The selectivity towards octene isomers decreased as the Nb concentration increased, suggesting strong contributions of secondary reactions, which convert the formed octene isomers to aromatics, cracked products and CO_x. Regardless, the ratio between 1-octene and internal octene isomers is almost the same over all catalysts (**Figure 4.11**). Therefore, it can be proposed that the primary dehydrogenation of a CH_2 segment in an alkane is mainly related to the operating temperature and the general characteristics of the catalyst.

Cracking is known to be due to the reaction of formed primary olefins or aromatics with acidic sites of heterogonous catalysts [4]. In addition, niobium is known as an acidic metal

oxide and its addition normally increased the density of acidic sites on the surface of the catalysts, as shown in **Table 4.2** [69]. Therefore, CO and cracked products increased upon the addition of Nb (**Figure 4.11**). However, 1Ni2NbAl shows a slightly higher specific yield to CO and cracked products than NbAl, which is possibly the effect of the rate of the reaction over the former catalyst (**Figure 4.11**). Higher specific yields for aromatic products were observed over 1Ni2NbAl, whereas the other catalysts have almost the same specific yields towards these products. Based on the data in **Figures 4.9** and **4.10**, the aromatics selectivity seems to be mainly dependant on pore volume and surface acidity, which determine the residence time of the formed octene isomers inside of the pores for further hydrogen abstraction. The specific yield to CO_2 follows the same trend, as the rate of the reaction seems to be mainly controlled by the direct combustion of the introduced paraffin and possibly this reaction is another primary reaction involved in the oxidative conversion of *n*-octane.

The effect of changing the concentration of oxygen in the reaction steam on the catalytic performance is shown in **Figure 4.12**. The amount of O_2 in the reaction has a direct correlation with observed conversion. NiAl showed the best selectivity to octene isomers at the different C:O ratios, while a low conversion was observed over this catalyst (**Figure 4.12**). 2Ni1NbAl and NbAl showed almost the same trend of deactivation and improved selectivity when the reaction proceeded at high C:O ratios (**Figure 4.12**). However, faster deactivation was observed for 1Ni2NbAl than for the other catalysts when the concentration of oxygen in the reaction steam was lowered. Also, the positive impact of this change in selectivity to octene isomers and CO_x was more significant than over the other catalysts. The introduction of a smaller quantity of oxidant seems to slow the reaction by limiting the redox capability of these catalysts, resulting in better selectivity to octenes and lower selectivities to

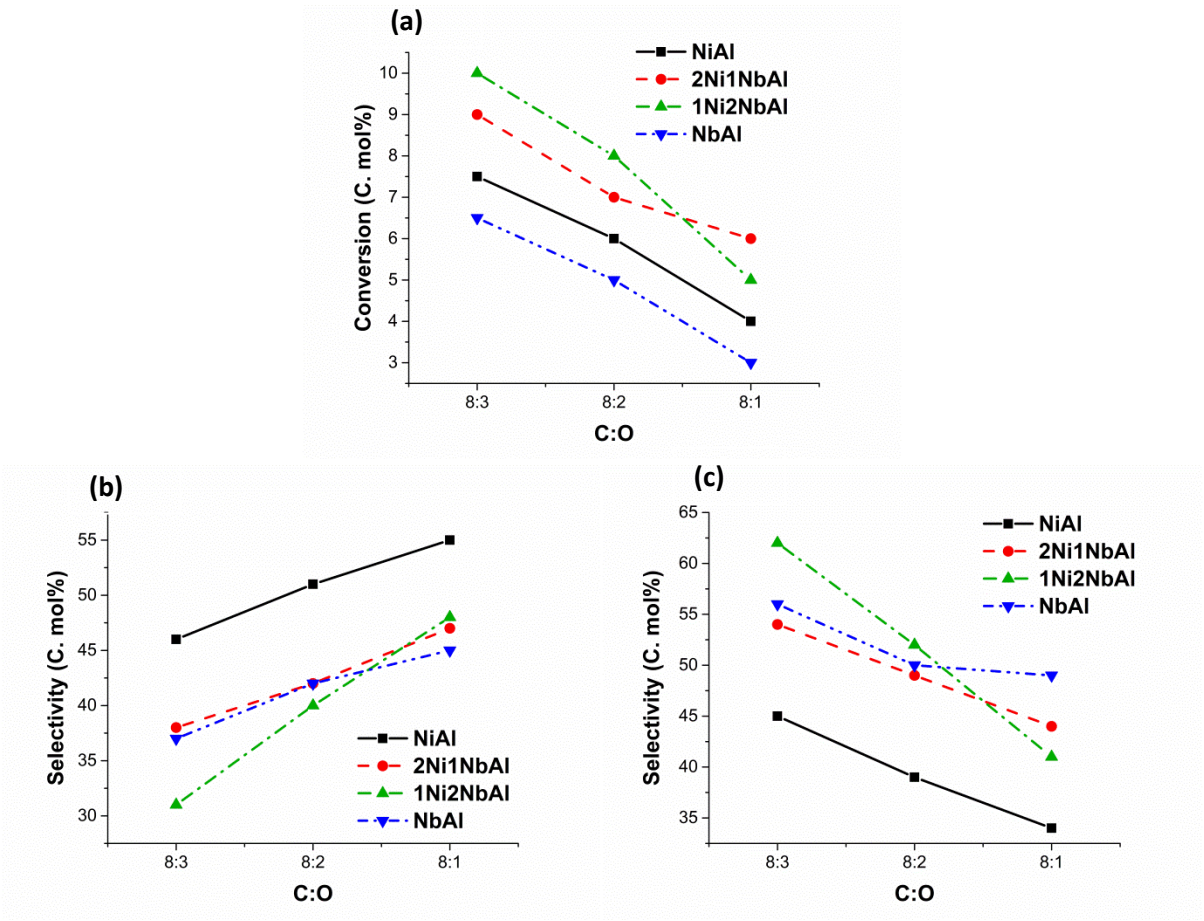

Figure 4.12 The effect of C:O ratio variation on oxidative conversion of *n*-octane over all catalysts. a) *n*-octane conversion, b) selectivity to octene isomers and c) selectivity to CO_x. Reaction conditions: GHSV = 16000 h^{-1}, temperature = 400 °C and concentration of *n*-octane in the feed= 7%.

CO_x. On the other hand, the coking of undesired catalytic sites (like acidic sites) under more anaerobic conditions seems to also selectively lower the CO_x formation and enhance the selectivity to the desired and primary ODH reactions. The positive impact of coking also is shown in different catalytic applications [71-73].

The above discussed characterization and catalytic data showed that the introduction of niobium in the NiO catalyst mixture plays a major role on the properties of the obtained catalysts. The presence of a strong "confinement effect" seems to improve the catalytic performance. However, the addition of niobium decreased this effect and resulted in catalysts with a faster reduction step at relatively lower temperatures.

The catalyst with lowest reduction temperature and the weakest "confinement effect" (1Ni2Nb) was found to have the highest selectivity to CO_x, whereas the catalyst with highest reduction temperature and strongest "confinement effect" resulted in the best obtained selectivity to octene isomers. The increase in reduction temperature and slow reduction are found to positively impact the selectivity to desired ODH products and lower the conversion, which is in agreement with many reports [16, 20, 30, 33]. However, fast reduction at low temperature does not seem to suite this reaction and accelerates the CO_x formation [16, 20, 30, 33]. The reduction only refers to the release of lattice oxygen ($O^{-2}_{\ latt.}$), therefore, the rate of its release can be linked to the entropy of this type of ionic oxygen. The entropy in this system can be qualitatively speculated from an immediate and high concentration release of $O^{-2}_{\ latt.}$ (according to onset temperature and consumed hydrogen in TPR analysis) as well as operating temperatures. Therefore, it can be proposed that $O^{-2}_{\ latt.}$ with high entropy (available in 1Ni2NbAl) accelerates the combustion of the *n*-octane, while $O^{-2}_{\ latt.}$ with low entropy (available in 2Ni1NbAl) accelerates the ODH selectivity.

Other important parameters are the contributions of radical reactions and the presence of electrophilic oxygen species on the surface of the catalyst. Nb_2O_5 is known to have no redox properties at the chosen operating conditions [16, 26]. However, it showed considerable

conversion with high selectivity to CO_2 in the oxidative conversion of *n*-octane. Therefore, the production of unstable C_8 oxygenated products and their combustion to CO_2 through a radical mechanism can be proposed as another important parameter [70]. However, these radical reactions might be suitable in ODH of C_2 and C_3 paraffins [74]. The charge-transfer through the available positive holes in the lattice of the semiconductor NiO seems to result in high a concentration of charge on its surface, which will form electrophilic oxygen when it is in contact with atmospheric air [20, 30]. Therefore, the catalyst with highest nickel content was expected to have highest selectivity to CO_x, which was the case only at 440 °C. This observation shows the contribution of the electrophilic oxygen species in the combustion reaction.

The last parameter for high selectivity to CO_x over Nb content catalysts can be correlated to the increase of acidity by addition of this element. It is a well-accepted phenomenon that the acidic sites are suitable for ODH of ethane and propane, while medium-chain paraffins like *n*-octane require a high concentration of basic sites (for better desorption of the formed products) [4]. Therefore, it can be briefly mentioned that Nb introduction into the lattice of NiO does not only modify the sites for different oxygen species, but also modifies the acidic and radical sites of the catalysts that play important roles in the performance of the catalysts.

4.4) Conclusion

Different characterisation techniques showed the presence of nanorods, which resulted in ordered mesoporous structures for these nano-composites, prepared using the glycol-thermal synthesis. In addition, OMA was successfully synthesised, using this technique. The similarity of the surface textures of all four catalysts allowed the better understanding of the chemistry behind these nano-composites. Nb introduction seems to weaken the observed

"confinement effect" and results in the shift of reduction temperatures to lower temperatures than found for the catalyst without niobium. In addition, Nb addition was found to increase the density of acidic sites, which is responsible for the production of cracked products and CO from the primary products. The strong "confinement effect" is found to enhanced the selectivity to octene isomers. The aromatics selectivity was found to be mainly dependant on pore size and acidity of the catalysts. Finally, the fast release of nucleophilic oxygen spices with high entropies, radical reaction via the addition of Nb, the presence of electrophilic oxygen species (especially at high temperatures) and the presence of acidic sites seem to be the main parameters for CO_x formation from *n*-octane.

4.5) Acknowledgements

We thank SASOL and the National Research Foundation, South Africa (NRF) for their financial supports. We also thank the Electron Microscopy Unit at the University of KwaZulu-Natal (Westville campus).

4.6) References

[1] J.J.H.B. Sattler, J. Ruiz-Martinez, E. Santillan-Jimenez, B.M. Weckhuysen, Chem. Rev., 114 (2014) 10613-10653.

[2] R. Grabowski, Catal. Rev., 48 (2006) 199-268.

[3] F. Cavani, N. Ballarini, A. Cericola, Catal. Today, 127 (2007) 113-131.

[4] C.A. Gärtner, A.C. van Veen, J.A. Lercher, ChemCatChem, 5 (2013) 3196-3217.

[5] S. Pradhan, J.K. Bartley, D. Bethell, A.F. Carley, M. Conte, S. Golunski, M.P. House, R.L. Jenkins, R. Lloyd, G.J. Hutchings, Nat Chem, 4 (2012) 134-139.

[6] J.C. Vedrine, J. Energy. Chem., 25 (2016) 936-946.

[7] H.B. Friedrich, A.S. Mahomed, Appl. Catal., A, 347 (2008) 11-22.

[8] M.I. Fadlalla, H.B. Friedrich, Catal. Sci. Tech., 4 (2014) 4378-4385.

[9] B. Pillay, M.R. Mathebula, H.B. Friedrich, Appl. Catal., A, 361 (2009) 57-64.

[10] E.A. Elkhalifa, H.B. Friedrich, Appl. Catal., A, 373 (2010) 122-131.

[11] E.A. Elkhalifa, H.B. Friedrich, Catal. Lett., 141 (2011) 554-564.

[12] B. Pillay, M.R. Mathebula, H.B. Friedrich, Catal. Lett., 141 (2011) 1297-1304.

[13] E.A. Elkhalifa, H.B. Friedrich, J. Mol. Catal. A: Chem., 392 (2014) 22-30.

[14] J. Chetty, V.D.B.C. Dasireddy, S. Singh, H.B. Friedrich, React. Kinet. Mech. Cat., 120 (2017) 307-321.

[15] E. Romera, C. Lamotte, P. Bodart, Process for the purification of medium-chain olefins, Fina Research S.A., 1998.

[16] E. Heracleous, A.A. Lemonidou, J. Catal., 237 (2006) 162-174.

[17] E. Heracleous, A.A. Lemonidou, J. Catal., 237 (2006) 175-189.

[18] F. Rubio-Marcos, E. Rojas, R. López-Medina, M.O. Guerrero-Pérez, M.A. Bañares, J.F. Fernandez, ChemCatChem, 3 (2011) 1637-1645.

[19] S.-B. Ivan, I. Popescu, I. Fechete, F. Garin, V.I. Parvulescu, I.-C. Marcu, Catal. Sci. Tech., 6 (2016) 6953-6964.

[20] H. Zhu, D.C. Rosenfeld, M. Harb, D.H. Anjum, M.N. Hedhili, S. Ould-Chikh, J.-M. Basset, ACS Catal., 6 (2016) 2852-2866.

[21] E. Heracleous, A.A. Lemonidou, J. Catal., 270 (2010) 67-75.

[22] E. Heracleous, A. Delimitis, L. Nalbandian, A.A. Lemonidou, Appl. Catal., A, 325 (2007) 220-226.

[23] B. Savova, S. Loridant, D. Filkova, J.M.M. Millet, Appl. Catal., A, 390 (2010) 148-157.

[24] W. Weng, M. Davies, G. Whiting, B. Solsona, C.J. Kiely, A.F. Carley, S.H. Taylor, Phys. Chem. Chem. Phys., 13 (2011) 17395-17404.

[25] H. Zhu, S. Ould-Chikh, D.H. Anjum, M. Sun, G. Biausque, J.-M. Basset, V. Caps, J. Catal., 285 (2012) 292-303.

[26] Z. Skoufa, E. Heracleous, A.A. Lemonidou, Catal. Today, 192 (2012) 169-176.

[27] X. Sun, B. Li, H. Metiu, J. Phys. Chem. C, 117 (2013) 23597-23608.

[28] J. Santander, E. López, A. Diez, M. Dennehy, M. Pedernera, G. Tonetto, Chem. Eng. J., 255 (2014) 185-194.

[29] I. Popescu, Z. Skoufa, E. Heracleous, A. Lemonidou, I.-C. Marcu, Phys. Chem. Chem. Phys., 17 (2015) 8138-8147.

[30] H. Zhu, D.C. Rosenfeld, D.H. Anjum, V. Caps, J.-M. Basset, ChemSusChem, 8 (2015) 1254-1263.

[31] A. Qiao, V.N. Kalevaru, J. Radnik, A. Martin, Catal. Today, 264 (2016) 144-151.

[32] N. Madaan, N.R. Shiju, G. Rothenberg, Catal. Sci. Tech., 6 (2016) 125-133.

[33] H. Zhu, D.C. Rosenfeld, D.H. Anjum, S.S. Sangaru, Y. Saih, S. Ould-Chikh, J.-M. Basset, J. Catal., 329 (2015) 291-306.

[34] B. Solsona, F. Ivars, A. Dejoz, P. Concepción, M.I. Vázquez, J.M. López Nieto, Top. Catal., 52 (2009) 751-757.

[35] B. Solsona, J.M. López Nieto, P. Concepción, A. Dejoz, F. Ivars, M.I. Vázquez, J. Catal., 280 (2011) 28-39.

[36] S. Agouram, A. Dejoz, F. Ivars, I. Vázquez, J.M. López Nieto, B. Solsona, Fuel Process. Technol., 119 (2014) 105-113.

[37] J.M. López Nieto, B. Solsona, R.K. Grasselli, P. Concepción, Top. Catal., 57 (2014) 1248-1255.

[38] J.P. Bortolozzi, E.D. Banús, N.L. Courtalón, M.A. Ulla, V.G. Milt, E.E. Miró, Catal. Today, 273 (2016) 252-258.

[39] B. Farin, C. Swalus, M. Devillers, E.M. Gaigneaux, Catal. Today, 203 (2013) 24-31.

[40] J.P. Bortolozzi, T. Weiss, L.B. Gutierrez, M.A. Ulla, Chem. Eng. J., 246 (2014) 343-352.

[41] L. Smoláková, M. Kout, E. Koudelková, L. Čapek, Ind. Eng. Chem. Res., 54 (2015) 12730-12740.

[42] L. Smoláková, M. Kout, L. Čapek, Top. Catal., 58 (2015) 843-853.

[43] L. Smoláková, L. Čapek, Š. Botková, F. Kovanda, R. Bulánek, M. Pouzar, Top. Catal., 54 (2011) 1151.

[44] Z. Skoufa, G. Xantri, E. Heracleous, A.A. Lemonidou, Appl. Catal., A, 471 (2014) 107-117.

[45] B. Solsona, P. Concepción, B. Demicol, S. Hernández, J.J. Delgado, J.J. Calvino, J.M. López Nieto, J. Catal., 295 (2012) 104-114.

[46] B. Solsona, J.M. López Nieto, S. Agouram, M.D. Soriano, A. Dejoz, M.I. Vázquez, P. Concepción, Top. Catal., 59 (2016) 1564-1572.

[47] J.P. Bortolozzi, L.B. Gutierrez, M.A. Ulla, Appl. Catal., A, 452 (2013) 179-188.

[48] B.R. Jermy, B.P. Ajayi, B.A. Abussaud, S. Asaoka, S. Al-Khattaf, J. Mol. Catal. A: Chem., 400 (2015) 121-131.

[49] E. Heracleous, A.F. Lee, K. Wilson, A.A. Lemonidou, J. Catal., 231 (2005) 159-171.

[50] X. Lin, K.R. Poeppelmeier, E. Weitz, Appl. Catal., A, 381 (2010) 114-120.

[51] K. Fukudome, A. Kanno, N.-o. Ikenaga, T. Miyake, T. Suzuki, Catal. Lett., 141 (2011) 68-77.

[52] B. Solsona, P. Concepción, S. Hernández, B. Demicol, J.M.L. Nieto, Catal. Today, 180 (2012) 51-58.

[53] B. Solsona, P. Concepción, J.L. Nieto, A. Dejoz, J. Cecilia, S. Agouram, M. Soriano, V. Torres, J. Jiménez-Jiménez, E.R. Castellón, Catal. Sci. Tech., 6 (2016) 3419-3429.

[54] P. Brussino, J.P. Bortolozzi, V.G. Milt, E.D. Banús, M.A. Ulla, Ind. Eng. Chem. Res., 55 (2016) 1503-1512.

[55] J.-M. Basset, H. Zhu, D.C. Rosenfeld, P. Laveille, Solid-state synthesis of nickel oxide-based oxidative dehydrogenation catalysts for alkene manufacture from alkanes, Dow Global Technologies LLC, USA . 2016, p. 19pp.

[56] G. Tanimu, B.R. Jermy, S. Asaoka, S. Al-Khattaf, J. Ind. Eng. Chem., 45 (2017) 111-120.

[57] W. Li, J. Liu, D. Zhao, Nat. Rev. Mater., 1 (2016) 16023.

[58] D. Gu, F. Schuth, Chem. Soc. Rev., 43 (2014) 313-344.

[59] Q. Yuan, A.-X. Yin, C. Luo, L.-D. Sun, Y.-W. Zhang, W.-T. Duan, H.-C. Liu, C.-H. Yan, J. Am. Chem. Soc., 130 (2008) 3465-3472.

[60] S.M. Morris, P.F. Fulvio, M. Jaroniec, J. Am. Chem. Soc., 130 (2008) 15210-15216.

[61] M.D. Farahani, J. Valand, A.S. Mahomed, H.B. Friedrich, Catal. Lett., 146 (2016) 2441-2449.

[62] Y. Zeng, H. Ma, H. Zhang, W. Ying, D. Fang, Fuel, 137 (2014) 155-163.

[63] Y. Kathiraser, W. Thitsartarn, K. Sutthiumporn, S. Kawi, J. Phys. Chem. C, 117 (2013) 8120-8130.

[64] A.M. Zhao, W.Y. Ying, H.T. Zhang, H.F. Ma, D.Y. Fang, Catal. Commun., 17 (2012) 34-38.

[65] X.J. Zou, X.G. Wang, L. Li, K. Shen, X.G. Lu, W.Z. Ding, Int. J. Hydrogen Energy, 35 (2010) 12191-12200.

[66] K. Jabbour, P. Massiani, A. Davidson, S. Casale, N. El Hassan, Appl. Catal., B, 201 (2017) 527-542.

[67] E. Yuan, C. Wu, G. Liu, L. Wang, Appl. Catal., A, 525 (2016) 119-127.

[68] Q. Liu, J.J. Gao, F.N. Gu, X.P. Lu, Y.J. Liu, H.F. Li, Z.Y. Zhong, B. Liu, G.W. Xu, F.B. Su, J. Catal., 326 (2015) 127-138.

[69] K. Nakajima, Y. Baba, R. Noma, M. Kitano, J. N. Kondo, S. Hayashi, M. Hara, J. Am. Chem. Soc., 133 (2011) 4224-4227.

[70] S. Furukawa, T. Shishido, K. Teramura, T. Tanaka, J. Phys. Chem. C, 115 (2011) 19320-19327.

[71] D. Teschner, E. Vass, M. Hävecker, S. Zafeiratos, P. Schnörch, H. Sauer, A. Knop-Gericke, R. Schlögl, M. Chamam, A. Wootsch, A.S. Canning, J.J. Gamman, S.D. Jackson, J. McGregor, L.F. Gladden, J. Catal., 242 (2006) 26-37.

[72] J. McGregor, Z. Huang, E.P.J. Parrott, J.A. Zeitler, K.L. Nguyen, J.M. Rawson, A. Carley, T.W. Hansen, J.-P. Tessonnier, D.S. Su, D. Teschner, E.M. Vass, A. Knop-Gericke, R. Schlögl, L.F. Gladden, J. Catal., 269 (2010) 329-339.

[73] S. Gomez Sanz, L. McMillan, J. McGregor, J.A. Zeitler, N. Al-Yassir, S. Al-Khattaf, L.F. Gladden, Catal. Sci. Tech., 5 (2015) 3782-3797.

[74] J. Grant, C. Carrero, F. Goeltl, J. Venegas, P. Mueller, S. Burt, S. Specht, W. McDermott, A. Chieregato, I. Hermans, Science, 354 (2016) 1570-1573.

Chapter five

Summary and conclusion

Solution combustion Synthesis (SCS) and Sol-Gel auto Combustion Synthesis (SGCS) were used for the synthesis of NiO/Al_2O_3. It was found that the physicochemical properties of the NiO/Al_2O_3 catalysts, such as crystallite size, phase composition, surface area, active metal dispersion, surface acidity and reducibility can be tuned with the careful control of the fuel and water concentration. Furthermore, the effects of these alterations in catalytic applications were probed using the hydrogenation of octanal as a model reaction.

The use of urea as a fuel gave NiO/Al_2O_3 catalysts with high surface areas, small crystallite sizes and low formation of $NiAl_2O_4$ spinel phase, which was highly dependent on the water concentration during the combustion synthesis. These materials provided high conversion at low temperature (110 °C) in the hydrogenation of octanal due to their enhanced surface characteristics, as well as the presence of a significant quantity of β-NiO (a large peak in the H_2-TPR data).

The use of oxalyldihydrazide as a fuel in preparation of NiO/Al_2O_3 resulted in catalysts with low surface areas, large crystallite sizes and high formation of the $NiAl_2O_4$ spinel phase, depending on the concentration of the water used during the combustion synthesis. In contrast of what was observed for the catalysts prepared by urea, the catalysts synthesised with oxalyldihydrazide showed low activity at low temperature (110 °C) in hydrogenation, due to their poor surface characteristics and presence of the hard to reduce $NiAl_2O_4$ spinel phase.

Interestingly, the catalytic activity of catalysts with oxalyldihydrazide were comparable with the ones synthesised using urea as a fuel at higher temperatures (150 °C and 180 °C), since

the rate of reaction on small detected α-NiO (from the H_2-TPR data) sites is higher at these elevated temperatures. In addition, available nickel on the surface of the $NiAl_2O_4$ spinel seems to be reduced at these temperatures and improves the catalytic activity. Finally, the formation of $NiAl_2O_4$ was found to enhance the selectivity to octanal from hydrogenation of octanal by blockage of acidic sites of the Al_2O_3. $NiAl_2O_4$ was also believed to slowly generate the metallic nickel in hydrogenation system, which will possibly be helpful for an enhanced time on stream application of the NiO/Al_2O_3 catalysts in hydrogenation of aldehydes.

To further study the chemistry of the $NiAl_2O_4$ spinel, the Sol-Gel auto Combustion synthesis (SGCS) with oxalyldihydrazide as a fuel was used to synthesis the Nb doped $NiAl_2O_4$ spinel catalysts that were used for the oxidative activation of *n*-octane. Nb showed a great tendency to occupy the octahedral sub-lattices of the spinel structure that have both Ni and Al, since $NiAl_2O_4$ is known to have an inverse spinel structure. Generally, the crystallite sizes of the catalysts increased upon the addition of Nb in the lattice of $NiAl_2O_4$. Furthermore, the substitution of Nb in the lattice of $NiAl_2O_4$ seems to alter the degree of inversion of these spinel based catalysts. Based on H_2-TPR data and the ODH (oxidative dehydrogenation) catalytic data, the addition of Nb in the lattice of spinel seemed to decrease the reducibility of $NiAl_2O_4$.

The addition of Nb was found to decrease the activity of these catalysts in the ODH of *n*-octane. Generally, the selectivity to octenes improved with the addition of Nb. The physical characteristics of the surface, the concentration of active sites and the operating temperature were found to be important factors for aromatic formations in the ODH of *n*-octane over these catalysts. In addition, the ratio between $Ni_{[Oct]}/Ni_{(Tet)}$ was found to be very important in the selectivity to CO_x.

The characterisation of the used catalysts showed that the crystallite sizes of these were consistently smaller than their corresponding fresh equivalent, and the difference between the crystallite sizes of the used and fresh catalysts decreased as the Nb doping increased. The *in situ* XRD analysis under reducing and oxidising conditions showed that the appearance of smaller crystallite sizes of the used catalysts, in comparison to the fresh catalysts, does not seem to be due to the occurrence of the redox cycles during the catalytic testing. In addition, TGA analysis of the used catalysts under flow of air showed that all catalysts were covered with a thin layer of coke during the ODH of *n*-octane under somewhat anaerobic conditions. The formed coke over the spinel was shown to have different characteristics to the coke formed over the NiO phase and Nb doping shifted the coke gasification towards higher temperatures. Finally, HR-TEM images, as well as the XRD diffractograms, of the used SP-0.02 Nb showed that the formed smaller crystals have the characteristics of spinel and the coking seems to result in the formation of smaller crystallites in the used catalysts compared to the fresh ones. In addition, this coking was found to modify the nickel distribution between the two available sub-lattices in the cubic structure of spinel.

To investigate the effect of porosity of the NiO/Al_2O_3 based catalysts containing Nb in oxidative reactions, the glycol-thermal synthesis technique was used to prepare mesoporous catalysts with nanorod morphology. In addition, the use of this synthesis technique provided Al_2O_3 with ordered mesoporous structure in the absence of any template. Similar surface textures were obtained for these catalysts, which allowed the investigation of the chemical properties of these catalysts. The addition of Nb seems to weaken the observed "confinement effect" and resulted in the lowering of the reduction temperatures. Therefore, the catalysts with no niobium has similar characteristics as nickel oxide loaded on alumina, whereas the catalyst with the lowest nickel and highest niobium loading showed similar characteristics for bulk NiO. These characteristics were confirmed using *in situ* XRD, N_2 physisorption, SEM,

TEM and HR-TEM techniques. NH_3-TPD data showed that Nb addition increases the acidity of the catalysts, with the highest acidity observed for Nb_2O_5/Al_2O_3. The increase of acidity was found to have a direct impact on selectivity to CO, cracked products and benzene when these catalysts were used for the oxidative activation of *n*-octane. The strong "confinement effect" was also found to enhance the selectivity to octenes, while the selectivity to C_8 aromatics was found to be dependent on the pore size, as well as the acidity of the catalysts. This study showed that the fast release of nucleophilic oxygen species with high entropies, radical reactions via the addition of Nb, the presence of electrophilic oxygen species (especially at high temperatures) and the presence of the acidic sites seem to be the main factors for high selectivity to CO_x during the oxidative activation of *n*-octane. Therefore, two different synthetic techniques used in this study to prepare the NiO/Al_2O_3 based catalysts gave materials with different physicochemical properties, which in turn showed different catalytic performances in the chosen reaction models.

This study shows that both combustion synthesis and glycol-thermal synthesis can be used as two strong tools for the preparation of heterogeneous materials with tuneable characteristics. The use of combustion synthesis for the preparation of the materials with the same molecular formula gives materials with different physicochemical characteristics, depending on the type of fuel used and the amount of water added. Accordingly, this technique can be used to synthesise doped binary oxides or mesoporous materials. Although mesoporous NiO/Al_2O_3 catalysts could be synthesised using both aforementioned techniques, only glycol-thermal synthesis resulted in the materials with ordered-mesoporous structures. The effect of Nb loading on glycol-thermal synthesis was explored in this study and found to strongly affect the physicochemical properties of NiO/Al_2O_3 based catalysts. As a result, different catalytic performances in the chosen reaction models were observed for these catalysts.

Appendix

Chapter three

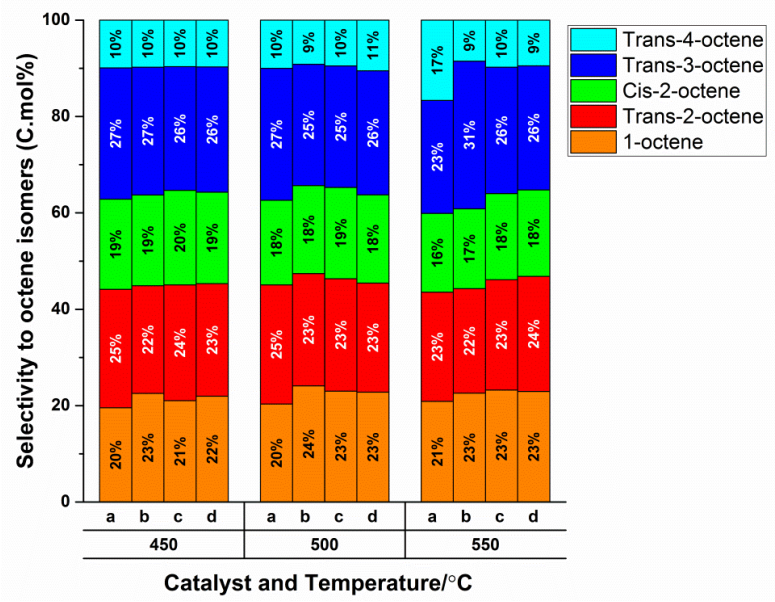

Appendix 3.1 Selectivity towards different octene isomers; a) Sp, b) Sp-0.02 Nb, c) Sp-0.06 Nb and d) Sp-0.10 Nb

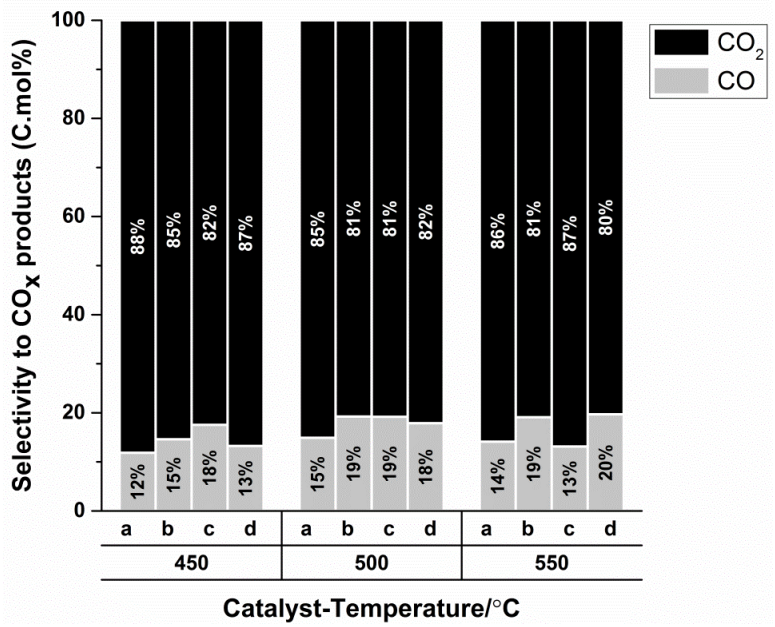

Appendix 3.2: Selectivity towards CO and CO_2; a) Sp, b) Sp-0.02 Nb, c) Sp-0.06 Nb and d) Sp-0.10 Nb.

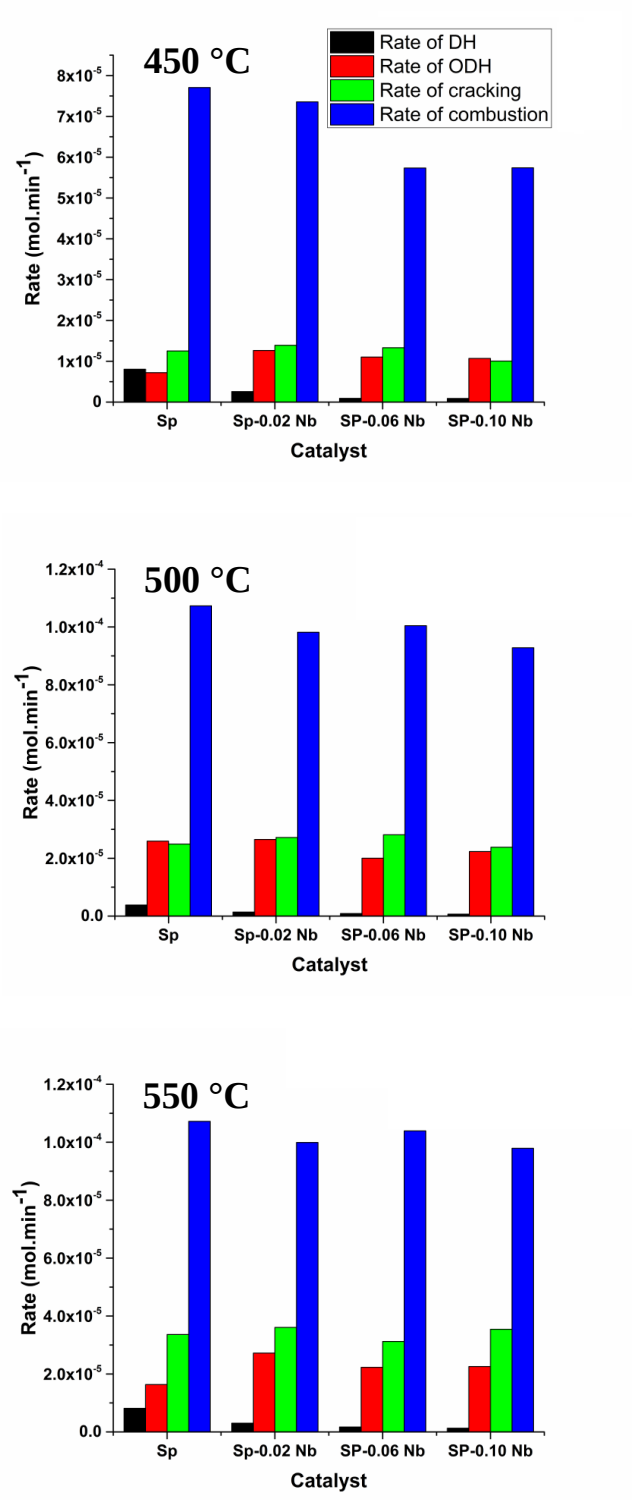

Appendix 3.3 Different involved pathways during the reaction at different temperatures. (DH: dehydrogenation [based on detected H_2 in the TCD], ODH: oxidative dehydrogenation [estimated, based on the formed products])

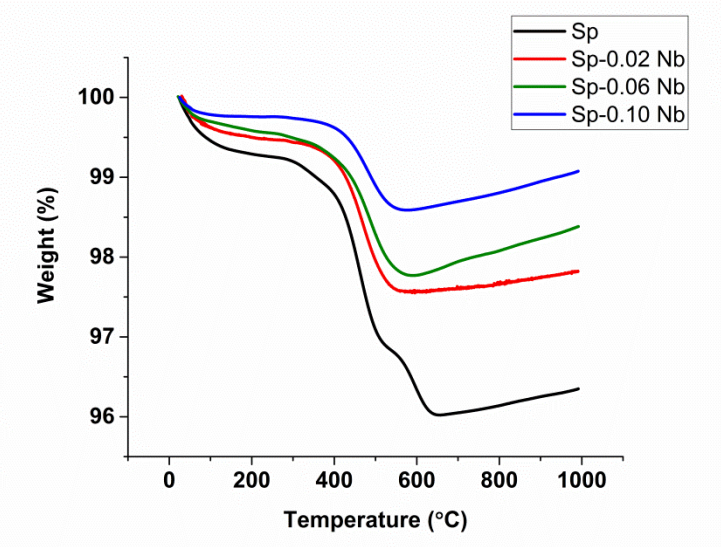

Appendix 3.4 Calculated mass lost using TGA analysis of the used SP-x Nb (x: 0, 0.02, 0.06 and 0.10) under flow of air.

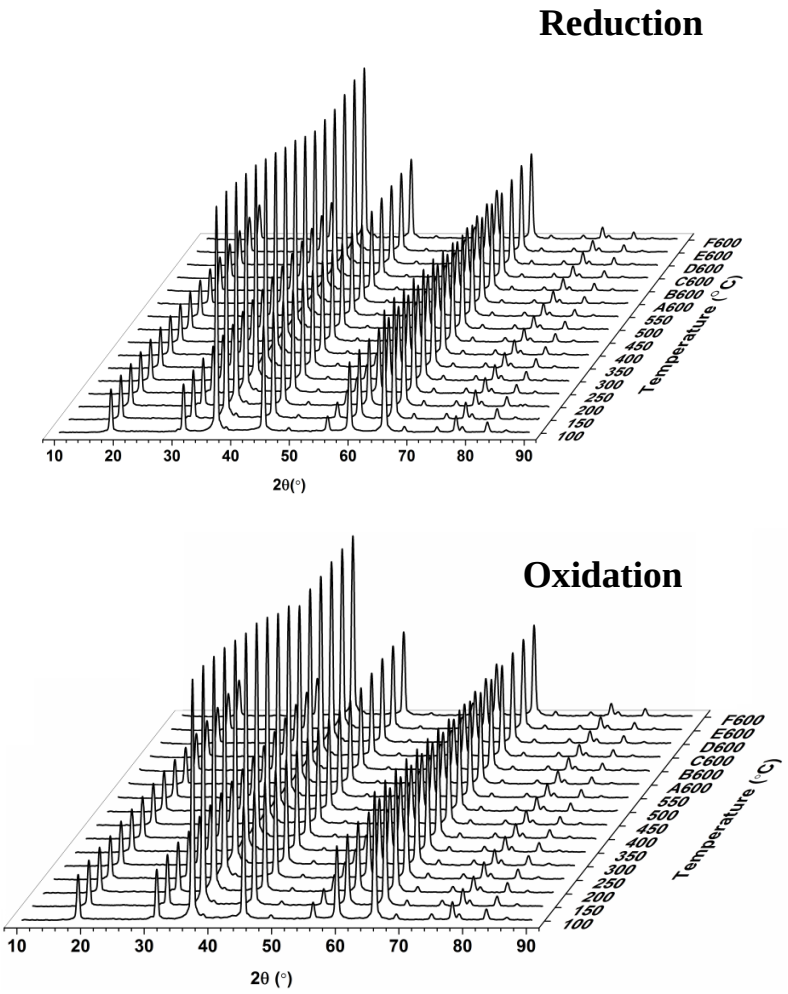

Appendix 3.5 *In situ* XRD of Sp-0.02 Nb under reducing and oxidizing conditions (the A600-F600 diffractograms are in isothermal conditions)

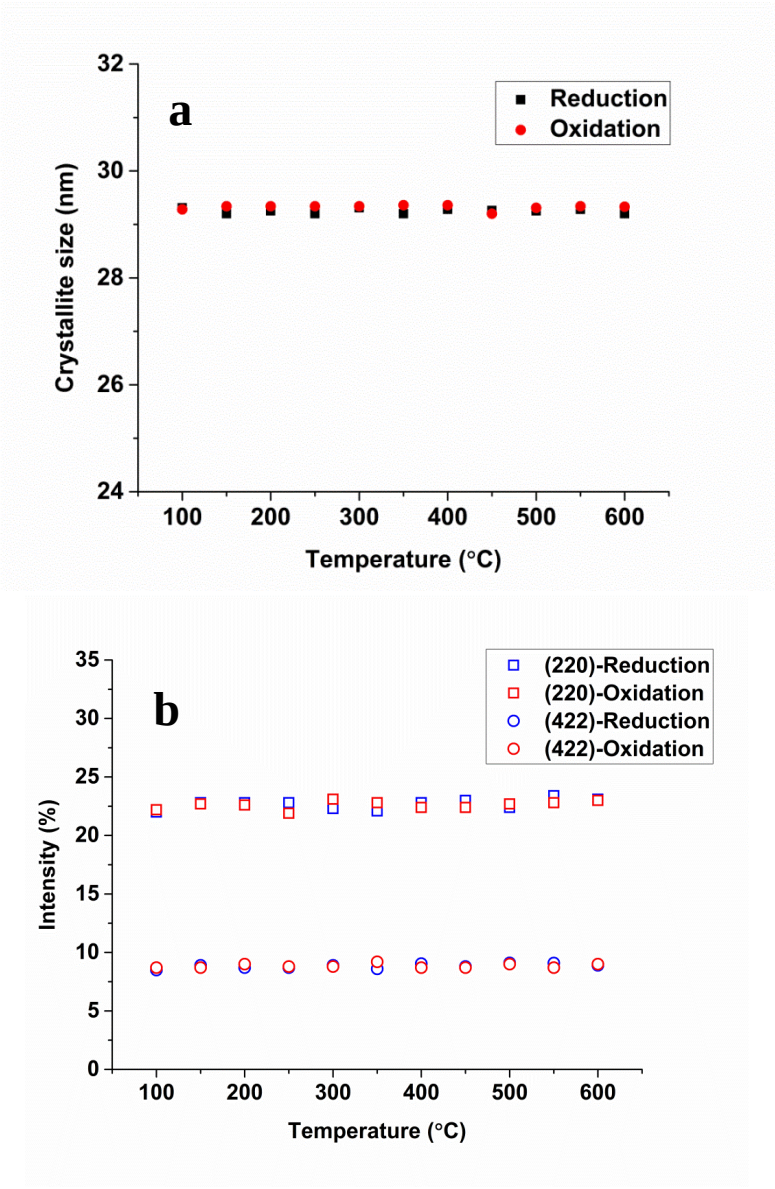

Appendix 3.6 a) Crystallite size [using Scherrer equation] analysis at different temperatures and redox conditions using *in situ* XRD of Sp-0.02 Nb **b)** The change in intensities of plane (220) and (422) at different temperatures and redox conditions using *in situ* XRD of Sp-0.02 Nb (The intensity of the Peak with *hkl* value of (311) was used as a reference in each diffractogram)

Appendix

Chapter four

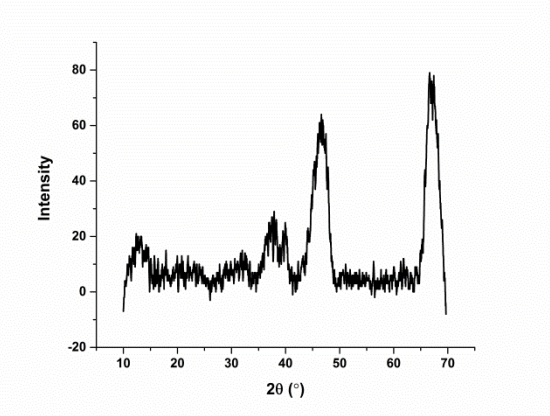

Appendix 4.1 The PXRD of Al_2O_3 synthesised by glycol-thermal technique.

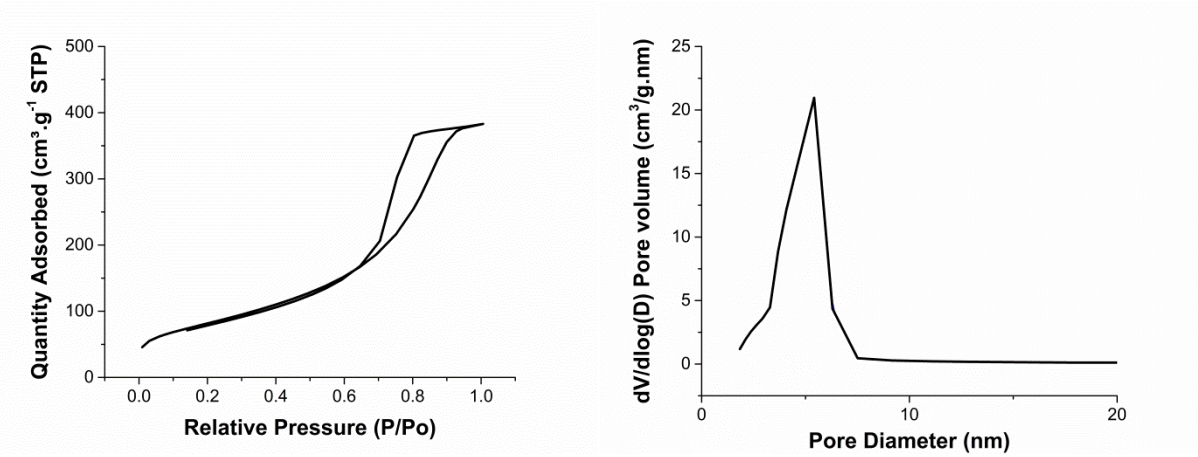

Appendix 4.2 (a) The N_2 adsorption-desorption isotherm and (b) pore size distribution of Al_2O_3 synthesised using glycol-thermal technique.

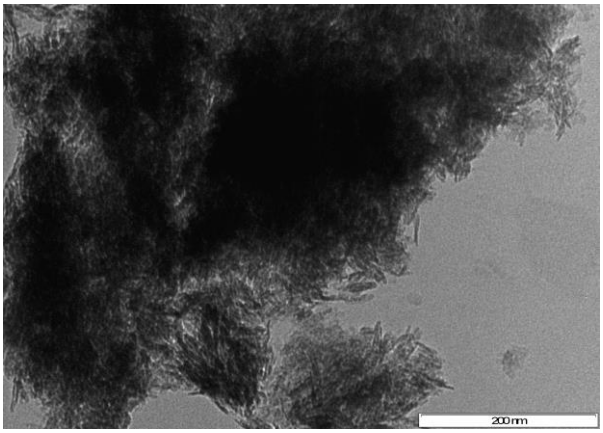

Appendix 4.3 TEM image of Al_2O_3 synthesised using glycol-thermal technique.

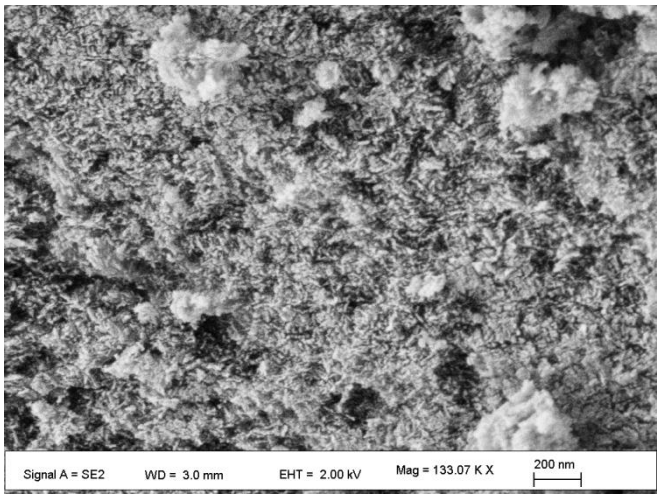

Appendix 4.4 SEM image of Al_2O_3 synthesised using glycol-thermal technique.

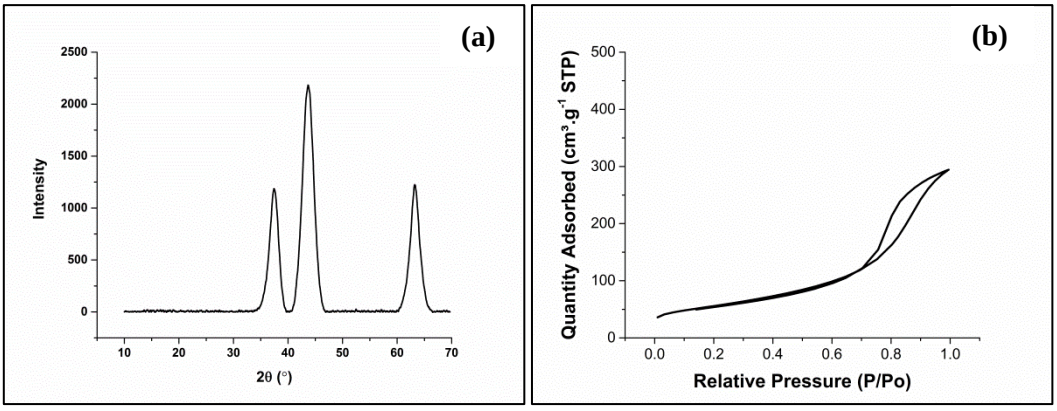

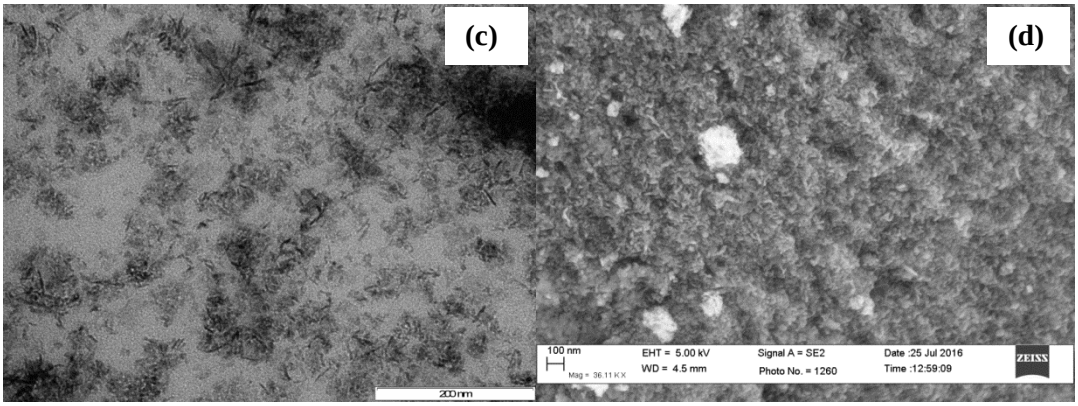

Appendix 4.5 The basic characterisations of the synthesised control catalysts with the composition of NiO=87.6 wt%, Nb_2O_5= 6.2 wt% and Al_2O_3=6.2 wt%. (a) PXRD, (b) N_2 adsorption-desorption isotherm, (c) TEM image and (d) SEM image.

Appendix

General

Table 1 The continues flow hydrogenation reactor setup.

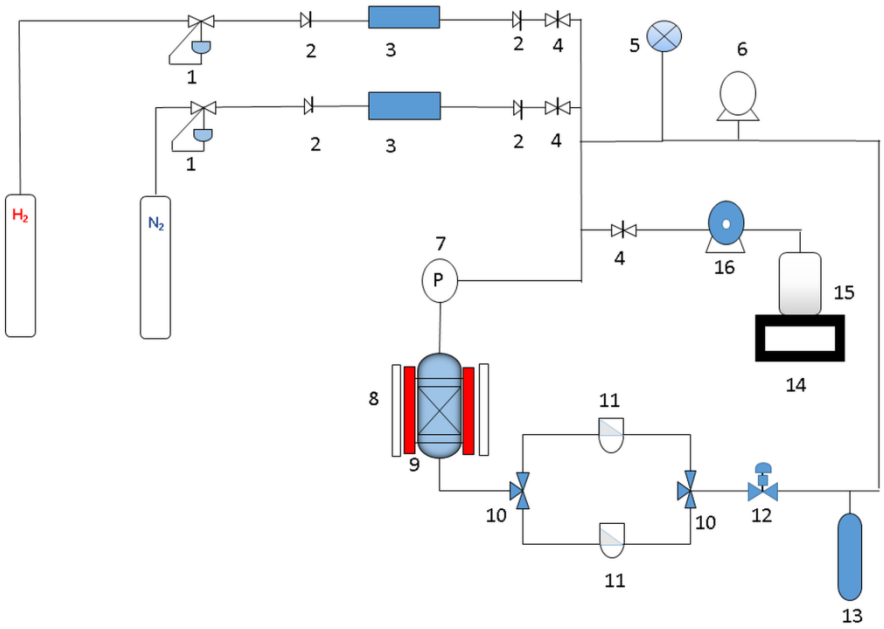

Part number	Description	Part number	Description
1	High pressure regulator	9	Fixed bed reactor
2	Check valve	10	Three way valve
3	Mass flow controller	11	Filter
4	Load valve	12	Back pressure gauge
5	Pressure relief valve	13	Catchpot
6	Wet gas flow meter	14	Balance
7	Pressure gauge	15	Octanal container
8	Heating jacket	16	HPLC pump

Fig 1 An image of a continues flow hydrogenation reactor setup.

Table 2 The continues flow oxidative dehydrogenation reactor setup.

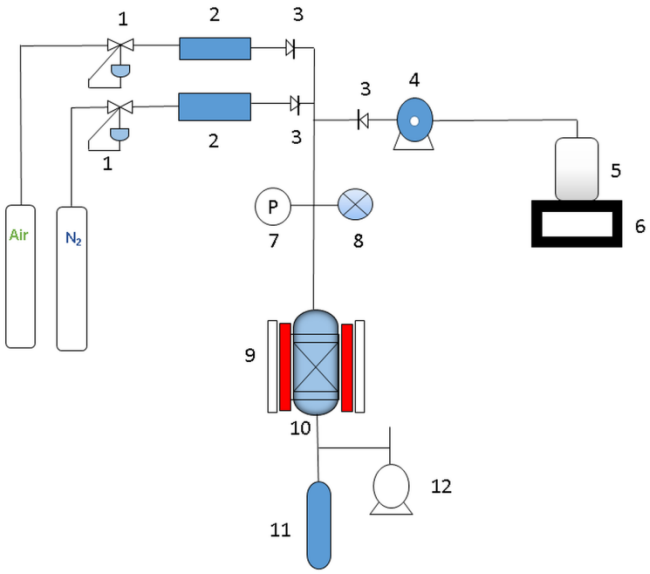

Part number	Description	Part number	Description
1	Pressure regulator	7	Pressure gauge
2	Mass flow controller	8	Pressure relief valve
3	Check valve	9	Heating block
4	HPLC pump	10	Fixed bed reactor
5	*n*-Octane container	11	Catchpot
6	Balance	12	Wet gas flow meter

Fig 1 An image of a continues flow oxidative dehydrogenation reactor setup.